1991

Design of an air test loop and turbine exhaust end models for performance improvement study

Behzat Turegun
Lehigh University

DESIGN OF AN AIR TEST LOOP AND TURBINE EXHAUST END MODELS FOR PERFORMANCE IMPROVEMENT STUDY

by

Behzat Türegün

A Thesis

Presented to the Graduate Committee

of Lehigh University

in Candidacy for the Degree of

Master of Science

in

Mechanical Engineering

Lehigh University

June 1991

This thesis is accepted and approved in partial fulfillment of the requirements for the degree of Master of Science.

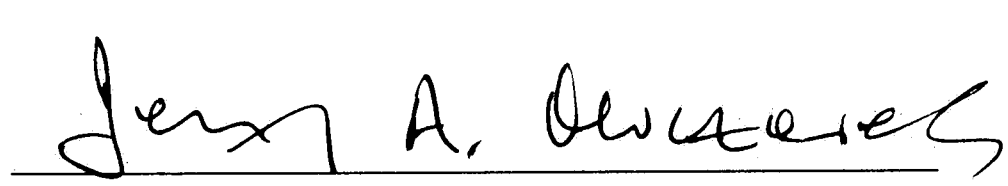

Professor in Charge

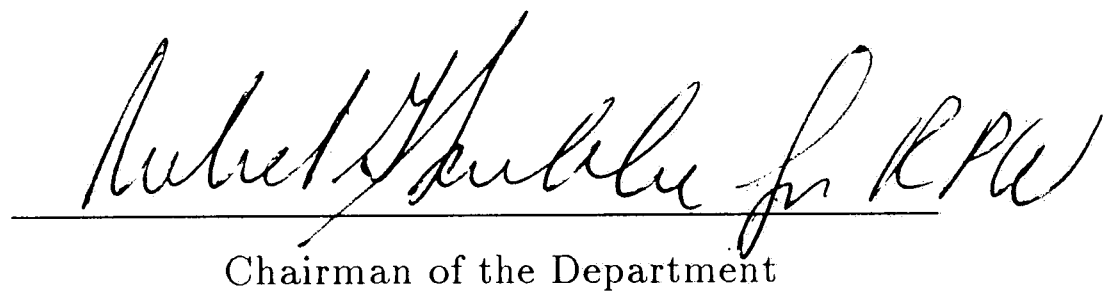

Chairman of the Department

May 8, 1991

Date

Dedicated to

My Father, Riza Türegün

and

My Mother, Gülüzar Türegün

ACKNOWLEDGEMENTS

The author would like to express his appreciation for the financial support provided by the Pennsylvania Power and Light Company, Allegheny Power Company, Duquesne Lights Company, and Houston Lighting and Power Company. The author would also like to thank Dr. Art Warnock of Energy Research Center.

Special thanks to Prof. Jerzy Owczarek of this department. He has been a constant source of help and motivation during the course of this study. Finally, the author gratefully thanks Mrs. Selime Dinc for the financial aid which was of crucial importance in the realization of the authors' graduate study.

CONTENTS

LIST OF TABLES

LIST OF FIGURES

LIST OF DRAWINGS

G−13C	Insert to change height
G−13D	Insert to change height
G−13E	Insert to change height
G−14A	Outlet duct for D/L=8.15
G−14B	Outlet duct for D/L=7.5
G−14C	Outlet duct for D/L=7.0
G−15	Open model (assembly)
H−1A	Condenser neck plan view
H−1B	Condenser neck (section A−A)
H−1C	Condenser neck (section B−B)
BV−1A	Assembly (elevation)
BV−1B	Assembly (plan view)
BV−1C	Side view (section A−A)
BV−1D	Side view (section B−B)
BV−2A	Condenser neck (struts only)
BV−2B	Condenser neck (steam dumps only)
BV−3	Guide vane
BV−4	Bearing cone
BV−5	Insert to change height
BV−6	Insert to change length
BV−7	Outlet duct
BV−8	Extraction piping
BV−9	Strut group 1
BV−10	Strut group 2
BV−11	Strut group 3

NOMENCLATURE

A	cross-sectional area, hood annulus length
A_B	blocked area
A_E	effective area
AR	area ratio , A_2/ A_1
B	blocked area fraction, hood length
C	distance shown in Figure 15
C_p	pressure recovery coefficient
C_{pi}	ideal pressure recovery coefficient
D	distance shown in Figure 15, hood width
E	effective area fraction
H	total pressure loss, hood height
H_L	total pressure loss coefficient
H_{Lm}	total pressure loss coefficient along the streamline of maximum velocity
h	specific enthalpy
HL	hood loss
(H+C)L	hood and condenser neck loss
L	last stage rotor blade height
L_v	guide vane length
$\overline{L}$	average wall length for annular diffuser, $(L_o + L_i)/2$
LL	leaving loss
M	Mach number
N	diffuser axial length
P	static pressure

$P_{T,AN}$	average annulus total pressure
Q	volumetric flow rate
q	dynamic head based on mass averaged velocity , $\frac{1}{2}\rho V^2$
R	radius, gas constant
Re	Reynolds number
ΔR	difference in tip and hub radii
S	specific weight, screen solidity
s	specific entropy
T	temperature
V	mass averaged velocity
W	two dimensional diffuser width
x	axial coordinate

Greek Symbols

α	kinetic-energy-flux velocity-profile parameter
β	diffuser bend angle shown in Figure 7, diameter ratio of venturi meter
γ	ratio of specific heats
δ^*	boundary layer displacement thickness
ϵ	overall effectiveness of a diffuser
ν	dynamic viscosity
ρ	fluid density
ρ_{AN}^{FL}	average fluid density between annulus and flange
ϕ	divergence half angle
ψ	swirl angle

Subscripts

air	air
AN	annulus
ATM	atmospheric conditions
AVE	average
c	centerline
FL	flange
H	hub
i	inner, inlet
IDEAL	ideal conditions; no losses
LOCAL	particular location on the shroud or the hub in the annulus
m	maximum, mean
T	total conditions, tip or shroud
t	throat
w	water
∞	far downstream or upstream
1	diffuser inlet, annulus
2	diffuser exit, flange

Superscripts

$-$	average
$^\circ$	degrees
$''$	inches

ABSTRACT

The energy loss in a low pressure turbine exhaust hood is associated with the wall friction and friction caused by the flow separations within the hood. Another parameter of exhaust hood performance, the " hood loss " is a measure the energy loss and of the inability of the hood to properly diffuse the flow and to distribute it uniformly into the condenser neck. The final objective of this study is to carry out an experimental investigation using air to gather data needed to optimize the design of LP turbine exhaust hood and condenser neck for a range of large steam turbine designs. For this purpose, three hood and condenser neck models were designed. A generic model design will be used to determine the necessary hood size relative to the last rotating blade height. Exhaust ends of two existing steam turbines were also modeled in order to investigate their performance characteristics and the possible power gain resulting from modifications of the internal structures, and from redistribution of flow through the condenser neck.

An annular diffuser review is given to form a basis for the design of a diffusing type exhaust hood. Dimensionless parameters affecting the performance of a turbine exhaust hood are derived and their relative importance on the performance is discussed. The equations for computing the exhaust hood loss coefficient and exhaust hood and condenser neck loss coefficient are also given. A methodology for the determination of these coefficients has been established previously.

1. INTRODUCTION

The structural component connecting a turbine and a condenser, and providing a flow path for the steam into the condenser neck is called the exhaust hood. In most designs, the flow leaving the last row of rotating blades has to turn 90 degrees in order to flow into the condenser neck. Exhaust hood of a turbine includes the inlet annulus, flow guide, bearing cone (which form a diffuser passage), turbine outer shell, reinforcing members, and the condenser or exhaust hood flange, as shown in Figure 1. The part between the exhaust hood flange and the condenser tube bundles, not shown in Figure 1, is referred to as the condenser neck. It includes the flange, reinforcing structural beams, feedwater heaters and associated piping.

The total exhaust loss, which represents the hood loss and the leaving loss, of a turbine represents a loss in available energy to the turbine. This loss depends on the overall geometry of the exhaust hood and on the kinetic energy of the steam exiting the last row of blades. Typically, the Mach number of the steam leaving the blades is in the range of 0.6 to 0.8. The total exhaust loss can add up to a total of 10% of all the fluid dynamic losses within the turbine [1]. The leaving loss is the energy equivalent of the absolute velocity leaving the last row of blades. The hood loss is the available enthalpy loss which exists when the mean static pressure at the exit of the last turbine stage, P_{AN}, is higher than the mean pressure at the condenser flange. This pressure difference is caused by friction along the exhaust hood walls and the associated structural components, flow separation, and lack of diffusion. The components of the total exhaust loss are shown on an h-s diagram in Figure 2 [2]. A reduction in P_{AN} means power gain for the turbine generator unit.

The factors affecting the performance of a turbine exhaust hood have been investigated by researchers to some extent and tests have been run to figure out their effects. The flow in a hood is extremely complex as a consequence of the nonuniformity of the flow leaving the blades, surface friction, and turbulence produced by the flow separation from structural members. Most researchers prefer experimentation to obtain an insight into this complex flow. However, a three dimensional analytical model of a particular hood has been developed [3]. The analysis involves the conservation equations for pressure and three momentum equations. Although the inlet conditions were not very realistic in that a uniform mass flow rate and axial momentum were assumed, the researchers were able to get an insight into the flow field in the hood and the condenser neck.

At the inlet to the annular diffuser, the flow velocity and the static pressure are nonuniform [4]. The radial and circumferential variations of the static pressure in the last blade annulus are caused by the swirl and turning of the flow towards the condenser, respectively. In order to attain minimum kinetic energy loss, the absolute velocity at the blade exit must be approximately uniform in magnitude and have direction which is close to axial. This implies a roughly constant mass flow rate per unit area and low swirl angles between blade tip and hub boundaries.

The non-uniform velocity profile in the condenser neck is a major problem because it causes poor heat transfer in the condenser. In order to fill in the neck with a nearly uniform flow, several modifications to the exhaust hoods are possible. Addition of guide vanes, splitter vanes, and modifications to the hood casing are various changes that can be considered to correct the pressure loss problem and to improve

performance.

This study has two objectives. The first one is directed toward the experimental determination of the necessary hood size relative to the last blade height for significant diffusion in the flow passage between the guide vane and the bearing cone. The second objective is determination by experiments of performance of existing exhaust hoods and improvement of the performance by modifications.

2. ANNULAR DIFFUSERS IN TURBINE EXHAUST HOODS

The exhaust hood losses in an exhaust hood can be reduced significantly by designing a diffusing type hood [2]. The use of a well designed diffuser in the exhaust hood is very important. Figure 3 shows a survey of performance of annular diffusers used in turbomachinery applications. In that figure C_p represents the pressure recovery coefficient defined as the ratio of the pressure rise in the diffuser to the inlet kinetic pressure, AR denotes the area ratio of a diffuser, and $\bar{L}/\Delta R_1$ the dimensionless length. It is clear that some of the diffusers are not operating effectively, so there is a potential for improvement.

In the design of an annular diffuser to be used in the exhaust hood of a turbine, the length is usually the most important parameter. Also, the high Mach number at the inlet of the diffuser is another factor. The design of a diffuser in the hood can not be separated from the total structure. The diffuser which gives the most pressure recovery in an optimum exhaust hood may not be operating at the optimum line in the performance chart which is determined for the diffuser exhausting into an open space. It should be designed considering the passage that turns the flow.

Zeryankin and Drokonov [5] tested a turbine exhaust hood with and without a diffuser and they found that installation of a diffuser raised the efficiency of the turbine stage by 3 per cent. For a particular turbine unit, the increase in the thermal efficiency resulting from addition of a diffuser was about 0.5% at 0.7-0.8 axial Mach number [6].

Performance characteristics of diffusers of two dimensional, conical and annular types have been studied by many workers. The performance charts for diffusers contain two optimum diffuser lines that are very useful for design purposes. The line denoted by the symbol C_p^* is the locus of points which defines the diffuser area ratio producing the maximum pressure recovery for a given non-dimensional length. The line denoted by C_p^{**} defines the diffuser non-dimensional length producing maximum pressure recovery for a given area ratio. The performance charts for straight walled annular and curved annular diffusers are given in Figures 4 and 5, respectively. The symbol R in Figure 5 represents the radius of curvature of the diffuser, and ΔR_1 is the difference between the annulus radii at diffuser inlet. There is a considerable difference in the value of the pressure recovery coefficient between curved and straight walled annular diffusers at the same length. However, the difference is less at the same area ratio, as shown in Figure 6.

The optimum operating points of diffusers change with the inlet conditions, such as the flow Mach number. However, there is not sufficient data for all types of diffusers to predict the effect of inlet conditions on the optimum operating line. The physical phenomena affecting the flow conditions in diffusers have been determined, and, for most of the diffuser types exhausting into an open space, flow regime charts have been obtained.

In practical design of a certain type of diffuser, the designer can use the existing data and he can extrapolate between various diffuser types. Geometric conditions, flow conditions, and inlet conditions should be considered together.

2.1. Geometry and Performance Parameters

The annular diffusers are common in turbomachinery applications. However, the investigation of annular diffusers has been less extensive than that of other types. The main reason for this is the large number of geometrical parameters. Four parameters are required to specify the geometry of a straight walled annular diffuser. They are the two wall angles, the inlet radius ratio, and the non-dimensional length. Annular diffuser geometries and associated geometrical parameters are explained in Figure 7.

The geometric parameters for straight walled diffusers are divided into two groups according to the degree of effect on the diffuser performance. The area ratio and the non-dimensional length are the most important parameters. The inlet radius ratio, $R_{T,1}/R_{H,1}$, and the wall angle are the complementary variables.

Relative measures of diffuser performance are obtained by comparing the measured pressure rise with either the maximum value that is theoretically obtainable, or with the ideal pressure rise. The ideal pressure rise is obtained when the flow is steady, inviscid, and one-dimensional. The maximum obtainable pressure rise is achieved when the exit velocity of the diffuser is zero, that is, when the diffuser has an infinite area at the exit. The ideal conditions refer to the process without any losses. Derivation of performance parameters for diffusers is given below [7].

With the assumption of uniform incompressible inviscid flow i.e., no losses, and effect of change in elevation, the Bernoulli equation becomes

$$\frac{P_1}{\rho} + \frac{V_1^2}{2} = \frac{P_2}{\rho} + \frac{V_2^2}{2} \tag{2.1}$$

and the continuity equation reads

$$V_1 A_1 = V_2 A_2 \tag{2.2}$$

where the subscripts 1 and 2 refer to the inlet and exit sections respectively. Combining equations (2.1) and (2.2) we obtain

$$\frac{(P_2 - P_1)_{IDEAL}}{\frac{1}{2}\rho V_1^2} = 1 - \frac{1}{AR^2} \tag{2.3}$$

where AR= A_2/A_1. The term on the right hand side of equation (2.3) is referred to as the ideal pressure recovery coefficient, and it is denoted by the symbol C_{pi}.

$$C_{pi} = 1 - \frac{1}{AR^2} \tag{2.4}$$

The pressure recovery coefficient, C_p, is the ratio of actual pressure rise to the maximum attainable pressure rise at the particular flow rate with one dimensional flow. When the exit velocity is assumed to be zero, equation (2.1) gives

$$\Delta P_m = \frac{1}{2}\rho V_1^2 \tag{2.5}$$

Equation (2.5) shows the maximum attainable pressure rise, hence the pressure recovery coefficient becomes

$$C_p = \frac{\Delta P}{\Delta P_m} = \frac{P_2 - P_1}{\frac{1}{2}\rho V_1^2} \tag{2.6}$$

Another common parameter used for the evaluation of a diffuser performance is the diffuser effectiveness which relates the actual pressure rise to that which would be obtained in an inviscid one dimensional flow at the same flow rate, i.e.,

$$\epsilon = \frac{\Delta P}{\Delta P_i} = \frac{C_p}{C_{pi}} \tag{2.7}$$

Because of the uniform flow assumption, the value of effectiveness may exceed unity although it is not likely to. One should notice that the pressure recovery coefficient is sometimes defined in a way that the denominator of equation (2.6) is replaced by the dynamic pressure difference between inlet and exit of the diffuser, which is $\frac{1}{2}\rho {V_1}^2 - \frac{1}{2}\rho {V_2}^2$.

The total pressure loss for a real incompressible flow is given by the following equation

$$H = \left(\frac{P_1}{\rho} + \frac{1}{2}{V_1}^2 \right) - \left(\frac{P_2}{\rho} + \frac{1}{2}{V_2}^2 \right) \tag{2.8}$$

Dividing equation (2.8) by $\frac{1}{2}{V_1}^2$, the non-dimensional loss coefficient can be defined as

$$H_L = \frac{H}{\frac{1}{2}{V_1}^2} = \left(1 - \frac{{V_2}^2}{{V_1}^2} \right) - \frac{P_2 - P_1}{\frac{1}{2}{V_1}^2} \tag{2.9}$$

Using the continuity equation (2.2) , the loss coefficient can be written as

$$H_L = C_{pi} - C_p \tag{2.10}$$

2.2. Flow Regimes

A major problem in a diffusing passage is the separation of flow. Stall may cause a non-uniformity in the flow and subsequent excessive losses. Sometimes the outlet velocity distribution from the diffusers can be of as much importance as the velocity reduction or pressure rise. For example, when a turbomachine is tied to a diffuser discharge, the performance of the turbomachine, especially when it is a compressor, can be affected by the diffuser discharge non-uniformity or lack of steadiness. The designer should know beforehand what kind of an internal flow will exist in the diffuser. For these reasons the flow regimes in the diffuser flow must be clearly understood.

The separation of flow or stall can be explained by the theory of boundary layers. Flow separation is thought to start when the velocity gradient in the perpendicular direction to the wall over which the fluid flows is zero or, in other words, when the shear stress at the wall becomes zero. Experiments show that the separated laminar boundary layer may reattach to the wall. Between the separation and reattachment points of a laminar boundary layer, the flow often becomes turbulent. During this process a laminar separation bubble is formed. Inside the bubble, the fluid makes a circulatory motion between the points of separation and reattachment. There is no accepted prediction method for the start of separation in a turbulent boundary layer.

In a diffuser flow, as the divergence angle is increased from zero degrees four regimes of flow are observed [8]: the well behaved flow regime, the large transitory stall regime, the steady fully developed stall regime and the jet flow regime. The schematic diagrams of diffuser flow regimes are given in Figure 8.

2.2.1. Well Behaved Flow Regime

Well behaved flow regime is an unseparated flow. The pressure gradient along the wall of the diffuser remains favorable, i.e., pressure increases along the diffuser, and its magnitude is relatively small. Well behaved flow regime should be expected when the area ratio of the diffuser is not very large and when the diffuser is relatively long since the area ratio alone does not ensure a suitable pressure gradient. In this flow regime, at high Reynolds numbers, the core flow is approximately irrotational and the boundary layers are close to the walls.

From the definition of the pressure recovery coefficient one can notice that in the case of well behaved flow regime, the recovery coefficient is expected to be relatively small. The reason for that is simply the small pressure rise in the diffuser due to the small area ratio. The same reasoning applies to the ideal pressure recovery coefficient. In fact, the coefficients are close to each other and therefore the effectiveness of the diffuser in this flow regime is high.

2.2.2. Large Transitory Stall Flow Regime

This is the regime in which the separation varies in size, intensity, and in position with time. This unsteady flow regime is encountered at higher pressure gradients than those in the well behaved flow regime. The area ratio of a diffuser which has a large transitory stall regime is presumably greater than that of a well behaved diffuser. Therefore, greater ideal pressure recovery coefficients are expected. However, the unsteadiness of the flow reduces the effectiveness.

2.2.3 Fully Developed Stall Regime

In this flow regime, a major portion of the diffuser is filled with a recirculation region extending from a position close to the inlet to the exit of the diffuser. The fully developed stall is very much like the classical stall pattern propounded by Prandtl. This pattern is steady with far less fluctuation than in the large transitory flow regime. This regime occurs when the pressure gradient becomes too large to support uniform flow. Pressure recovery coefficients and effectiveness for this flow regime are small because of large losses. As can be seen in the Figure 8, the inner core of the flow is not decelerated and the pressure is not recovered.

2.2.4. Jet Flow Regime

In the jet flow regime, the main flow is separated from all the walls. This regime occurs at high angles of divergence. The pattern of flow is relatively steady. A complete reversed flow near the walls of the diffuser is observed. As in the case of fully developed stall flow regime the pressure recovery and effectiveness are poor. In order for the jet flow to occur, the diffuser walls must all diverge because of the fact that, for separation, the pressure gradient must be adverse on all walls of the diffuser.

A flow regime chart has been obtained experimentally for curved annular diffusers. A sharp transition between the flow regimes does not exist, so the definition of a certain limit involves a degree of subjectivity. The chart for curved annular diffusers is presented in Figure 9. Unfortunately, no such charts exist for straight walled annular diffusers. Only the first stall line has been established [9].

2.3. Effect of Inlet Conditions on Performance

2.3.1. Effect of Inlet Turbulence

Significant improvements in the pressure recovery of diffusers have been obtained with turbulent inlet boundary layer flow rather than laminar boundary layer flow because of the well known fact that the turbulent boundary layers are more resistant to separation of flow than the laminar boundary layers. For a given adverse pressure gradient, the laminar separation point falls upstream of the turbulent separation point.

Hoffmann and Gonzales [10] studied the effects of inlet free-stream turbulence on flow in two-dimensional diffusers. Two dimensional diffusers with divergence angles of 9° to 20° were studied to determine the flow direction along the walls and internal velocity profiles for conditions with and without inlet turbulence which was obtained by an arrangement of rods upstream of the diffusers. The mean divergence half-angle, ϕ_m is defined in Figure 7-(b). For the divergence half-angle of 9°, the condition of no upstream rods resulted in a pressure recovery coefficient of 0.72, while with the rods placed upstream the pressure recovery coefficient was determined to be 0.79. The increase in the pressure recovery of the diffuser with a divergence angle of 20 degrees was observed to be 22 per cent. When rods were used, the velocity profiles along the diffuser were flattened.

The effects of various small blade vortex generators, for the same thickness of the boundary layer at the inlet, have been studied by Senoo and Nishi [11]. The type of

diffuser studied was conical; however, in the qualitative sense the results are applicable to all types of diffusers. Two different kinds of blade arrangements were used in the experiments. One is co-rotating type which consists of equally spaced blades like a cascade, and the other is counter-rotating type where two adjacent blades are symmetrically placed and form a pair. The co-rotating type demonstrated a better performance since with this configuration the generators have dual effects: the trailing vortices exchange momentum between the main flow and the boundary layer, and also introduce a swirling flow which also contributes to prevention of flow separation. As a result of the vortex generation, there was an appreciable increase in the pressure recovery of the conical diffusers which had divergence angles between 8° to 30°. The maximum increase in the pressure recovery coefficient produced by vortex generators was found to occur around 16 degrees divergence angle.

The effects of inlet turbulence for annular diffusers have also been investigated by Stevens and Williams [12]. The results of the investigation showed a marked improvement in the stability of the outlet flow and increases in pressure recovery up to 20 per cent with only small rises in the total pressure loss.

The increase in the value of C_p as a result of increased inlet turbulence is caused by the reduction in flow velocity profile distortion and by the delay of separation. The results may be applicable to other flows which encounter adverse pressure gradients.

2.3.2. Effect of Swirl at the Inlet

In a flow downstream of a pump or turbine, some swirl is usually present. The designer must be aware of the effects of swirling flow which is a very important practical inlet flow distortion.

The effects of swirling inlet flow on pressure recovery coefficient were determined to be a function of the flow regime which would exist for axial inlet flow [13]. Swirling inlet flow produces large performance increases for diffusers in which the flow was separated. However, in the case of well behaved flow the swirling inlet flow does not provide any performance increases. Therefore, the geometry of the optimum diffuser with swirling inlet flow differs from that for axial inlet flow. The optimum lines for conical diffusers with swirling inlet flow can be found in reference 13.

The annular diffusers used in turbomachinery operate in the presence of swirl. Annular diffusers with various lengths, area ratios and cant angles were tested over a range of inlet flow swirl angles up to 48 degrees [14]. For a free-vortex flow, the tangential velocity in a swirling flow through an annular diffuser decreases in radially outward direction. Consequently, as the mean radius of flow increases, a reduction in the tangential velocity with a corresponding rise in the static pressure is observed. This implies that the cant angle of the diffuser is an important geometric parameter. Another difference between the pressure recovery for an axial inlet flow and swirling inlet flow may be attributed to the modification of the diffusion of the meridional component of velocity because of coupling with the tangential flow. This has an adverse effect on the pressure recovery particularly in highly canted diffusers due to

flow separation from the inner wall. However, if the distortion of the exit velocity profile does not matter, then the pressure recovery from the tangential component of the velocity can be very high.

Figure 10 shows the effect of the inner wall cant angle, ϕ_i, and inlet swirl angle, ψ_1, on the pressure recovery. The swirling flow in a diffuser which has a negative cant angle results in low pressure recovery, while it improves the performance of a diffuser with positive cant angle. The cant angle is said to be negative when the cross-section of hub decreases in the flow direction.

The stall characteristics of diffusers with swirling inlet flow are different than those for axial inlet flow. The presence of swirling inlet flow reduces the stall boundary of the diffuser. When swirling flow exists, stall free operation is unattainable at large area ratios regardless of the length of the diffuser. However, if the flow in the diffuser is axial, at the same area ratio, a stall-free operation can be achieved by increasing the length of the diffuser.

2.3.3. Effect of Inlet Boundary Layer Thickness

Figure 11 shows schematically the boundary layer blockage concept. The mass averaged stagnation pressure of an incompressible internal flow system at any cross-section can be expressed as [15]

$$P_T = P + \alpha q \tag{2.11}$$

where q denotes the dynamic head based on the mass averaged flow velocity, and α

represents $\overline{V^2}/V^2$. Physically, α is the ratio of actual kinetic energy flux to the kinetic energy flux corresponding to a uniform velocity profile at the same cross-section and flow rate. When there is some velocity nonuniformity, the value of α at that cross-section becomes greater than unity. For an incompressible flow, the difference in static pressure at two locations is then given as

$$P_2 - P_1 = (\alpha_1 q_1 - \alpha_2 q_2) - (P_{T,1} - P_{T,2}) \qquad (2.12)$$

Using the already defined total pressure loss coefficient for the whole diffuser, the effectiveness can be expressed as

$$\epsilon = \frac{\alpha_1 \left(1 - \frac{\alpha_2}{\alpha_1} \frac{1}{AR^2} \right)}{C_{pi}} - \frac{H_L}{C_{pi}} \qquad (2.13)$$

The above equation shows that the effectiveness of diffusers is affected by the kinetic energy flux coefficient ratio and the total pressure loss. Any increase in the value of α represents a loss in pressure recovery availability. The insufficient diffusion and the losses due to viscosity effects reduce the effectiveness of the diffusers.

The effective area, A_E, of an internal flow system is defined as the area that would pass the particular flow rate if the velocity were uniform and equal to the maximum velocity in the cross section. The blocked area, A_B, is then equal to the difference between the geometric area, A, and the effective area . The effective and blocked area fractions are defined by the following equations :

$$E = \frac{A_E}{A} \leq 1 \tag{2.14a}$$

$$B = \frac{A_B}{A} \geq 0 \tag{2.14b}$$

$$E = 1 - B \tag{2.14c}$$

Expressing the volumetric flow rate through any cross section in terms of the mass averaged velocity and the maximum velocity in the cross section, the effective area fraction can be written as

$$E = \frac{V}{V_m} \tag{2.15}$$

After some manipulations of the equations derived so far and utilizing the loss coefficient along the stream line of maximum velocity, the effectiveness can be expressed by the following equation [15]:

$$\epsilon = \frac{1}{E_1^2} \left\{ 1 - \frac{(E_1/E_2)^2}{AR^2} \right\} \frac{1}{C_{pi}} - \frac{H_{Lm}}{C_{pi}} \tag{2.16}$$

Since the viscous effects in the core are very small, the velocity profile distortion term (the first term in the right-hand-side of the last equation) is the largest term in the above equation. That is, insufficient diffusion rather than the inefficient diffusion, is the main problem in diffusers. For instance, the main effect of separation is not a large increase in internal losses but in area blockage. Before the analysis of Sovran and Klomp, the total pressure loss term was thought to be the dominant factor affecting the performance of the diffusers. Figure 12 shows the effect of inlet boundary layer blockage on velocity profile parameter, E_2, of conical fiffusers operating near $C_p{}^*$. This curve can be used to find the effectiveness for optimum diffusers of two

dimensional, conical, or annular diffuser geometries with a potential core and turbulent boundary layers at the inlet with moderate blockage. The overall result of this analysis is that thickening of the inlet boundary layers reduces the pressure recovery of diffusers.

Stevens and Williams [12] also carried out tests with annular diffusers. They found that increasing the inlet boundary layer thickness degrades the performance until the value of B_1 reaches that of fully-developed pipe flow which is approximately .105. When fully developed conditions are reached, there is a significant rise in the pressure recovery. They have also shown that the correlation of Sovran and Klomp is quite consistent with their experimental results up to the fully developed conditions.

The above-mentioned investigations have shown that the state of the boundary layer at the inlet is very important for diffuser performance. In the absence of boundary layer control such as blowing fluid into the boundary layer or applying suction to remove the boundary layer, a thin boundary layer at the inlet is necessary to obtain high performance in a diffuser.

2.3.4. Mach Number Effects

The performance of a diffuser is affected by the Mach number. When the flow Mach number is higher than unity, shock boundary layer interaction may cause flow separation. The performance of the diffuser then degrades.

3. DETERMINATION OF MINIMUM HOOD SIZE

The following analysis has been developed by Prof. J. A. Owczarek of Lehigh University, for the experimental improvement study of LP turbine exhaust hoods [17]. The most important variables having dimensions of area and length are presented in Figure 13. These variables control the geometry and size of an exhaust hood. For the purpose of defining the geometry and relative hood size the following dimensionless parameters are utilized.

$$\frac{R_H}{L} = \frac{\text{last blade root radius}}{\text{last blade height (or annulus height)}}$$

$$\frac{H}{L} = \frac{\text{hood height}}{\text{last blade height}}$$

$$\frac{B}{L} = \frac{\text{hood length}}{\text{last blade height}}$$

$$\frac{D}{L} = \frac{\text{hood width}}{\text{last blade height}}$$

$$\frac{A}{B} = \frac{\text{annulus advance}}{\text{hood length}}$$

$$\frac{A_{CF}}{\frac{1}{2}A_{AN}} = \frac{\text{centerline flange open area}}{\frac{1}{2}(\text{annulus area})}$$

$$\frac{A_{FL}}{A_{AN}} = \frac{\text{condenser flange open area}}{\text{annulus area}}$$

$$\frac{A_{FL,EFF}}{A_{AN}} = \frac{\text{effective flange open area}}{\text{annulus area}}$$

Testing of all these parameters is a complex task and unnecessary since not all of these parameters are of equal importance. Furthermore, some of the parameters do not change from one design to another in large steam turbines. The value of R_H/L in steam turbines changes between 1.0 and 1.3. Similarly the ratio A/B is usually in the range of 0.3 to 0.5, and B/L varies from 4.0 to 4.6. Considering the exhaust hoods which are going to be tested in this study, the parameters R_H/L, B/L, and A/B are fixed and equal to 1.0, 4.4, and 0.5 respectively. The parameter D/L rather than B/L was chosen to be a variable because of the fact that for experimental and practical purposes, no change in the bearing cone and the guide vane is required when changing the parameter A_{FL}/A_{AN}. A change in B/L would require a change in the turbine bearing cone, which is not convenient.

With the help of Figure 13., the parameter $\frac{A_{FL}}{\frac{1}{2}A_{AN}}$ can be expressed as

$$\frac{A_{CF}}{\frac{1}{2}A_{AN}} \simeq \frac{\left(D - 2(L+R_H)\right) B}{\frac{1}{2}\pi(2R_H+L)\ L} = \frac{\left(\frac{D}{L} -2 - \frac{2R_H}{L} \right) \frac{B}{L}}{\frac{1}{2}\pi\left(\frac{2R_H}{L} + 1\right)} \qquad (3.1)$$

Once the fixed values are plugged into the equation (3.1), it becomes

$$\frac{A_{CF}}{\frac{1}{2}A_{AN}} \simeq 0.933\ \frac{D}{L} - 3.73 \qquad (3.2)$$

The significance of this parameter is that it indicates whether the flow from the upper half of the annulus can diffuse or not. When this parameter is less than 1.0, the flow can not diffuse. A large value of this parameter is desirable since the fluid from upper half of the annulus flows mainly through the centerline flange area near the front wall.

The parameter, A_{FL}/A_{AN}, can be written as

$$\frac{A_{FL}}{A_{AN}} = \frac{B\ D}{\pi(2R_H+L)\ L} = \frac{\frac{B}{L}\ \frac{D}{L}}{\pi\left(2\frac{R_H}{L}+1\right)} \tag{3.3}$$

When fixed values of parameters R_H/L and B/L are inserted into this equation it gives

$$\frac{A_{FL}}{A_{AN}} = 0.467\ \frac{D}{L} \tag{3.4}$$

It is important to note that the flange open area determined as (B*D) does not reflect the reality. The blockage due to the turbine cylinder, beams and struts makes this parameter much smaller than the value obtained from equation (3.4). The more realistic flange area ratio is expressed in the following form

$$\frac{A_{FL,EFF}}{A_{AN}} = \frac{D\ B-2(R_H+L)(A+L_v)}{\pi(2R_H+L)L} \tag{3.5}$$

In order to diffuse the flow further below the flange efficiently, turning vanes can be used. This would help the flow fill the condenser neck. Insufficient filling of the neck is a common problem in real applications. Another improvement resulting from the use of the vanes is the decrease in the sudden expansion losses. (There is a sudden

expansion section right below the flange.)

The generic exhaust hood model has variables D/L and H/L only. As will be discussed in later sections, the design allows testing of these variables for three different values of each parameter. Changes in the shape of bearing cone and of the guide vane are also possible to test. The effect of turning vanes on the performance of the turbine exhaust hood-condenser neck unit will also be determined in future tests.

4. EQUATIONS FOR LOSS COEFFICIENTS AND METHODOLOGY

A sketch of a low pressure turbine exhaust hood is given in Figure 14. The thermodynamic states of the fluid at the exit from the last row of rotor blades and in the exhaust hood were previously given in Figure 2. This diagram shows the states of an expanding exhaust hood meaning that the annulus pressure, P_{AN} is higher than the condenser flange pressure, P_{FL}. The following derivation has been developed for improvement study of Indian Point Unit No. 2 exhaust hood [2].

The leaving loss can be expressed as

$$LL = \frac{V_{AN}^2}{2} = h_{T,AN} - h_{AN} \tag{4.1}$$

The working fluid in this study is air and we can assume it to behave like an ideal gas. Therefore, using the ideal gas equation, the leaving loss can be introduced in the following form

$$LL = C_p\, T_{T,AN}\left(1 - \frac{T_{AN}}{T_{T,AN}}\right) = C_p\, T_{T,AN}\left\{1 - \left(\frac{P_{AN}}{P_{T,AN}}\right)^{\frac{\gamma-1}{\gamma}}\right\} \tag{4.2}$$

Note that the specific heats are assumed to be constant. This assumption is valid due to low temperature difference between the total and static conditions, the difference being around 60°F. The hood loss corresponds to the enthalpy difference between the states 1 and $2'$ shown in Figure 2. Hence,

$$HL = h_1 - h_2' = (h_{T,AN} - h_2') - (h_{T,AN} - h_1) = (h_{T,AN} - h_2') - LL \quad (4.3)$$

since $h_1 = h_{AN}$.

The dimensionless hood loss coefficient, HL/LL, is defined as the ratio of the hood loss to the leaving loss. Similarly, the dimensionless hood and condenser loss coefficient, (H+C)L/LL, is the ratio of the hood and condenser neck losses to the leaving loss. For an ideal gas having constant specific heats, the hood loss coefficient can be expressed in form of equation

$$\frac{HL}{LL} = \frac{(h_{T,AN} - h_2') - LL}{LL} = \frac{C_p T_{T,AN}\left(1 - \frac{T_2'}{T_{T,AN}}\right)}{C_p T_{T,AN}\left\{1 - \left(\frac{P_{AN}}{P_{T,AN}}\right)^{\frac{\gamma-1}{\gamma}}\right\}} - 1$$

$$= \frac{1 - \left(\frac{P_{FL}}{P_{T,AN}}\right)^{\frac{\gamma-1}{\gamma}}}{1 - \left(\frac{P_{AN}}{P_{T,AN}}\right)^{\frac{\gamma-1}{\gamma}}} - 1$$

$$= \frac{\left(\frac{P_{AN}}{P_{T,AN}}\right)^{\frac{\gamma-1}{\gamma}} - \left(\frac{P_{FL}}{P_{T,AN}}\right)^{\frac{\gamma-1}{\gamma}}}{1 - \left(\frac{P_{AN}}{P_{T,AN}}\right)^{\frac{\gamma-1}{\gamma}}} \quad (4.4)$$

For an isentropic process, P/ρ^{γ} is constant, then

$$\frac{P}{P_T} = \left(\frac{\rho}{\rho_T} \right)^{\gamma} \tag{4.5}$$

But for a perfect gas $\frac{P}{(\rho T)} = \frac{P_T}{(\rho_T T_T)} = R$, therefore,

$$\frac{P_T}{P} = \left(\frac{T_T}{T} \right)^{\frac{\gamma}{\gamma-1}} \tag{4.6}$$

By combining equations (4.5) and (4.6) and remembering that speed of sound is equivalent to $\sqrt{\gamma RT}$, the ratio of static to total pressure can now be written as

$$\frac{P}{P_{T,AN}} = \left\{ \frac{1}{1 + \frac{\gamma-1}{2} M_{AN}^2} \right\}^{\frac{\gamma}{\gamma-1}} \tag{4.7}$$

Therefore, the common term in the numerator and denominator of equation (4.4) can be expressed in term of Mach number as follows

$$\left(\frac{P_{AN}}{P_{T,AN}} \right)^{\frac{\gamma-1}{\gamma}} = \frac{1}{1 + \frac{\gamma-1}{2} M_{AN}^2} \tag{4.8}$$

This term is only a function of annulus Mach number as the ratio of specific

heats, γ is constant. The ratio, $P_{FL}/P_{T,AN}$, will be determined from the air model tests for varying flow rates and annulus Mach numbers. The Reynolds and Mach numbers affect this ratio. However, the value of the Reynolds number in the air test is quite close to that in the steam turbines whose exhaust hoods are being modeled. For a typical turbine unit modeled, the Reynolds number based on the annulus exit speed and the last blade height at M_{AN}=0.75, is 1.01×10^6 for steam and 0.75×10^6 for the air model (see Appendix C). As a result, the ratio, $P_{FL}/P_{T,AN}$, becomes only a function of M_{AN}. Therefore, the whole hood loss coefficient becomes,

$$\frac{HL}{LL} = f_1(M_{AN}) \tag{4.9}$$

The terms $\left(\frac{P_{FL}}{P_{T,AN}}\right)^{\frac{\gamma-1}{\gamma}}$ and $\left(\frac{P_{AN}}{P_{T,AN}}\right)^{\frac{\gamma-1}{\gamma}}$ can be plotted against annulus Mach number, M_{AN}. The first term is obtained from the air tests and the second term is from relation (4.8). Referring to Figure 15, the hood loss is represented by the ratio

$$\frac{HL}{LL} = \frac{C}{D} \tag{4.10}$$

where $C = \left(\frac{P_{AN}}{P_{T,AN}}\right)^{\frac{\gamma-1}{\gamma}} - \left(\frac{P_{FL}}{P_{T,AN}}\right)^{\frac{\gamma-1}{\gamma}}$ and $D = 1 - \left(\frac{P_{AN}}{P_{T,AN}}\right)^{\frac{\gamma-1}{\gamma}}$, in view of equation (4.4).

The pressures and temperatures used in the above equations represent the average values obtained from the measurements. In the tests, the mass flow rate, W, will be measured using an ASME Standard flow nozzle or a venturi meter. In order to

use the Air Tables, we need to derive nondimensional mass flow equation. Equations (4.6) and (4.8) implies that

$$\frac{T_{T,AN}}{T_{AN}} = 1 + \frac{\gamma-1}{2} M_{AN}^2 \tag{4.11}$$

Utilizing the continuity equation for one dimensional flow, definition of Mach number and the above equation, we get

$$\frac{W}{A_{AN}} = \left(\frac{\gamma}{RT_{T,AN}} \right)^{1/2} P_{AN} M_{AN} \left(1 + \frac{\gamma-1}{2} M_{AN}^2 \right)^{1/2} \tag{4.12}$$

The annulus static pressure from the above equation can be eliminated with the help of equation (4.8), that is

$$\frac{W}{A_{AN}} = \left(\frac{\gamma}{RT_{T,AN}} \right)^{1/2} P_{T,AN} M_{AN} \left(1 + \frac{\gamma-1}{2} M_{AN}^2 \right)^{-\frac{\gamma+1}{2(\gamma-1)}} \tag{4.13}$$

or in dimensionless form,

$$\frac{W\sqrt{RT_{T,AN}}}{A_{AN} P_{T,AN}} = \sqrt{\gamma} M_{AN} \left(1 + \frac{\gamma-1}{2} M_{AN}^2 \right)^{\frac{\gamma+1}{2(\gamma-1)}} \tag{4.14}$$

which is listed in Gas Tables [18].

In order to ensure an accurate measurement of total pressure $P_{T,AN}$, tests will be run with the exhaust hood annulus without a hood as shown in Figure 16. The value of P_{AN} will be determined from the measured flow rates using equation (4.14), then the term

$$\left(\frac{P_{AN}}{P_{T,AN}}\right)^{\frac{\gamma-1}{\gamma}}$$

will be determined. The result will be compared to the values obtained from equation (4.8) in Figure 15. A good agreement between these values represents reliable total pressure measurements.

The equations derived so far will also used to obtain the hood and condenser loss coefficient, (H+C)L/LL, as a function of annulus Mach number. Static pressure measurements will made in 12 locations in the model on the shroud and hub of the annulus. This will be done to get the magnitude of last blade excitation which is a consequence of circumferential pressure variation in the annulus. The pressures will be nondimensionalized to form a pressure coefficient:

$$C_{P,LOCAL} = \frac{P_{AN,LOCAL} - P_{FL}}{\left(\rho\frac{V^2}{2}\right)_{AN}} \tag{4.15}$$

Because of the tendency of the fluid to flow around the hub, and the shape of the diffuser vane, the constant Mach number lines in the annulus followed by a diffuser are not straight radial lines but are curved. Therefore, the average static pressure in the last stage annulus, P_{AN} is not the same as the average of the local static pressures measured on the shroud and hub, $(P_{AN,LOCAL})_{AVE}$. Using the proper annulus static pressure, P_{AN}, in equation (4.15) the pressure coefficient becomes,

$$C_P = \frac{P_{AN} - P_{FL}}{\left(\rho \frac{V^2}{2}\right)_{AN}} \tag{4.16}$$

whose value is much higher than that of $C_{P,LOCAL}$. The isentropic relation, $Tds = dh - \frac{dP}{\rho} = 0$, states that

$$\frac{P_{AN} - P_{FL}}{\rho_{AN}^{FL}} = h_{AN} - h_{FL} = h_1 - h_2' = HL \tag{4.17}$$

where ρ_{AN}^{FL} is the average fluid density between annulus exit and flange of the hood. Therefore, the value of the pressure coefficient is close to the hood loss coefficient. The average annulus static pressure, P_{AN}, which is to be used in equation (4.16) should be determined from the relation

$$\frac{W\sqrt{RT_{T,AN}}}{A_{AN}\, P_{T,AN}} = \sqrt{\gamma}\, M_{AN} \left(1 + \frac{\gamma - 1}{2} M_{AN}^2\right)^{\frac{\gamma+1}{2(\gamma-1)}} = f_2\left(\frac{P_{AN}}{P_{T,AN}}\right) \tag{4.18}$$

since $M_{AN} = f_3\left(\frac{P_{AN}}{P_{T,AN}}\right)$ as given in equation (4.8). The mass flow rate, W, the total temperature of the air, $T_{T,AN}$, and the total pressure, $P_{T,AN}$, entering the above equation are measured quantities in the exhaust hood model.

Based on the equations derived up to this point, the experimental procedure for the determination of exhaust hood loss coefficient, HL/LL or exhaust hood and condenser neck loss coefficient, (H+C)L/LL, is given below :

- The model air mass flow rate, W is measured from a flow nozzle.
- The total temperature, $T_{T,AN}$ is measured upstream of the screen.
- The total pressure downstream of the annulus screen is determined by several traverses.
- The total pressure measurements are area averaged to get a good estimate of $P_{T,AN}$.
- Exit flange static pressure, P_{FL}, is measured.
- From the values of $P_{T,AN}$, $T_{T,AN}$, area A, and W the nondimensional mass flow rate can be computed, i.e.,

$$\frac{W\sqrt{RT_{T,AN}}}{A_{AN}\,P_{T,AN}}$$

- The average annulus Mach number and the pressure ratio, $\frac{P_{AN}}{P_{T,AN}}$ can be determined entering the nondimensional mass flow rate in the Air Tables.

- From the experimentally determined values of $P_{T,AN}$, P_{FL}, $P_{AN}/P_{T,AN}$ and W, the hood loss coefficient is computed as a function of Mach number, M_{AN}.

5. AIR TEST LOOP AND MODEL DESIGNS

5.1 Air Test Loop

A schematic of the air test loop is given in Figure 17. The test loop contains a compressor providing 10,000 scfm at 12.5 psig maximum. It is driven by a three phase electric motor which has a capacity of 800 HP at 3600 rpm. The blower is equipped with an inlet filter, inlet and discharge silencers and an aftercooler. The aftercooler will cool the air, exiting the compressor at about 250 °F, to 100 °F.

Before the air flows into an ASME standard venturi meter, there is a flow straightener 36 inches long. The length of the straightener was determined according to ASME recommendation [19]. The venturi meter has a diameter ratio of 0.524. A manometer is used to measure the static pressure difference between the inlet and throat of the venturi. Figure 18 indicates the variation of pressure difference between these two locations as a function of the ratio of the inlet pressure to atmospheric pressure. The procedure to compute the pressure difference in inches of water is given in Appendix A. The necessary height of the manometer columns which are filled with water, is determined to be at least 35 inches for a range of flow rates from 5,000 to 12,000 scfm.

Special attention has been given to ensure a uniform flow at the inlet to the model. After the flow turns 90° via a large radius elbow, as shown in Figure 17, it enters a diffuser which has an area ratio of 1.78. The diameter of the pipe is increased to 2 feet from 1.5 feet in order to have a large diameter at the inlet to the test stand. This way the flow speed in the test stand is kept very low, and the loop can conveniently be used

for other applications. The upward 90° turn is accomplished with a special elbow. Elevation view of this elbow is given in Drawing No. F-3. The turning vanes used in this elbow are designed in such a way that the flow at the exit flange is uniform. The number of vanes is determined according to reference 20. Drawing No. F-2 gives the geometry of these vanes. The pressure drop in the elbow was estimated to be 0.034 psi.

A contraction duct leading from the test stand to the model was designed to meet the inlet flow requirements of the exhaust hood models. A contraction ratio of 15 was achieved along a length of 19.3 inches. The contraction will be cast, together with the flanges at the inlet and exit sections as indicated in Drawing No. F-4. The design procedure of the contraction [21,22], is explained in Appendix B.

5.2. Generic Model Design

The design of the generic exhaust hood as well as other two existing hood models was based on similarity parameters of geometry, Mach number and Reynolds number. The annulus height is the characteristic length in the design of exhaust hood model. Both Mach and Reynolds numbers are based on this length.

An iterative procedure was followed to determine the model annulus height within the constraints of the annulus Mach number and the available pressure head of the compressor. The upper limit of Mach number in the annulus was set to be 0.8. For a given Mach number, starting from the upper limit, the required total pressure in the annulus was determined. The next step was to determine the maximum volumetric flow rate possible for this pressure requirement using the compressor performance curve

which was supplied by the vendor. Then the annulus height was determined for that maximum volume flow rate. As a result of these iterations, maximum attainable annulus Mach number was determined to be 0.75. The model annulus height was determined to be 1.5 inches. The calculations are given in Appendix C. The Reynolds numbers in the model and in a typical turbine unit are also compared in the appendix. The Reynolds number calculation for the actual unit was based on the data supplied by utility [2]. The Reynolds numbers in the air test model and in the steam turbine exhaust hood are quite close to each other.

The generic exhaust hood model is designed to allow testing at three different values of both B/L and H/L ratios, as mentioned in section 3 earlier. The values of these ratios were set considering the turbine units whose exhaust hoods are going to be tested and the common turbine units operating presently. Table 1 shows the characteristic dimensions of the model. Model drawings are given in Appendix G. As shown in the elevation view of the model (Drawing No. G-1A), the design includes the bearing cone, the turbine outer and inner shells, the annulus hub, the annulus screen, the guide vane and the outlet duct. Drawing No. G-1B shows that the exhaust hood height, H and the width, D are going to be changed with the use of several wooden inserts. The drawings indicate the locations of static and total pressure measurement locations. At five angular positions total pressure measurements will be taken using $1/8''$ diameter probes. With the given configuration of total pressure probes, it is possible to get pressure measurements at every 30° in the annulus, because two of the probes can pass through the hub. The numbers next to traverse locations in Drawing No. G-1B represent the sequence of pressure measurements.

Table 1. Characteristic Dimensionless Lengths for Generic Model

R_H/L	1.0		
B/L	4.4		
A/B	0.5		
L_v/L	0.75		
H/L	3.0	3.4	3.8
D/L	7.0	7.5	8.15
$\frac{A_{CF}}{1/2\ A_{AN}}=\frac{\left(D-2(L+R_H)\right)B}{\frac{1}{2}\pi(2R_H+L)L}$	2.8	3.27	3.87
$\frac{A_{FL}}{A_{AN}}=\frac{D\ B}{\pi(2R_H+L)L}$	3.27	3.5	3.81
$\frac{A_{FL,EFF}}{A_{AN}}=\frac{D\ B-2(R_H+L)(A+L_v)}{\pi(2R_H+L)L}$	2.12	2.36	2.66

Just downstream of the total pressure probes static pressure holes of $1/32''$ diameter are located at 12 angular positions at the hub and the shroud of the annulus as shown in the Drawing No. G-2. Tygon tubing is used to connect the static pressure taps to manometer banks or to pressure transducers.

Air from the compressor flows over the elliptical bullet nosed center body into the exhaust hood model. A screen is placed $1.0''$ upstream of the total pressure probes to provide a circumferentially uniform flow in the model annulus. The solidity of the screen was chosen to be 10%. The solidity of a screen is defined to be the ratio of the total projected screen wire area to the total cross-sectional area. Tests without the use of a screen would indicate a biased pressure recovery since the major portion of the mass

flow would then bypass the upper half of the hood model. The details of screen solidity selection is given in Appendix D. A round-wire-screen having a solidity of 10% produces a choked flow in the screen when the inlet Mach number is equal or greater than 0.65 [23]. Therefore, tests at Mach numbers greater than 0.65 will be run without a screen.

Special attention has been focused on the elimination of leakage. For that reason the design of the hood model was kept as simple as possible. O-ring seals were used at several locations to stop possible leakage.

In order to determine the leaving loss, LL, entering the low pressure turbine exhaust hood, an open annulus assembly was designed. The assembly drawing of the open annulus assembly has also been included in Appendix G. The open assembly will also be used to calibrate the total pressure probes.

5.3. Hatfield Ferry and Beaver Valley Unit Models

Exhaust end models for Beaver Valley and Hatfield Ferry Units were designed utilizing the information supplied by the Allegheny Power Company and the Duquesne Lights Corporation. Plant visits to these stations were also made in order to measure various dimensions and to look for the evidence of flow separation at critical locations such as the flow guide vane at the annulus exit. Photographs taken during the plant visits provided information about the flow field in the condenser necks of these units. The characteristic dimensionless parameters for both units are listed in Table 2. These parameters are the main geometrical variables used in modeling of the actual units.

The generic model is designed in such a way that addition of struts and other support structures, and change of a few of the model parts results in the turbine exhaust end models for the Beaver Valley and Hatfield Ferry Units. For both exhaust end models, only the guide vane, the bearing cone, the back plate and the outlet duct need to be changed. The other model parts are the same as in the generic model. All of the pressure measurement locations except the ones at the exhaust flange are taken at the same locations as in the generic model. The detail drawings of the model design for the Beaver Valley Unit is provided in Appendix I. Condenser neck drawings for the Hatfield Ferry Unit are presented in Appendix H.

The condenser neck models are designed to be attached to the hood model as one piece. The struts and support beams are grouped and each group of these members are screwed into either the body or the outer shell piece.

Diffuser geometry parameters for all of the air models are given in Table 3 with reference to Figures 4, 5 and 7. The table also lists the approximate expected ranges of pressure recovery coefficients of the diffusers.

Table 2. Characteristic Dimensionless Lengths for Hatfield Ferry & Beaver Valley Units

	Hatfield Ferry Unit	Beaver Valley Unit
R_H/L	1.0	1.0
B/L	4.64	4.0
A/B	0.51	0.45
L_v/L	0.77	0.56
H/L	3.8	3.1
D/L	8.13	7.5
$\frac{A_{CF}}{1/2\ A_{AN}} = \frac{\left(D-2(L+R_H)\right)B}{\frac{1}{2}\pi(2R_H+L)L}$	4.07	3.16
$\frac{A_{FL}}{A_{AN}} = \frac{D\ B}{\pi(2R_H+L)L}$	4.00	3.3
$\frac{A_{FL,EFF}}{A_{AN}} = \frac{D\ B-2(R_H+L)(A+L_v)}{\pi(2R_H+L)L}$	2.67	2.38

Table 3. Diffuser Dimensions and Approximate C_p values for air models

	Generic Model	Beaver Valley Unit	Hatfield Ferry Unit
$R_{T,1}$(in)	3.0	3.0	3.0
$R_{H,1}$(in)	1.5	1.5	1.5
ΔR_1(in)	1.5	1.5	1.5
β (deg.)	30	37	55
W(in)	1.73	1.75	1.48
$\overline{L}$(in)	1.1	2.25	2.2
$A_1(in^2)$	21.2	21.2	21.2
$A_2(in^2)$	29.1	30.8	30.5
AR	1.37	1.45	1.44
$\overline{L}/\Delta R_1$	0.73	1.45	1.46
C_p	< 0.2	0.1−0.3	0.1−0.3

6. CONCLUSIONS

A methodology for the testing of turbine exhaust ends has been established. Variation of hood loss coefficient or hood and condenser neck loss coefficient with the annulus Mach number can be determined using equations derived. The results from the tests on the generic model should be applicable to turbines having different geometries. The tests will serve as the basis for qualitative understanding of the flow field and parameters affecting the performance of the hood.

The effects on the performance of Beaver Valley and Hatfield Ferry units of changing the guide vanes, addition of splitter vanes, and using turning vanes will be determined. Modifications of internal structures like the struts or beams can also be considered as a source of improvement of the performance. Strengthening the hood outside instead of putting all the reinforcing members inside the turbine exhaust casing should appreciably increase performance. This is especially true for the Beaver Valley Unit.

It appears that the annular diffuser sections of both units are operating inefficiently. Based on photographs, there seems to be a flow separation from the guide vane of Hatfield Ferry Unit. It is possible to eliminate this problem by using a shorter guide vane. Another problem common to both Hatfield Ferry and Beaver Valley units is poor flow distribution in the condenser neck. This is concluded from the photographs of the units. Addition of splitter vanes should be considered in order to improve the flow distribution there.

APPENDIX A—Determination of Manometer Column Height

The inlet and throat diameters of the venturi meter used in the test loop are 17.25 and 9.1 inches, respectively. Denoting the inlet and throat states with the subscripts i and t, we can write the Bernoulli equation as

$$\frac{P_i}{\rho_i} + \frac{V_i^2}{2} = \frac{P_t}{\rho_t} + \frac{V_t^2}{2} \tag{A-1}$$

Assuming that $\rho_i \approx \rho_t = \rho$, the continuity equation for a uniform flow gives

$$V_t = \frac{1}{\beta^2} V_i \tag{A-2}$$

where β is the diameter ratio, D_t/D_i. Combining the above two equations, the following equation is obtained.

$$\frac{P_i - P_t}{\rho} = \frac{\Delta P}{\rho} = \frac{V_i^2}{2}\left(\frac{1}{\beta^4} - 1\right) \tag{A-3}$$

In order to get the pressure difference in inches of water, the above equation can further be manipulated to yield

$$\frac{\Delta P}{S_w} = \frac{6\ S_{air} V_i^2}{g\ S_w}\left(\frac{1}{\beta^4} - 1\right) \tag{A-4}$$

where symbol S_w stands for specific weight of water. S_w is constant and equal to 62.3 lbf/ft^3. In order to obtain the pressure ratio difference as a function of the flow rate (in scfm) of the compressor, the inlet speed to the venturi meter is factored in as follows:

$$V_i=\left(\frac{P_{ATM}}{P_i}\,\frac{T_i}{T_{ATM}}\right)V_{ATM}\simeq\left(\frac{P_{ATM}}{P_i}\,\frac{T_i}{T_{ATM}}\right)\frac{Q}{A_i} \qquad \text{(A-5)}$$

Assuming that the ratio, T_i/T_{ATM} is about unity and introducing the numerical values $g=32.174$ ft/sec^2, $A_i=1.767$ ft^2, $T_{ATM}=100$ °F, $P_{ATM}=14.4$ lbf/ft^2 and $\beta=0.524$, we get the following equation.

$$\frac{\triangle P}{S_w}= 2.63X10^{-7}\,Q^2\left(\frac{P_{ATM}}{P_i}\right) \qquad \text{(A-6)}$$

The pressure difference from equation (A-6) is obtained in inches of water when Q is entered in scfm.

APPENDIX B—Contraction Duct Design Procedure

The most important parameter in the design of a contraction duct is the area contraction ratio, CR. Once the value of CR is fixed, the contour and the contraction length can be determined based on design considerations which are the exit flow uniformity, avoidance of flow separation, exit boundary layer thickness, and space and cost. Figure B-1 shows the geometric design parameters for a contraction duct. The design parameters are the length, the wall shape and the Reynolds number. The procedure followed here [21], is aimed at the avoidance of separation and at producing an exit velocity profile with prescribed nonuniformity defined as

$$\bar{u}_2 = (V - V_c)_2 / V_{2,\infty} \tag{B-1}$$

where V_c is the centerline velocity and $V_{2,\infty}$ is the velocity further downstream of contraction. For the cubic family of wall shapes, the designer needs to know about the two wall-pressure coefficients defined as

$$C_{p,e} = 1 - (U_{2,\infty}/V_e)^2 \tag{B-2}$$

$$C_{p,i} = 1 - (V_i/U_{1,\infty})^2 \tag{B-3}$$

where subscripts e and i refer to the point of maximum and minimum wall velocities. For a separation free flow, based on the Stanford's separation criterion, $C_{p,i}$, must be less than 0.5. Exit velocity nonuniformity, $\bar{u}_2$, is found to be a function of $C_{p,e}$ for values of $C_{p,e}$ less or equal to 0.2. The relation between $\bar{u}_2$ and $C_{p,e}$ is given as

$$\overline{u}_2 \approx 0.35 C_{p,e} \tag{B-4}$$

Talapurkara and Bhalla [22] investigated Morel's method for wind tunnel contractions and they suggest that the values 0.06 and 0.39 for $C_{p,e}$ and $C_{p,i}$ be used. This will ensure that the velocity nonuniformity at the exit is not more than 2%, and will also ensure a separation-free flow throughout the contraction. They experimentally found out that the velocity nonuniformity is actually about 50% less than the presumed value which is 2% from equation (B-4). Morel points out that the exit velocity nonuniformity after the exit plane is reduced to about 10% in a straight section with a length of $0.3D_2$ at the exit of the duct.

For cubic family of wall shapes, the contour of the contraction is determined with the following two equations after the distances X and L, shown in Figure B-1, have been determined. Derivation of the following equations are given in reference [21].

$$\frac{D-D_2}{D_1-D_2} = 1 - \frac{1}{X^2}\left(\frac{x}{L}\right)^3 \qquad \frac{x}{L} \le X \text{ or } x \le x_m \tag{B-5}$$

$$\frac{D-D_2}{D_1-D_2} = \frac{1}{(1-X)^2}\left(1-\frac{x}{L}\right)^3 \qquad \frac{x}{L} > X \text{ or } x > x_m \tag{B-6}$$

X and L are computed using the diagrams given in Morel's paper, the following equations.

$$X^{1/2}(1-X)^{-2/3} = \zeta\, m^{1/2}(m-1) \tag{B-7}$$

$$\zeta = F_e^{1/3} G_i^{-1/2} \tag{B-8}$$

$$G_i = \frac{m-1}{m} \frac{1}{X} \sqrt{\frac{D_1}{L}} \tag{B-9}$$

where F_e, G_i and ζ are some convenient dimensionless parameters utilized in the design procedure, and the parameter m is the ratio of inlet to outlet diameters, D_1/D_2. For $C_{p,e}=0.06$ and $C_{p,i}=.39$, the values of F_e and G_i are determined from the charts to be 0.51 and 2.0 respectively. Subsequently, from equation (B-8), ζ becomes 0.564. The inlet and outlet diameter of the contraction are $23.25''$ and $6''$. Therefore the implicit equation (B-7) can be solved with these values. The solution gives $X=0.57$. From equation (B-9) the length of the contraction, L, is found to be $18.76''$. A straight section of length $0.5''$ has been added at the inlet to decrease the effects of possible velocity nonuniformity as a result of the upstream elbow.

APPENDIX C—Determination of Model Annulus Height

The following calculations are for the upper limit of the annulus Mach number, $M_{AN}=0.75$. Entering the Gas Tables for $\gamma=1.4$ with this Mach number, we find

$$\left(\frac{P}{P_T}\right)_{AN}=0.6886 \quad \left(\frac{T}{T_T}\right)_{AN}=0.8989 \quad \frac{W\sqrt{R\,T_{T,AN}}}{A_{AN}P_{T,AN}}=0.6465 \quad \left(\frac{\rho V^2}{2P_T}\right)_{AN}=0.2711$$

If we assume that the model inlet air temperature is 90 °F, then

$$T_{AN}=.8989*550=494.4\ ^\circ R$$

$$a_{AN}=\sqrt{\gamma R T_{AN}}=\sqrt{1.4*53.35*494.4*32.176}=1090\ \text{ft/sec}$$

$$V_{AN}=M_{AN}\,a_{AN}=0.75*1090=817.5\ \text{ft/sec}$$

For $P_{ATM}=14.7$ psia and assuming the value of loss coefficient, $(H+C)L/LL=0.5$ where

$$LL=\frac{\rho V^2}{2},$$

$$P_{AN}=P_{ATM}+\frac{1}{2}\left(\frac{\rho V^2}{2}\right)_{AN}=14.7+.5(0.2711)P_{T,AN}=0.6886\ P_{T,AN}$$

As a result, total annulus pressure can be found

$$P_{T,AN}=\frac{14.7}{0.6886-0.5\ (0.2711)}=26.58\ \text{psia}\ (11.88\ \text{psig})$$

and $P_{AN}=0.6886*26.58=18.30$ psia (3.60 psig).

The above calculations indicates that we should be able to obtain a total annulus pressure of 11.88 psig. If the ratio of the hub radius to the annulus height, R_H/L is equal to unity, then

$$\frac{R_T}{R_H}=\frac{R_H+L}{R_H}=1+\frac{L}{R_H}=2, \text{ and}$$

$$A_{AN}=\pi {R_H}^2\left(\left(\frac{R_T}{R_H}\right)^2-1\right)=3\pi {R_H}^2$$

Using the dimensionless mass flow ratio determined from Air Tables,

$$\frac{W}{A_{AN}}=0.6445\ \frac{P_{T,AN}}{\sqrt{RT_{T,AN}}}=0.6445\ \frac{26.58*32.176}{\sqrt{53.35*550*32.176}}=0.5672\ \text{lbm/in}^2\text{. sec}$$

The density of air at standard atmospheric conditions (14.7 psia, 60 °F), ρ_{ATM} is 0.07628 lbm/ft^3. As a result,

$$\frac{Q_{ATM}}{A_{AN}}=\left(\frac{W}{A_{AN}}\right)\frac{1}{\rho_{ATM}}=\frac{0.5672}{0.07628}*60=446.146\ \text{scfm/in}^2$$

For Q=11,000 scfm, $A_{AN}=\frac{11,000}{446.146}=24.655\ \text{in}^2=3\pi {R_H}^2$, therefore $R_H=1.617$ in. As can be seen from Figure C-1, at Q=11, 000 scfm it will be possible to get annulus total pressure of 11.88 psig. To be on the safe side with the volume flow rate and the Mach number in the annulus, R_H was chosen to be 1.5 in.

The Reynolds number, Re_L, for a typical turbine unit with an exhaust annulus pressure 1.5 in.Hg (0.743 psia) and temperature of 100°F, and with an average annulus steam velocity of 900 ft/sec is:

$$Re_L)_{steam} = \frac{V_{AN}L}{\nu} = \frac{900*45/12}{0.0034} = 1.01x10^6$$

The Reynolds number for the air model for T_{AN}=90°F and M_{AN}=0.75 is:

$$Re_L)_{air} = \frac{\rho V_{AN}L}{\mu} = \frac{0.0898*817.5*1.5/12}{3.8x10^{-7}*32.174} = 7.5x10^5$$

where $\rho = P_{AN}/RT_{AN}$. The difference between the two Reynolds numbers is relatively small.

APPENDIX D—Selection of Screen Solidity

The highest Mach number in the annulus is expected to be 0.75 as was determined in Appendix C. From Figure D-1(b), it can be seen that at M_{AN}=0.65, the flow is choked at 10% screen solidity which is denoted by the symbol S. Therefore, tests requiring annulus Mach numbers greater than 0.65 will be run without a screen.

At M=0.65, $\left(\frac{T}{T_{AN}}\right)_{AN}$ is found to be 0.9221 from Air Tables. Assuming that $T_{T,AN}$=60 °F,

T_{AN}=479.5 °R

a=1073.5 ft/sec

V_{AN}=697.75 ft/sec

The screen pressure loss coefficient, λ at this choked flow conditions is found to be 0.4 from Figure D-1.

$$\lambda=\frac{\Delta P_T}{\frac{1}{2}\rho V_1^{\,2}}=0.4=\frac{\Delta P}{\frac{1}{2}\rho V_1^{\,2}}$$

since the change in the velocity across a screen is small. The ratio, HL/LL is expected to be less than 0.65. Therefore, 10% solidity screen should produce a pressure loss not much lower than the hood loss. For that reason, the air flow in the annulus after the screen should be quite uniform circumferentially.

The screen wire diameter is selected to be 0.009 inches. For this wire diameter, the Reynolds number is given as [23]

$$\mathrm{Re}=\frac{V_1 d}{(1-S)\nu_1}=\frac{697.75*0.009}{(1-0.10)\ 1.5\mathrm{x}10^{-4}(12)}=3875$$

(kinematic density of air at 60 °F is $1.5\mathrm{x}10^{-4}$ $ft^2/sec.$)

APPENDIX E–Figures

The figures given in this section have either been created by the author or adapted from the references indicated in square brackets.

LIST OF FIGURES

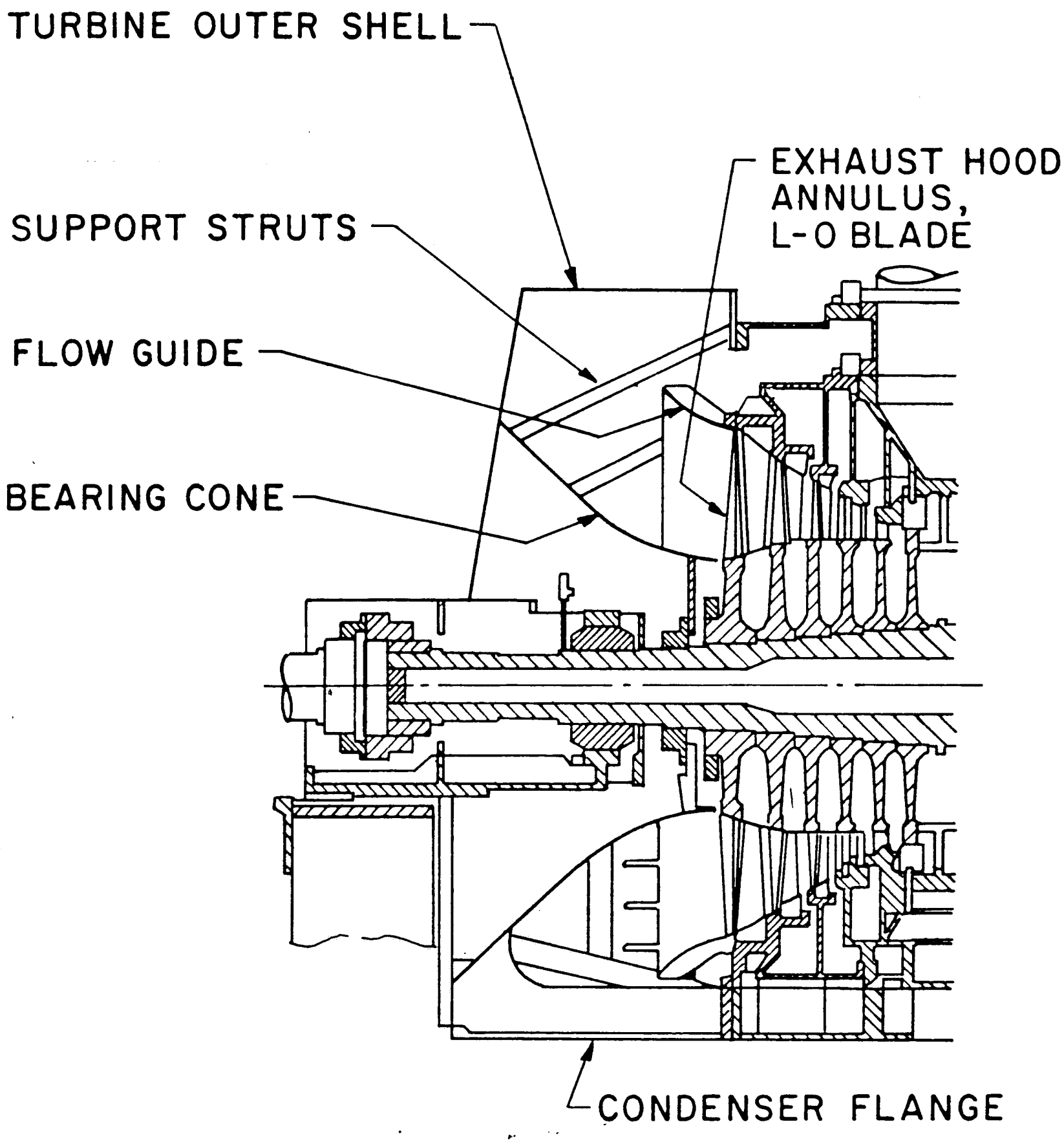

Figure 1. Schematic of a typical steam turbine exhaust hood [2]

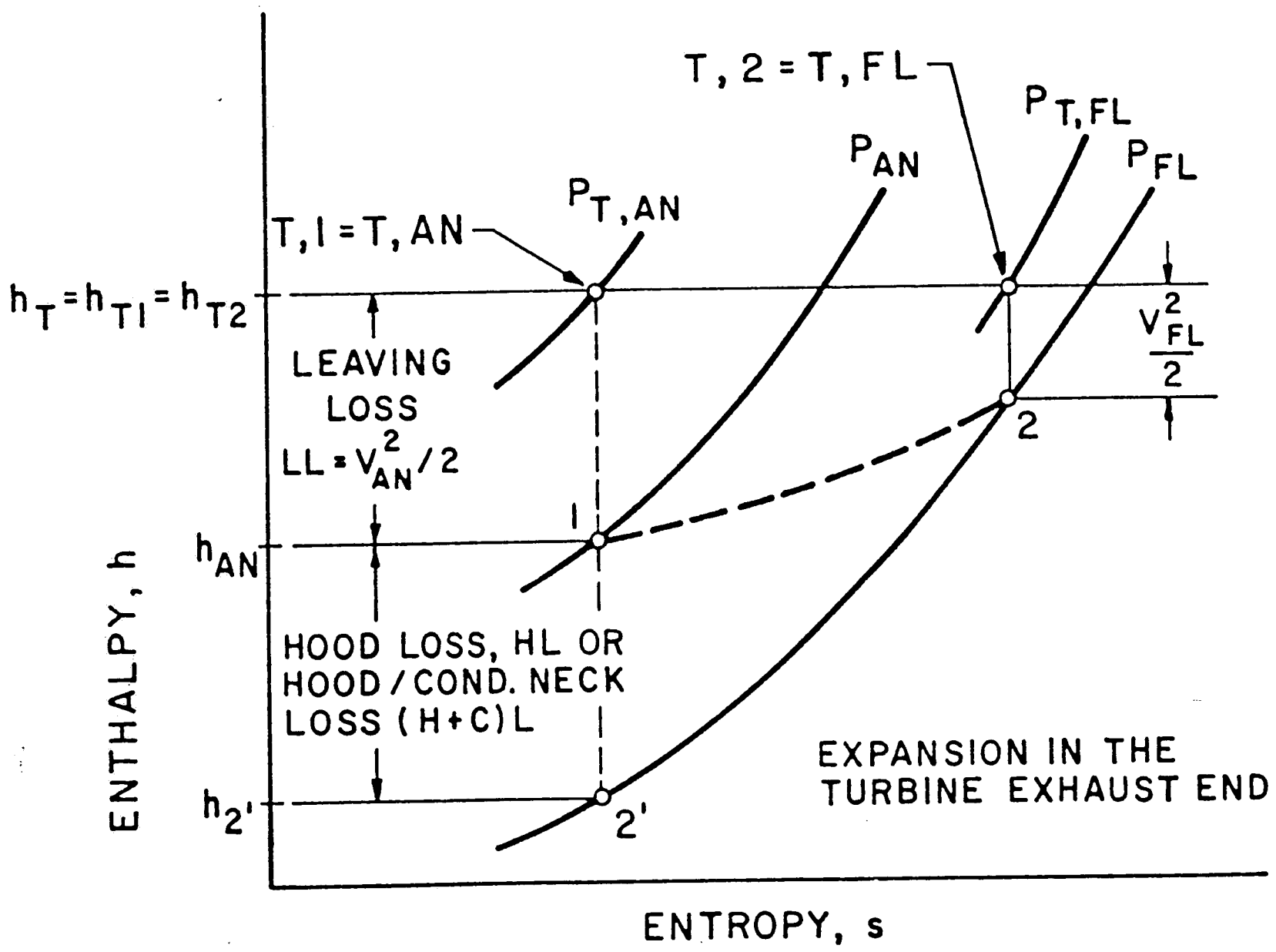

Figure 2. Thermodynamic states for an expanding exhaust hood ($P_{AN} > P_{FL}$) [2]

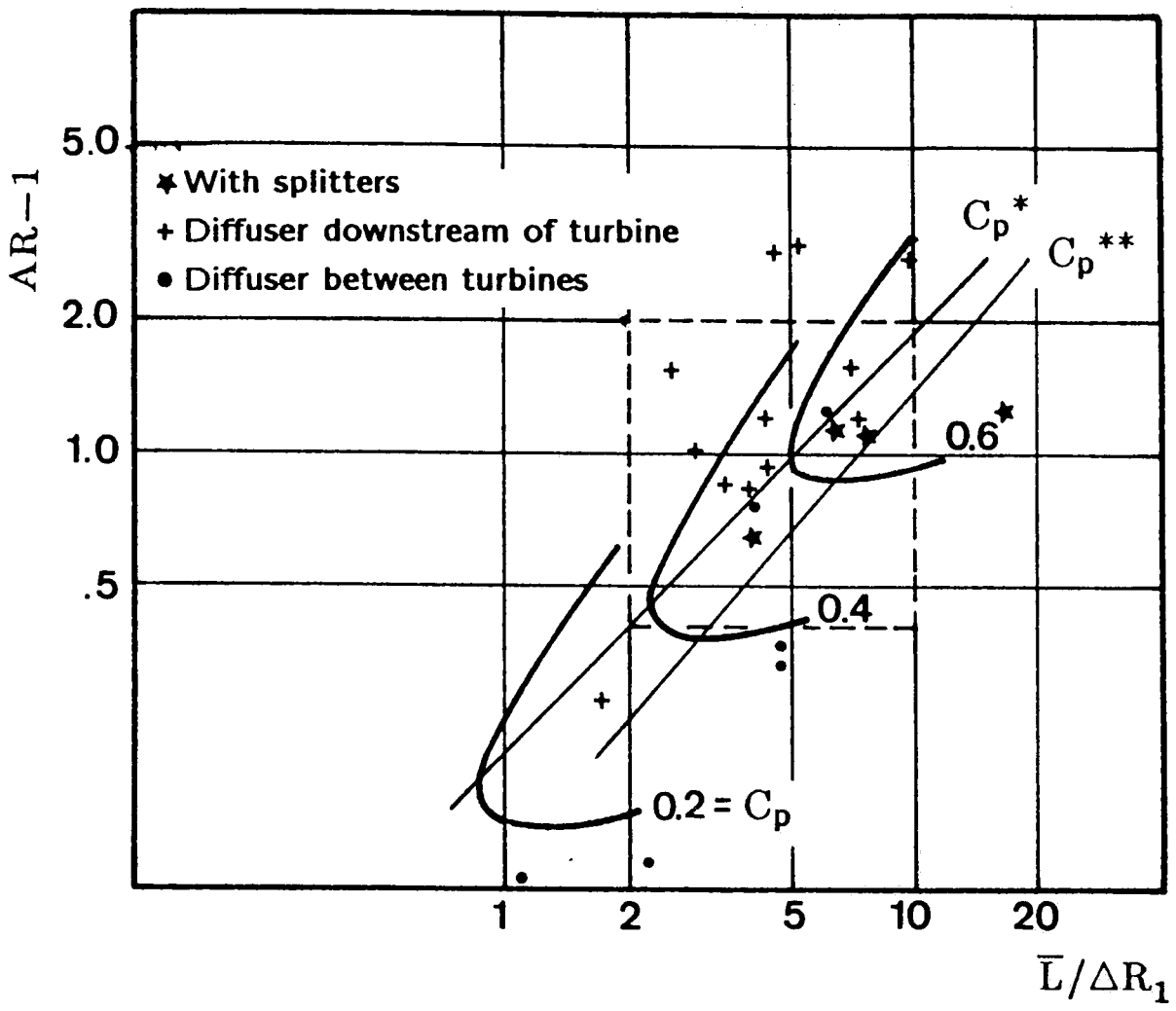

Figure 3. Survey of performance of annular diffusers in turbomachinery applications [15]

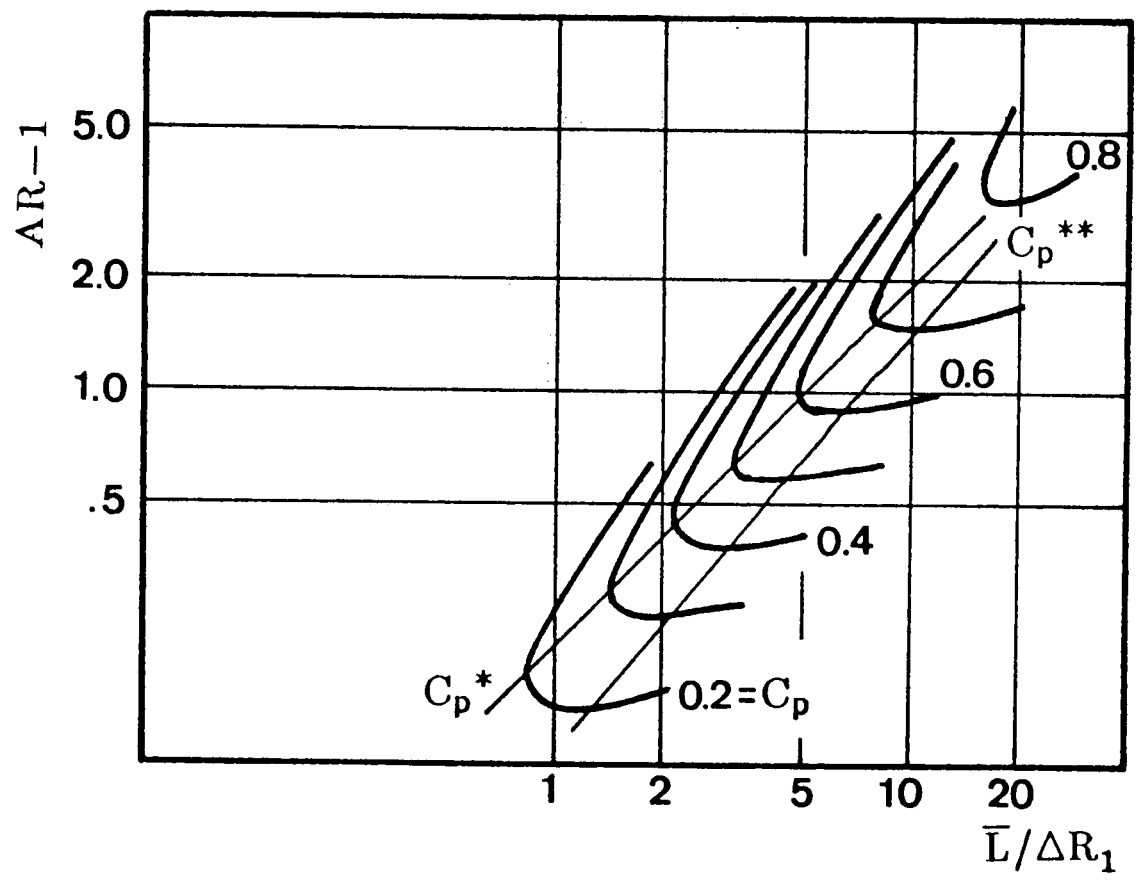

Figure 4. Performance chart for straight walled annular diffusers [15]

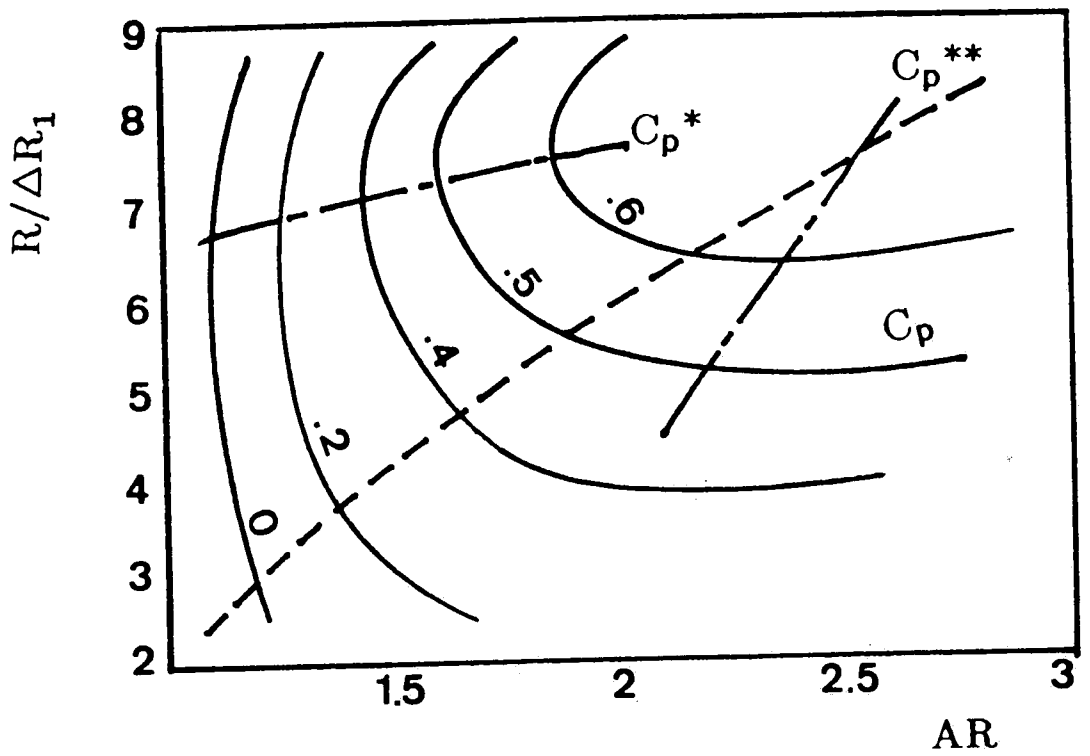

——— : starting of separation

Figure 5. Performance chart for curved annular diffusers [16]

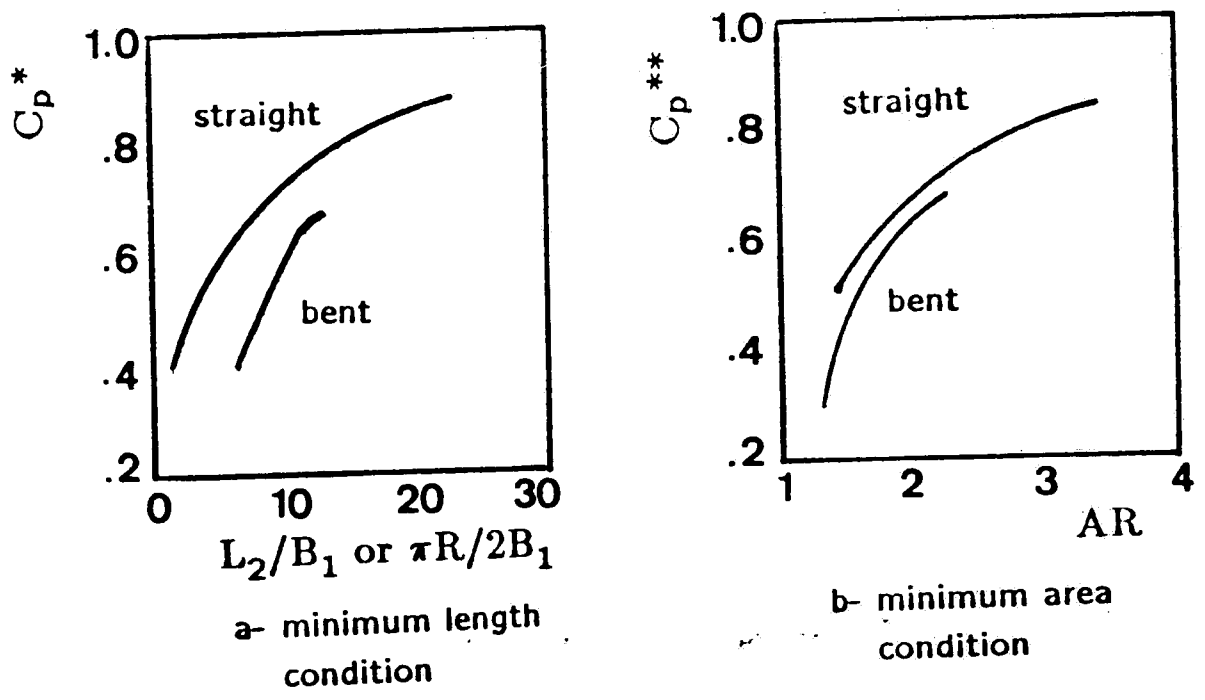

Figure 6. Comparison of curved and straight walled annular diffuser performances [16]

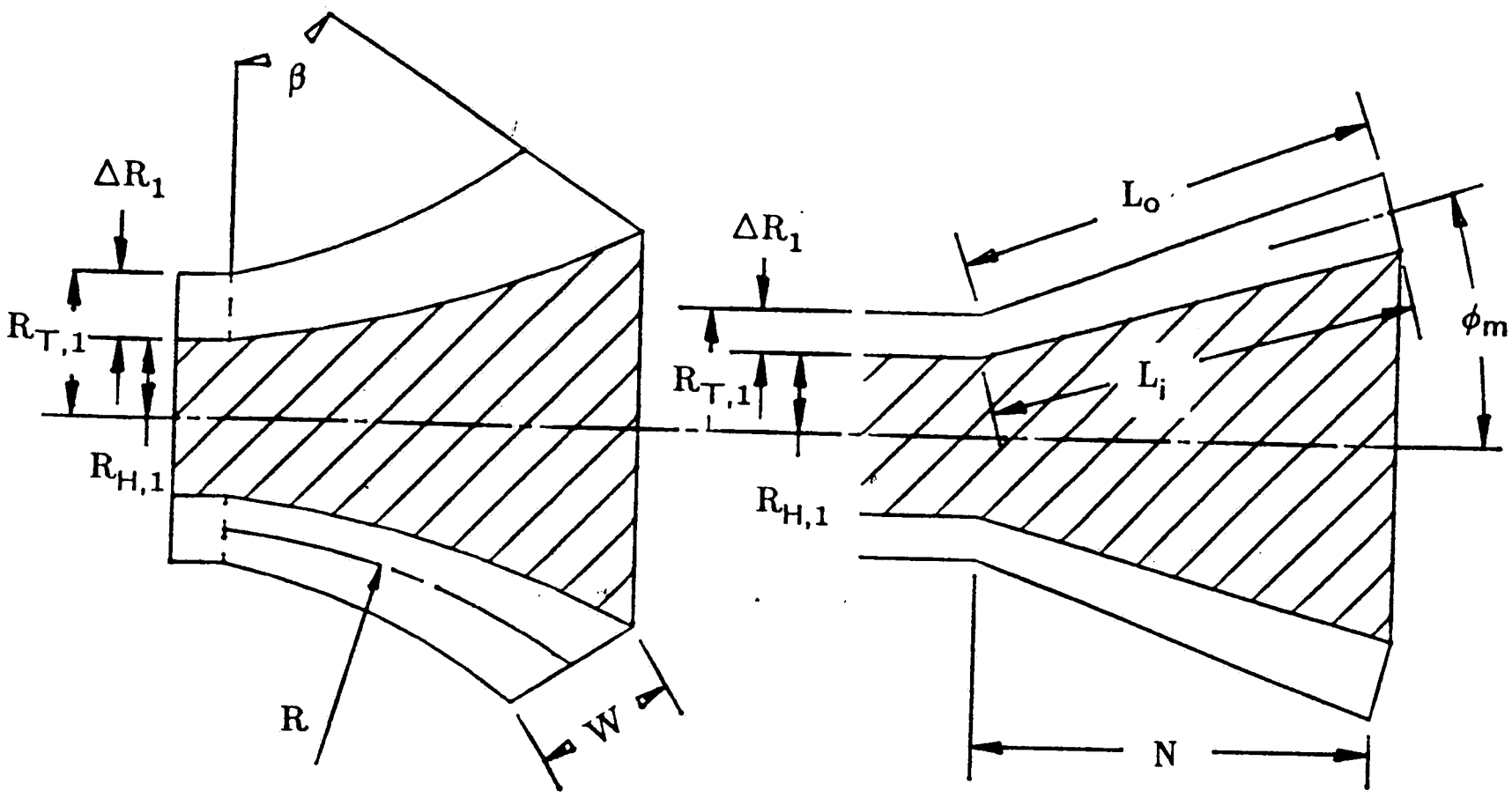

a—curved walled diffuser

b—straight walled diffuser

Figure 7. Curved and straight walled annular diffuser geometries[15, 16]

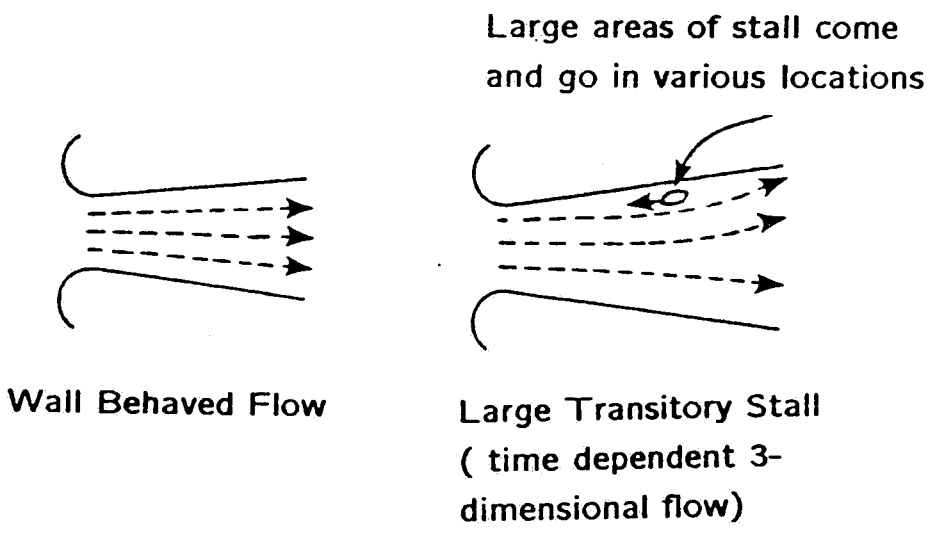

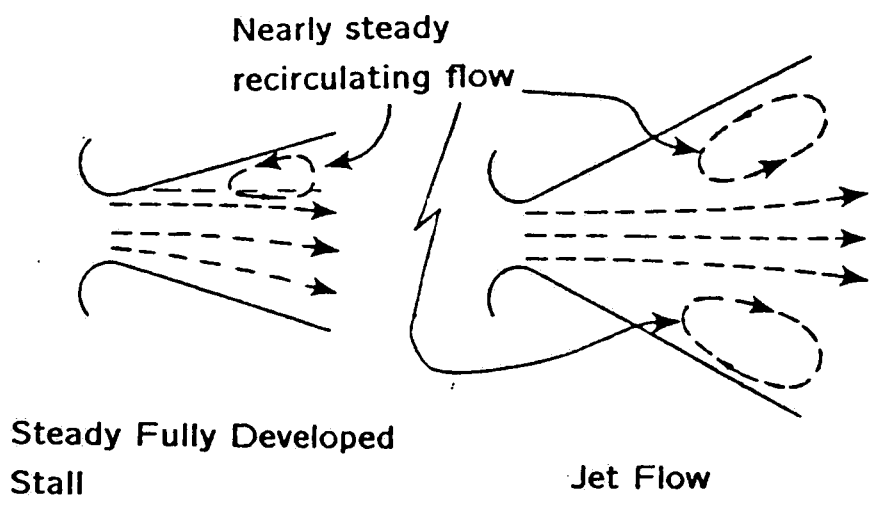

Figure 8. Schematic diagram of diffuser flow regimes[8]

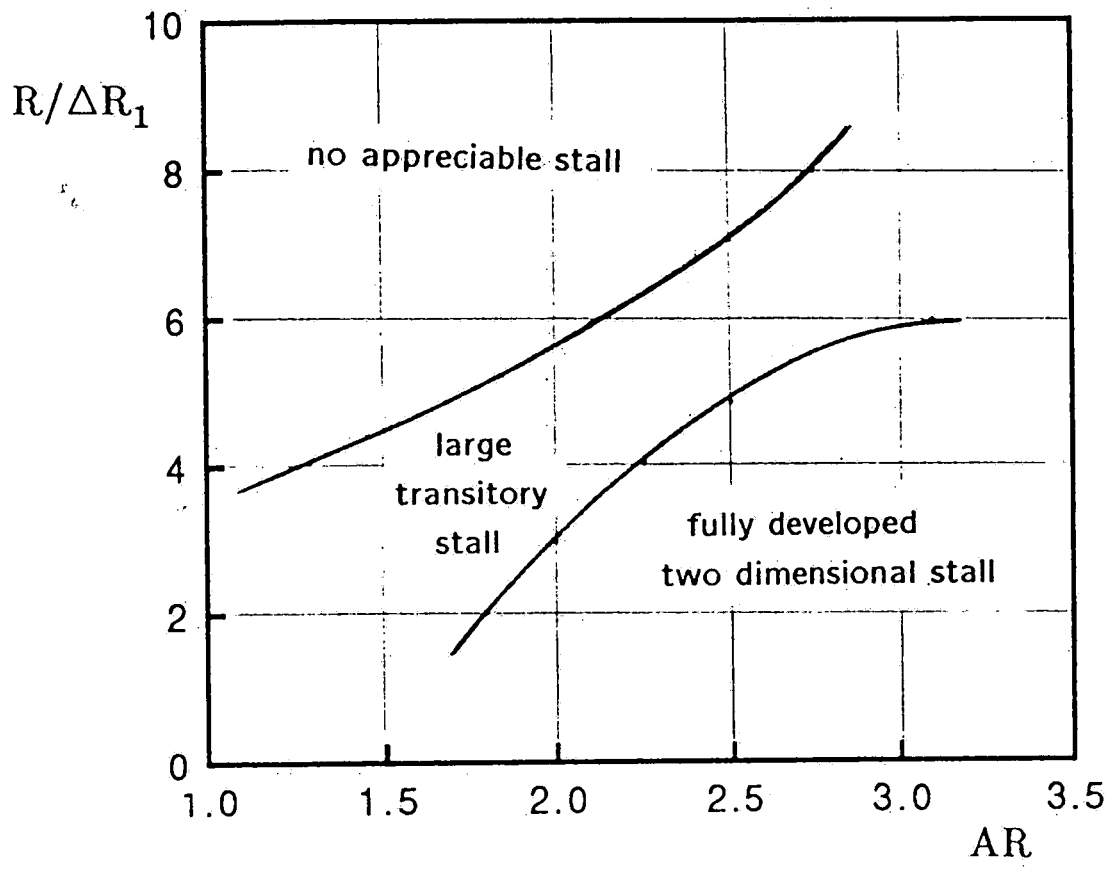

Figure 9. Flow regime chart for curved annular diffusers [16]

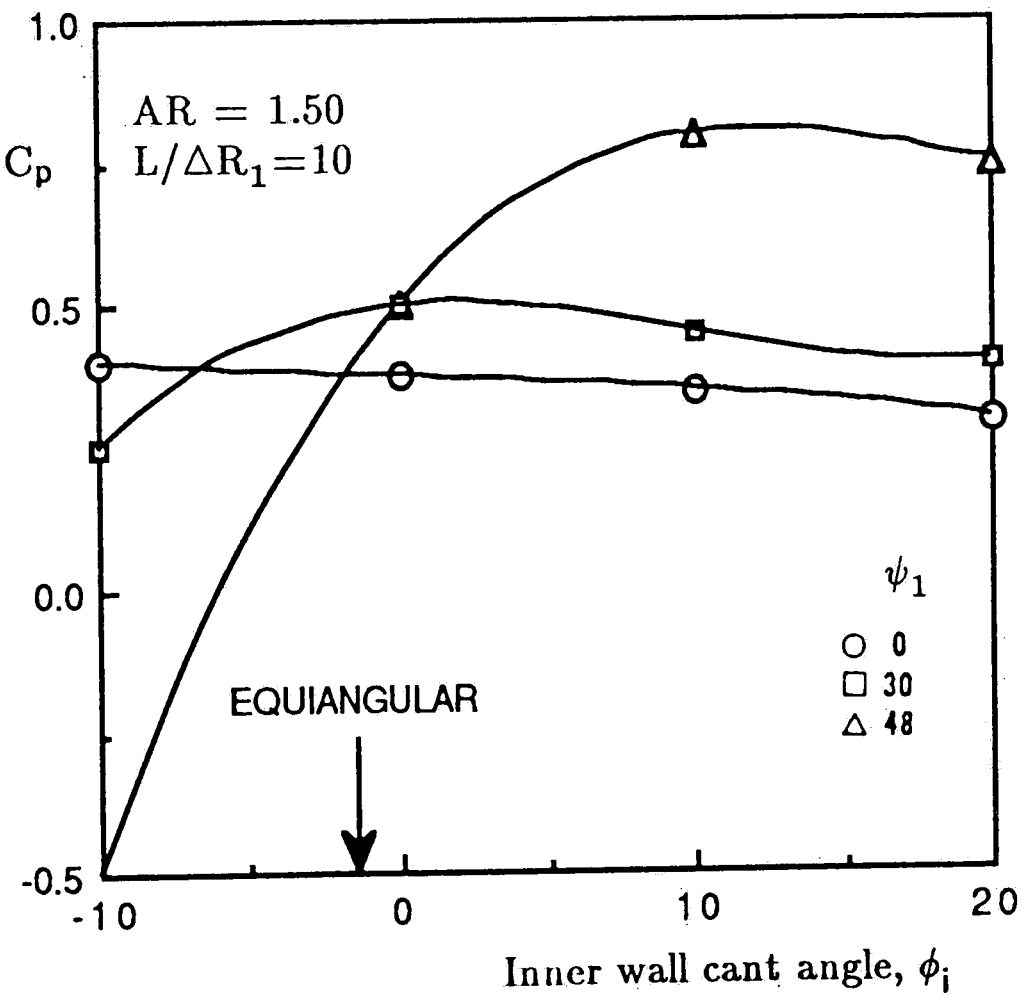

Figure 10. Effect of cant angle and swirl angle on pressure recovery of annular diffusers, ψ_1 denotes the swirl angle at inlet [10]

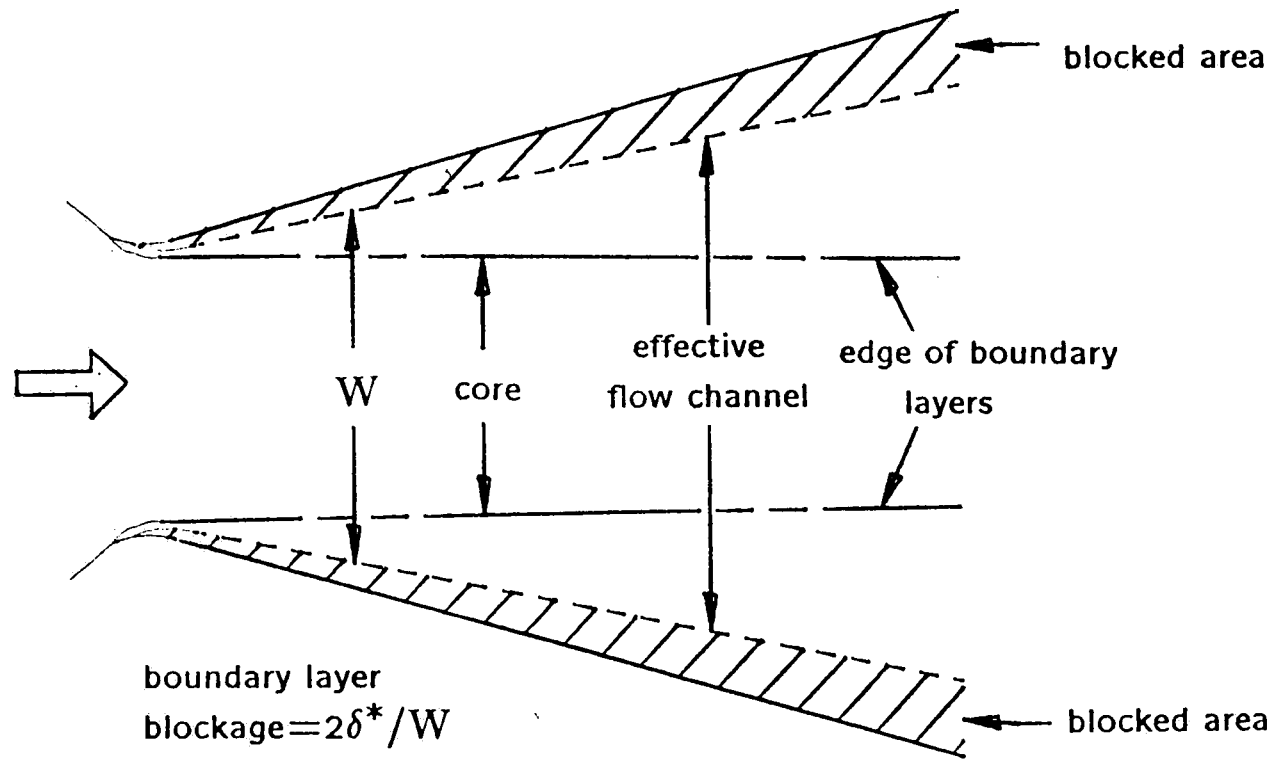

Figure 11. Boundary layer blockage [7]

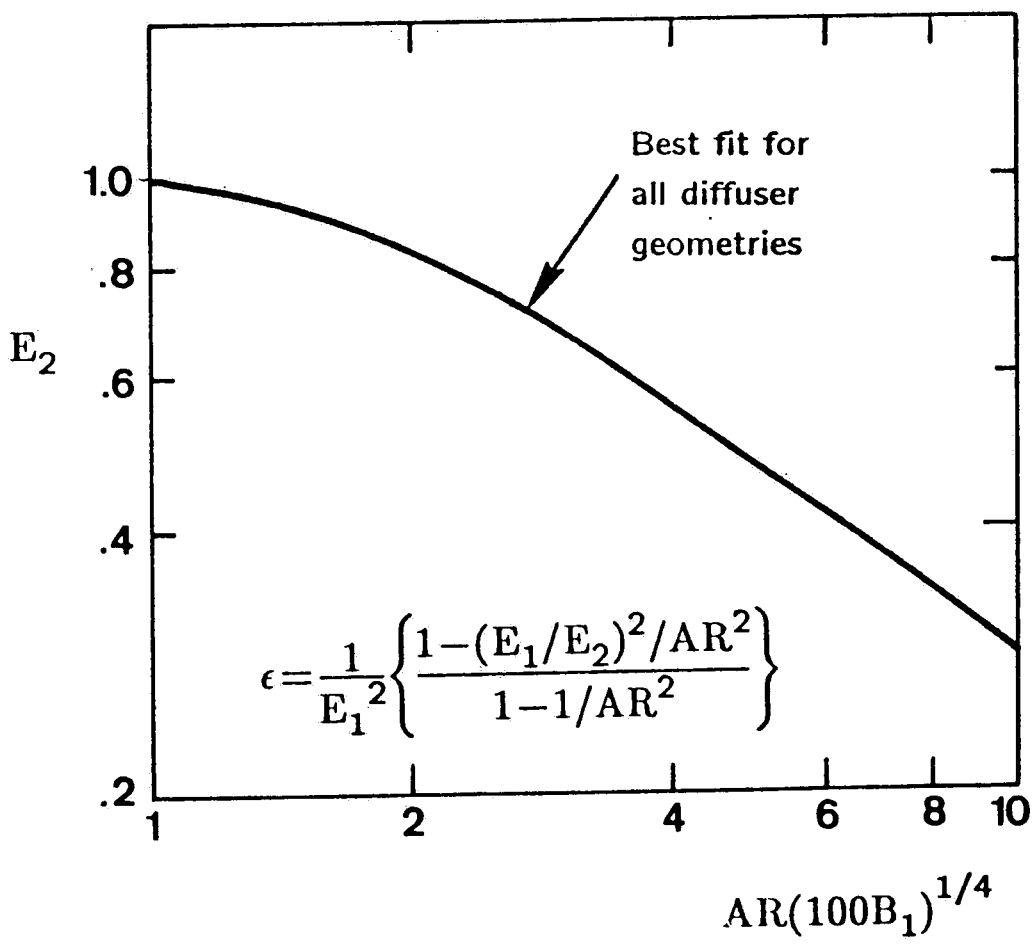

Figure 12. Effect of inlet boundary layer blockage on the velocity profile parameter at the exit, E_2, for conical diffusers near C^*_p [15]

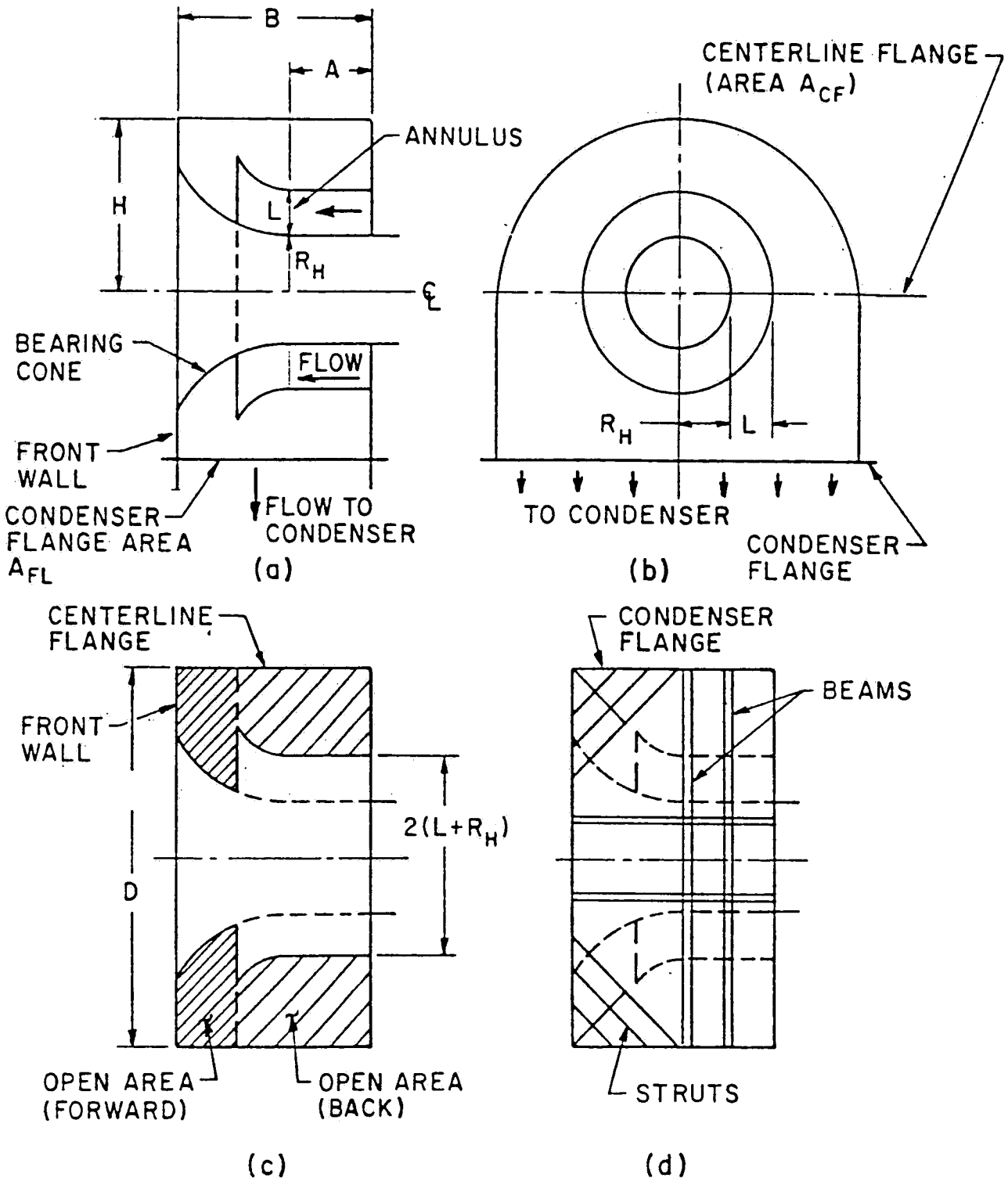

Figure 13. Variables used in the geometry description of an exhaust hood [17]

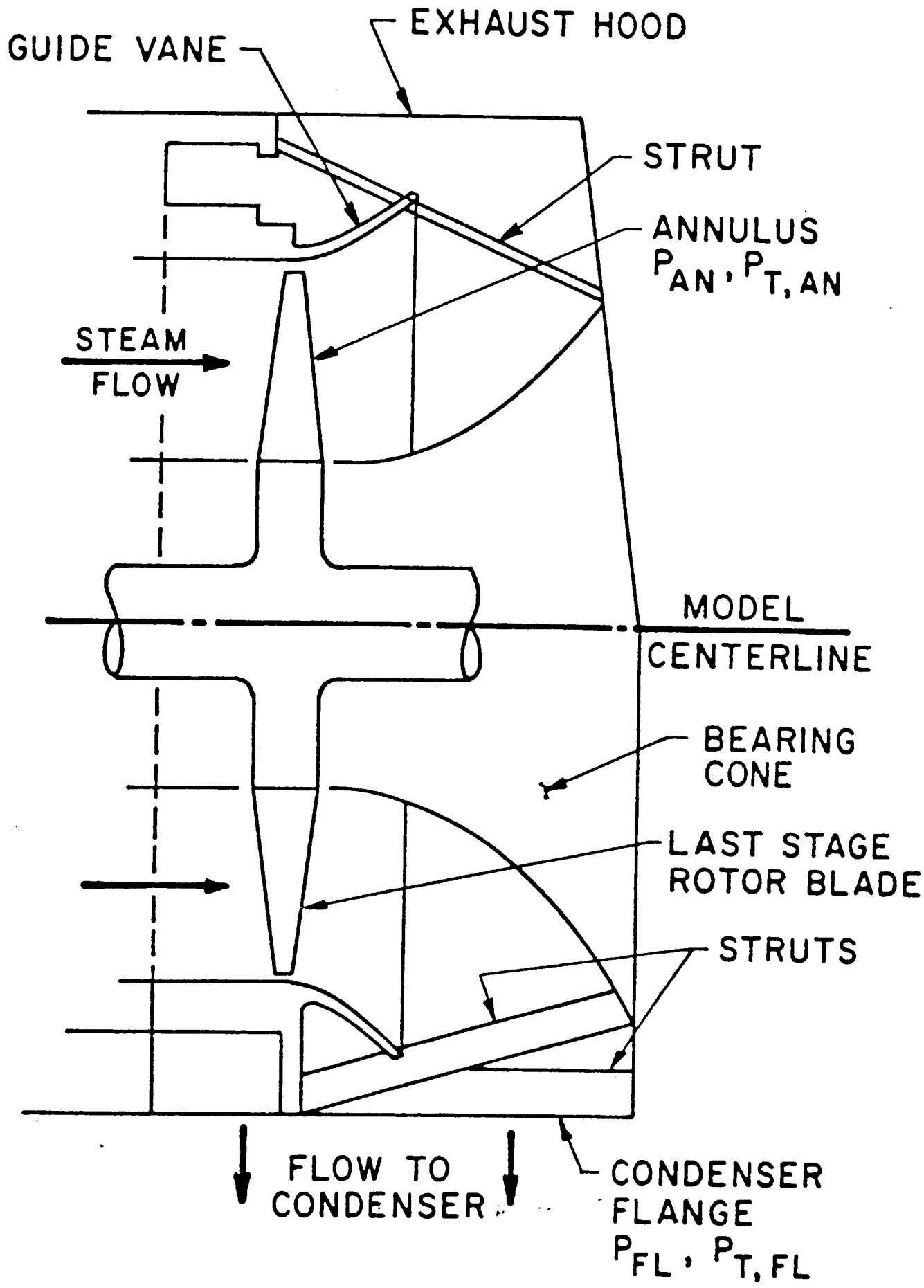

Figure 14. Sketch of a LP turbine end exhaust hood [2]

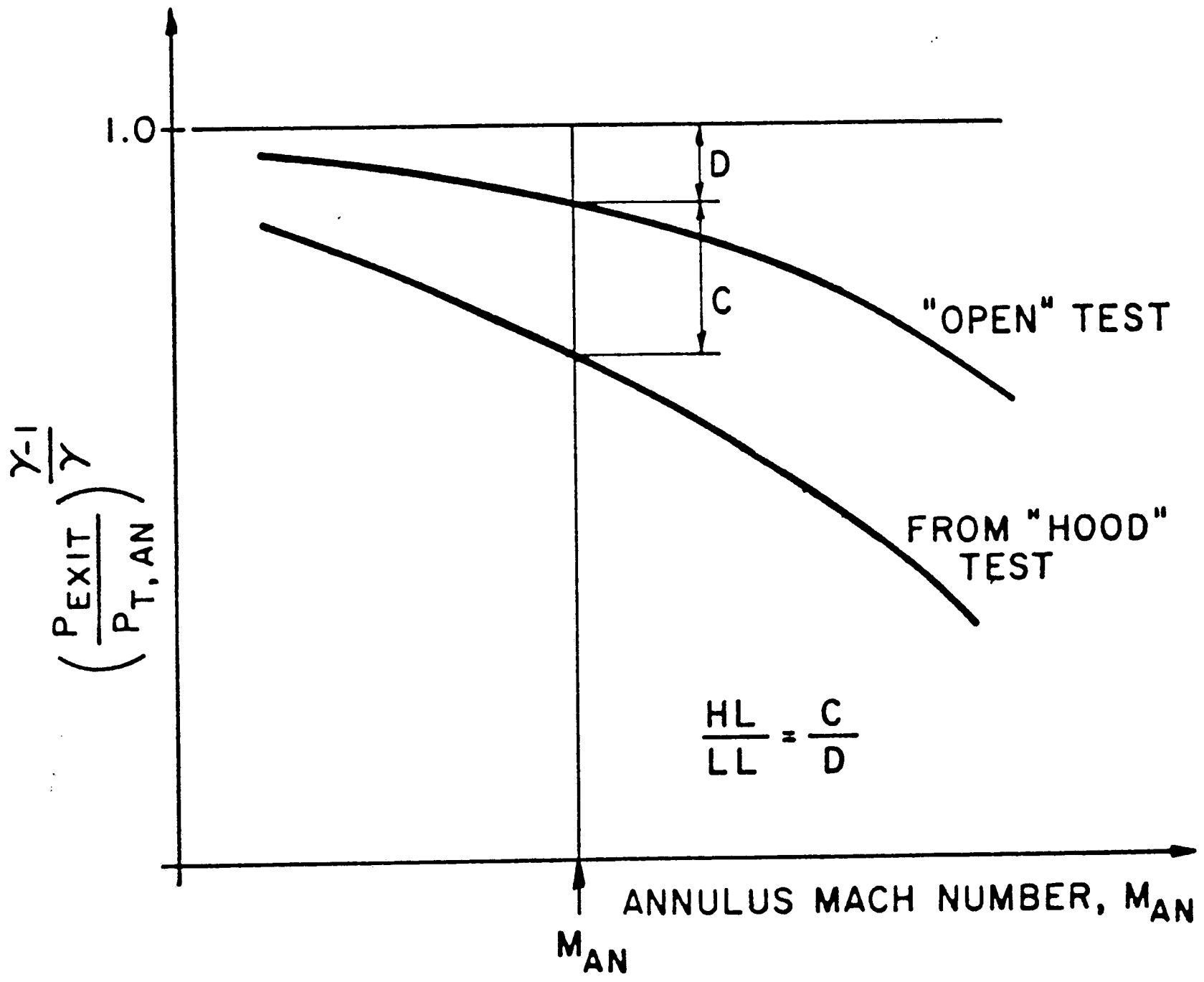

Figure 15. Graphical determination of hood loss coefficient using equation (4.4) when $T_{T,HOOD} = T_{T,OPEN}$, ($P_{EXIT} = P_{AN}$ or P_{FL}) [2]

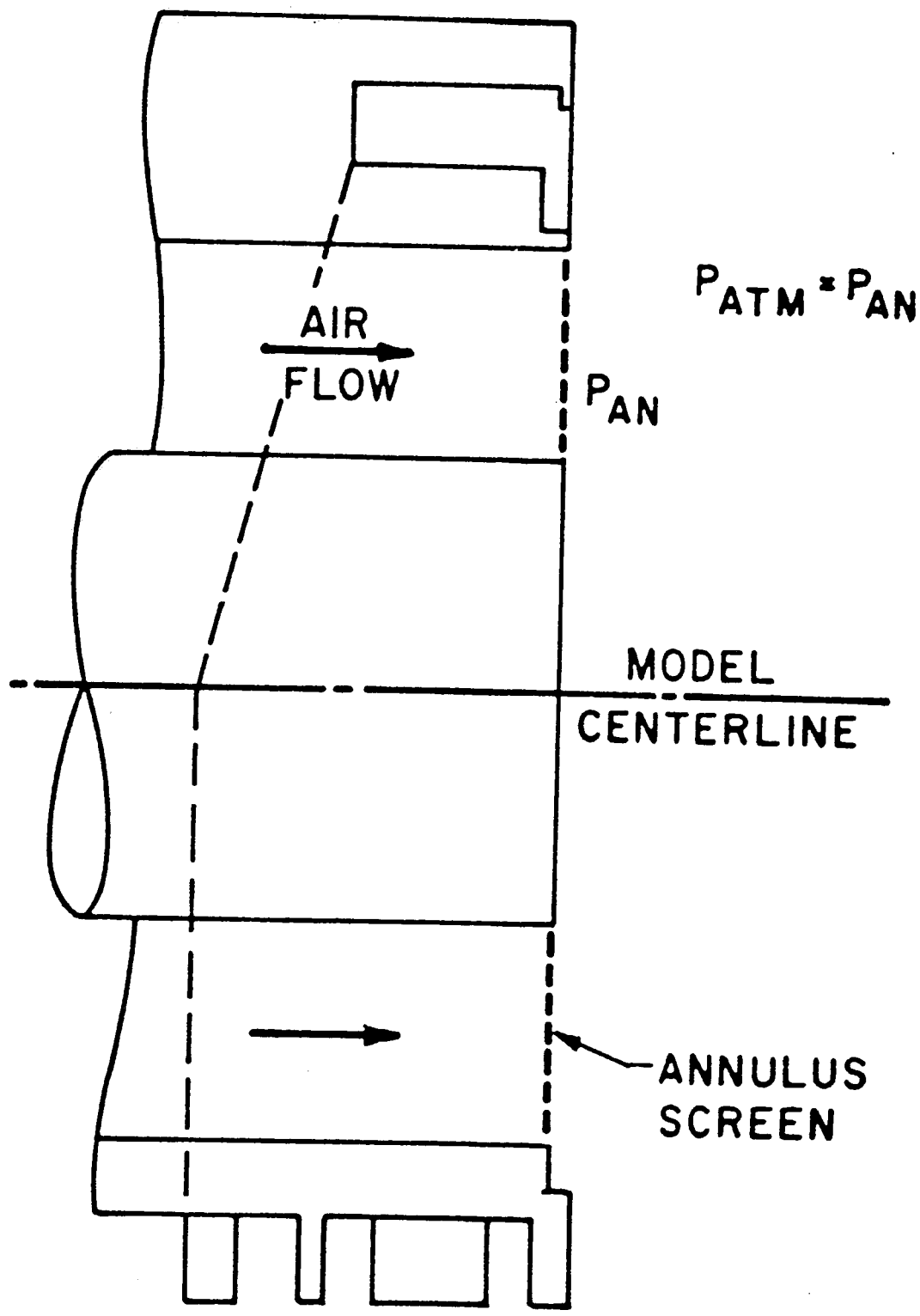

Figure 16. Schematic of an open test model [2]

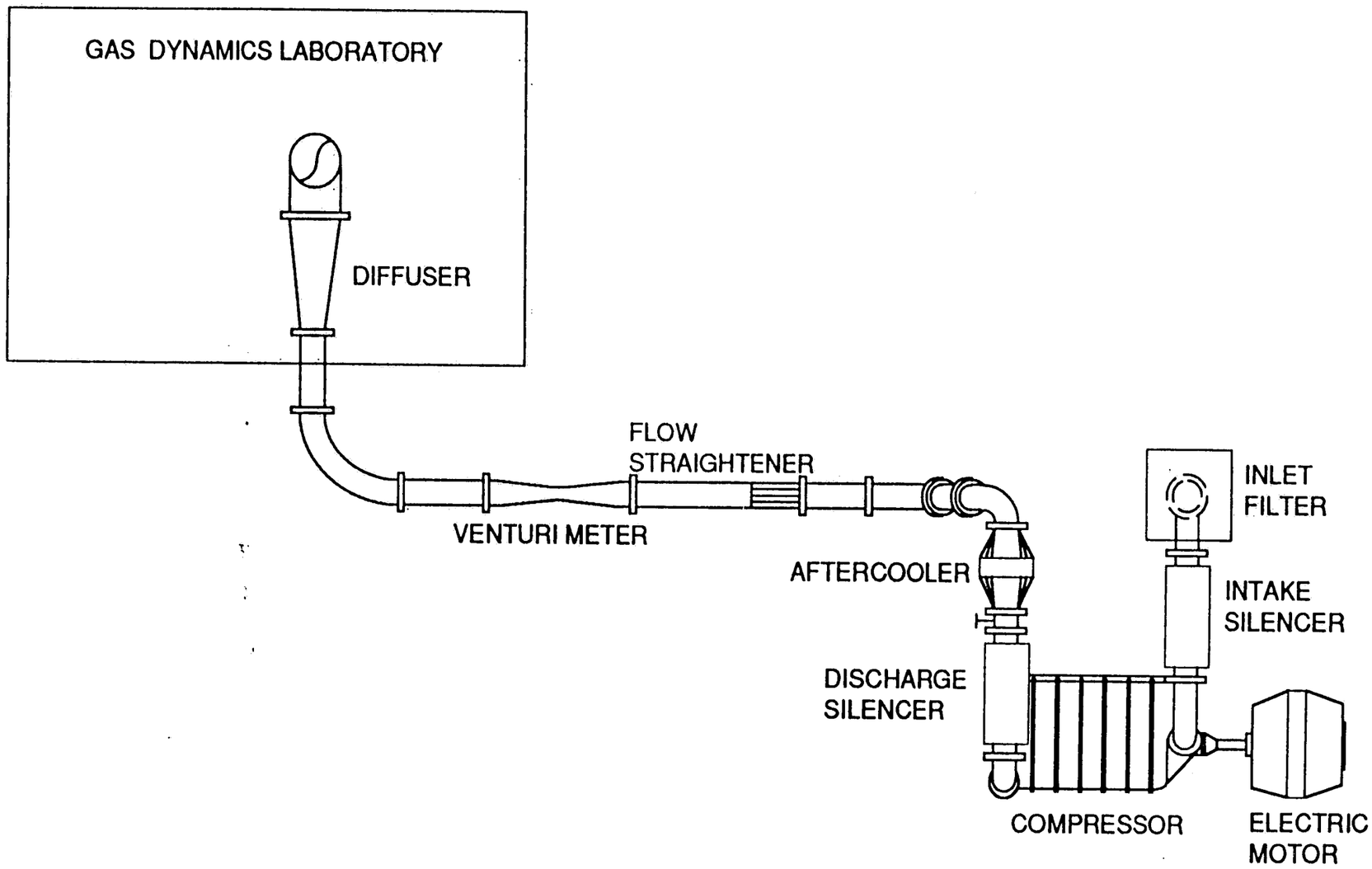

Figure 17. Schematic of air test loop

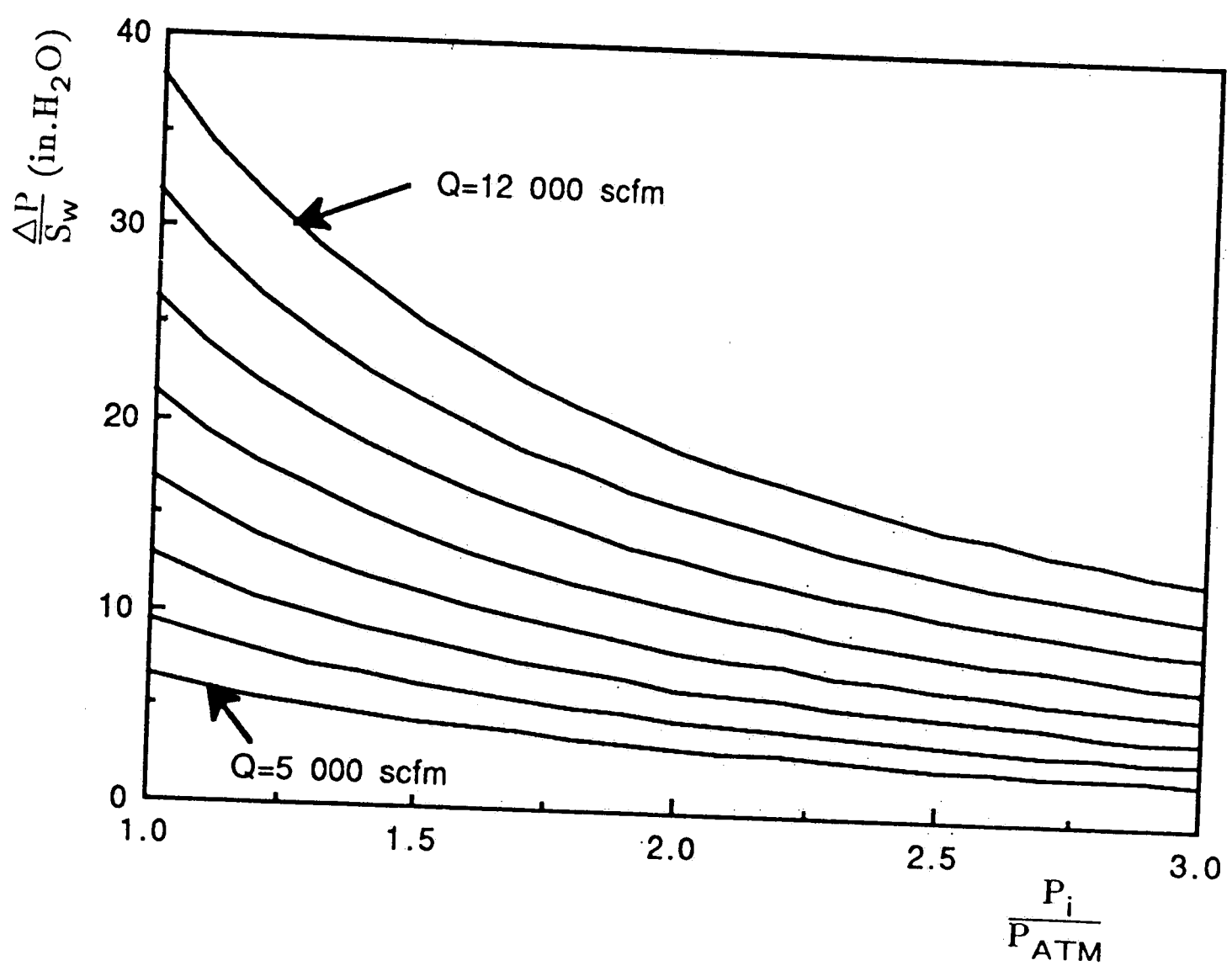

Figure 18. Variation of pressure difference across a venturi meter as a function of the ratio of inlet pressure to atmospheric pressure

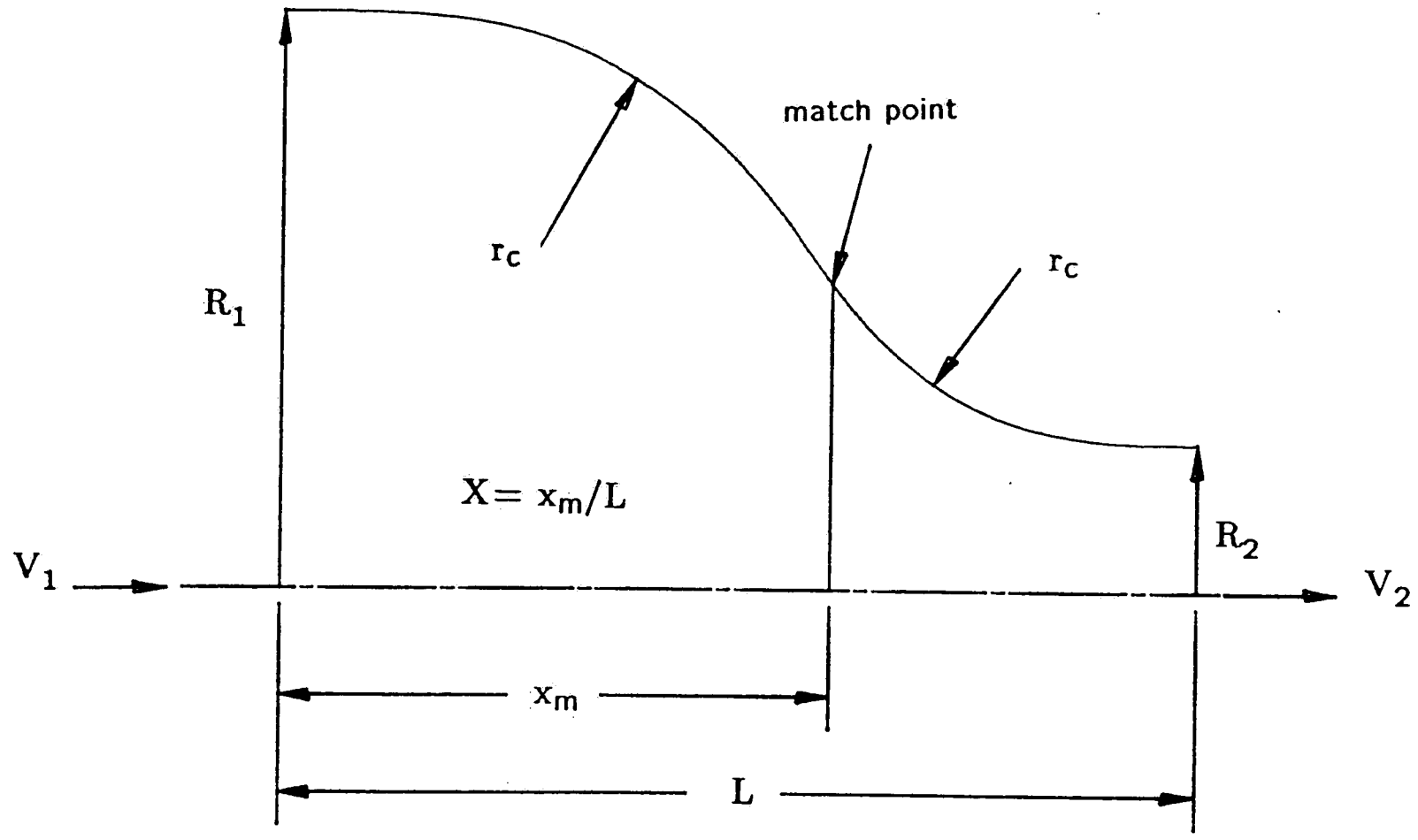

Figure B-1. Geometric parameters for contraction design [21]

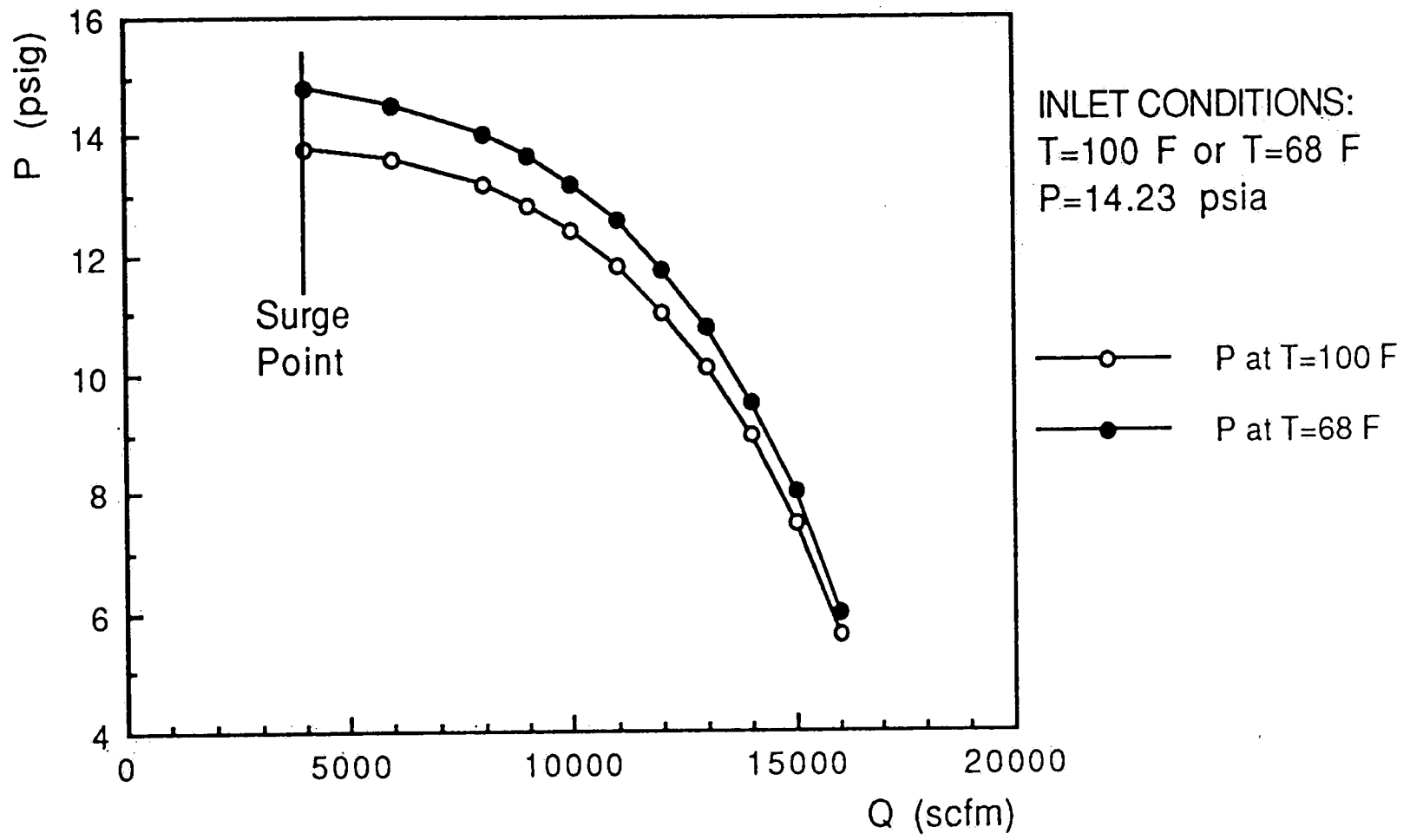

Figure C-1. Compressor performance curve (supplied by the vendor)

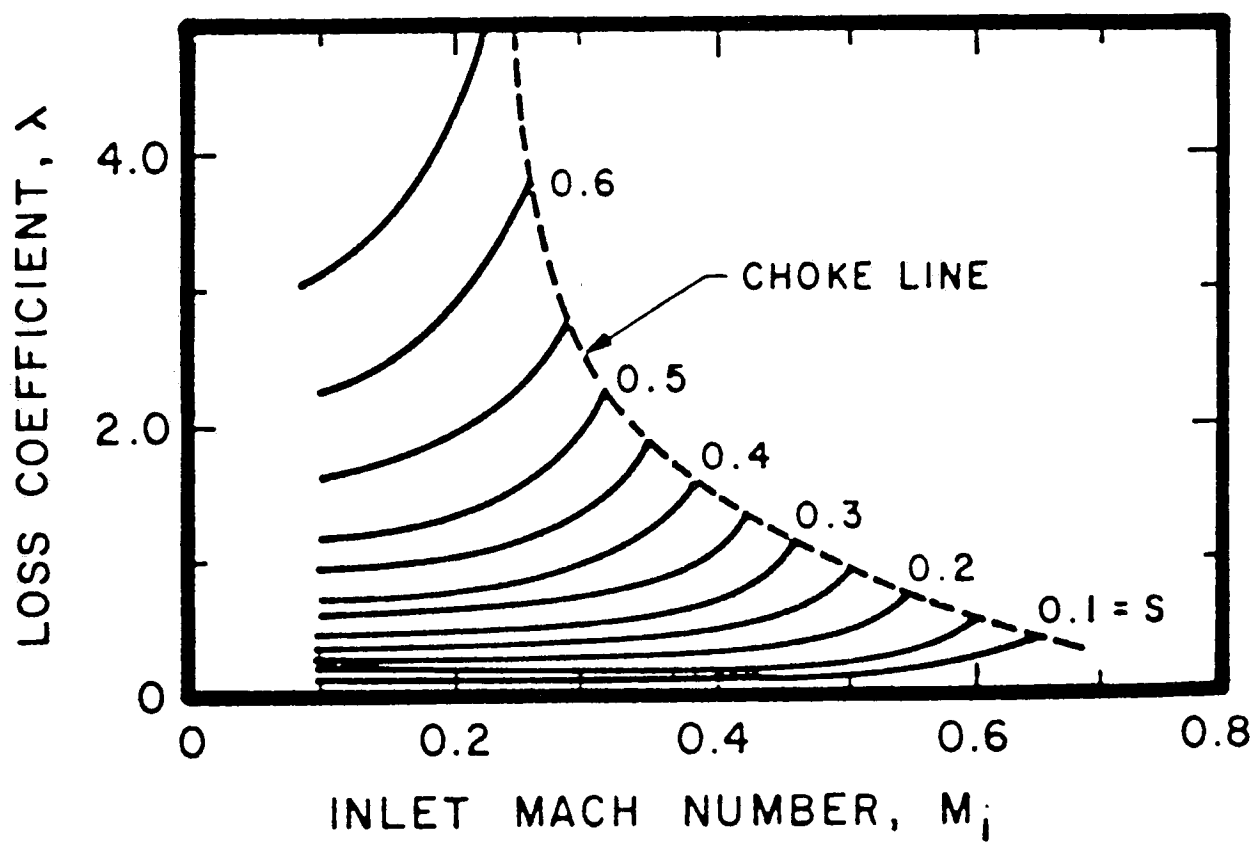

Figure D-1.Experimental results on round-wire-screen losses in high velocity flow normal to plane screens [2, 23]

APPENDIX F—Air Test Loop Drawings

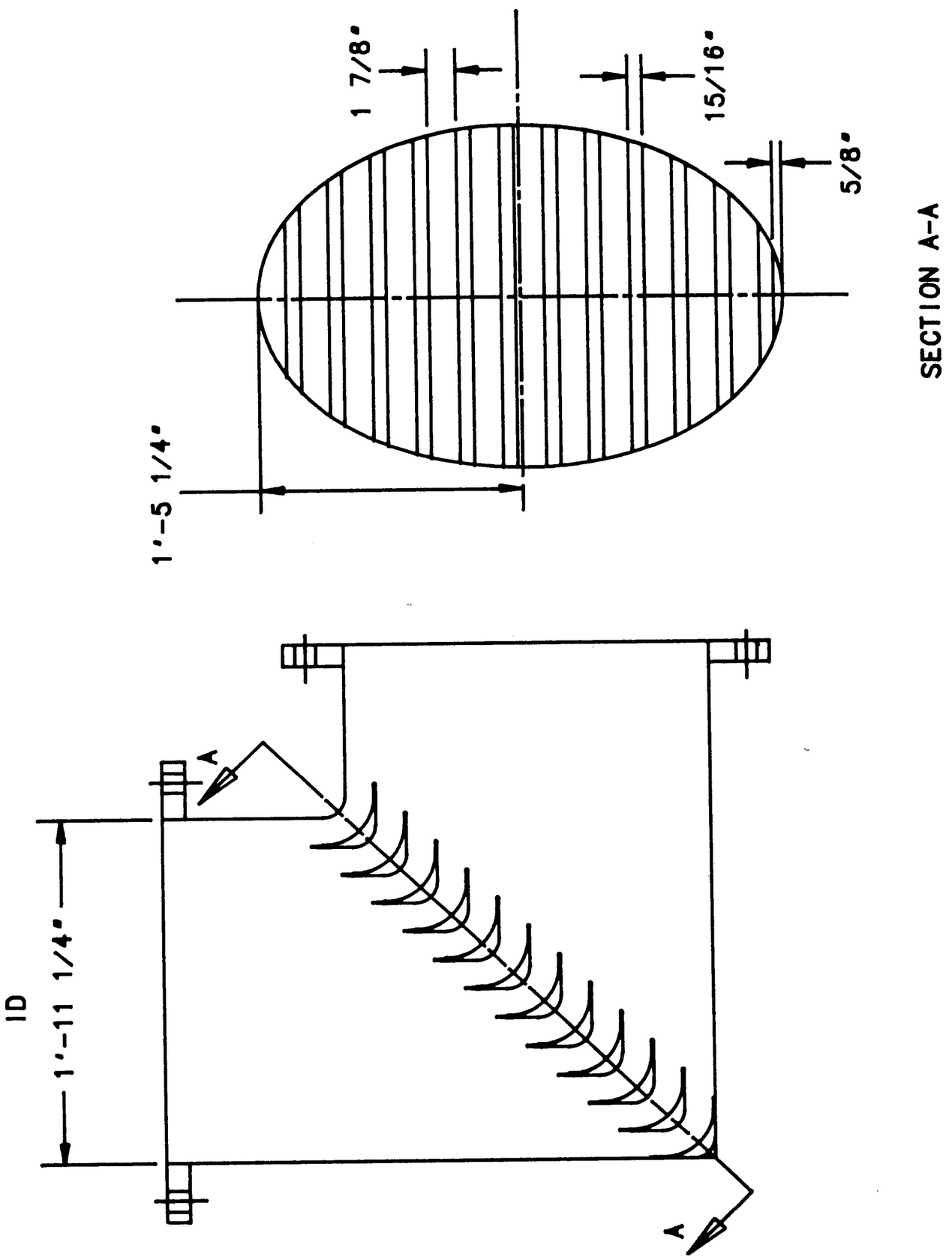

DRAWING NO. F-1
SPECIAL ELBOW
SCALE: 1/12

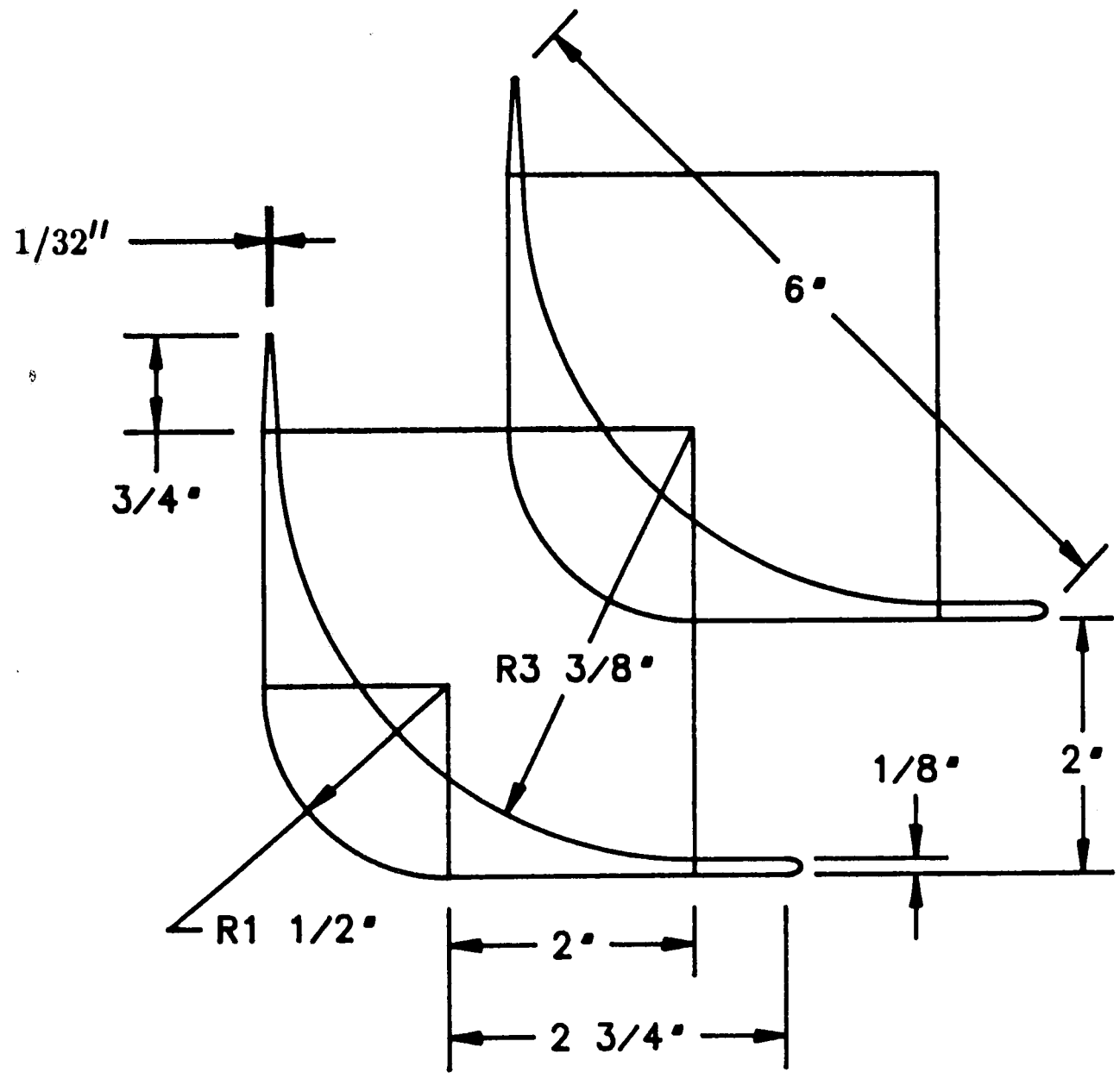

DRAWING NO. F-2
TURNING VANE DESIGN
SCALE:1/2

DRAWING NO. F-3
ELEVATION VIEW OF TEST STAND
SCALE: 9/160

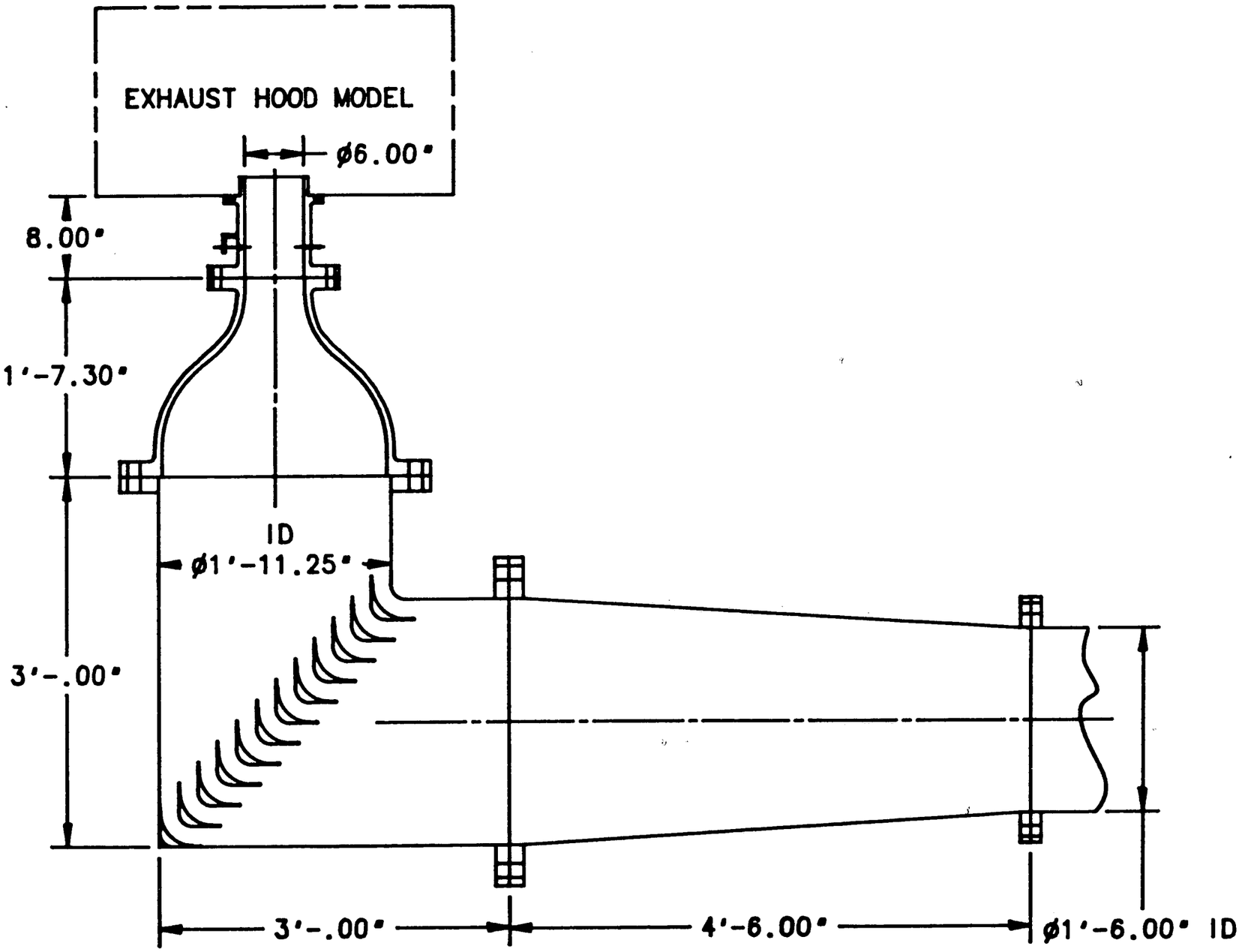

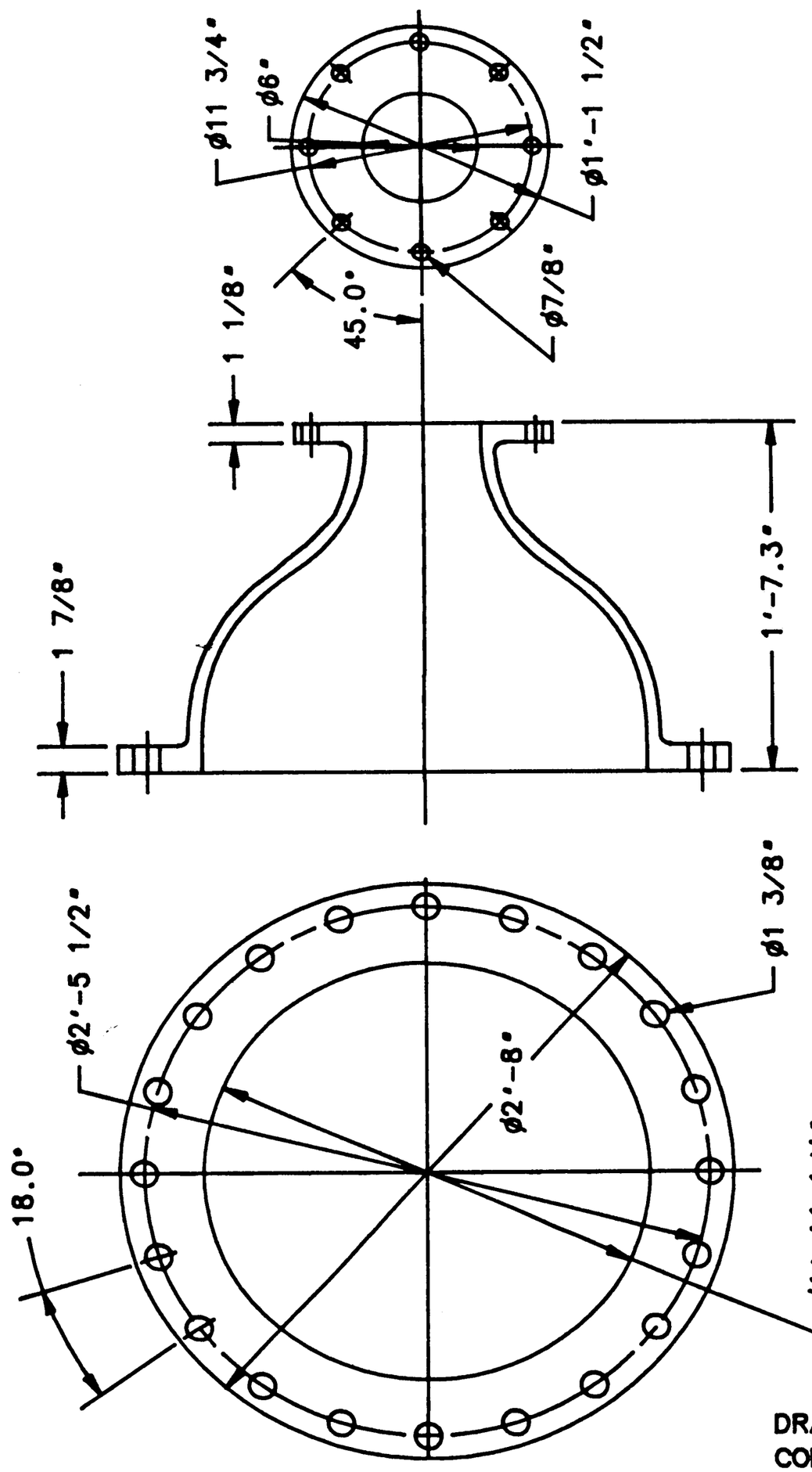

DRAWING NO. F-4
CONTRACTION CASTING
SCALE: 1/10

APPENDIX G—Generic Model Drawings

G—1A	Assembly (elevation view)
G—1B	Assembly (side view)
G—2	Hub
G—3	Elliptical nose
G—4	Ring piece
G—5	Back plate
G—6	Guide vane
G—7	Bearing cone
G—8	Annulus screen
G—9	Body
G—10A	Upstream pipe
G—10B	Upstream pipe
G—11	Shell
G—12A	Insert to change width
G—12B	Insert to change width
G—12C	Insert to change width
G—12D	Insert to change width
G—13A	Insert to change height
G—13B	Insert to change height
G—13C	Insert to change height
G—13D	Insert to change height
G—13E	Insert to change height
G—14A	Outlet duct for D/L=8.15
G—14B	Outlet duct for D/L=7.5
G—14C	Outlet duct for D/L=7.0
G—15	Open model (assembly)

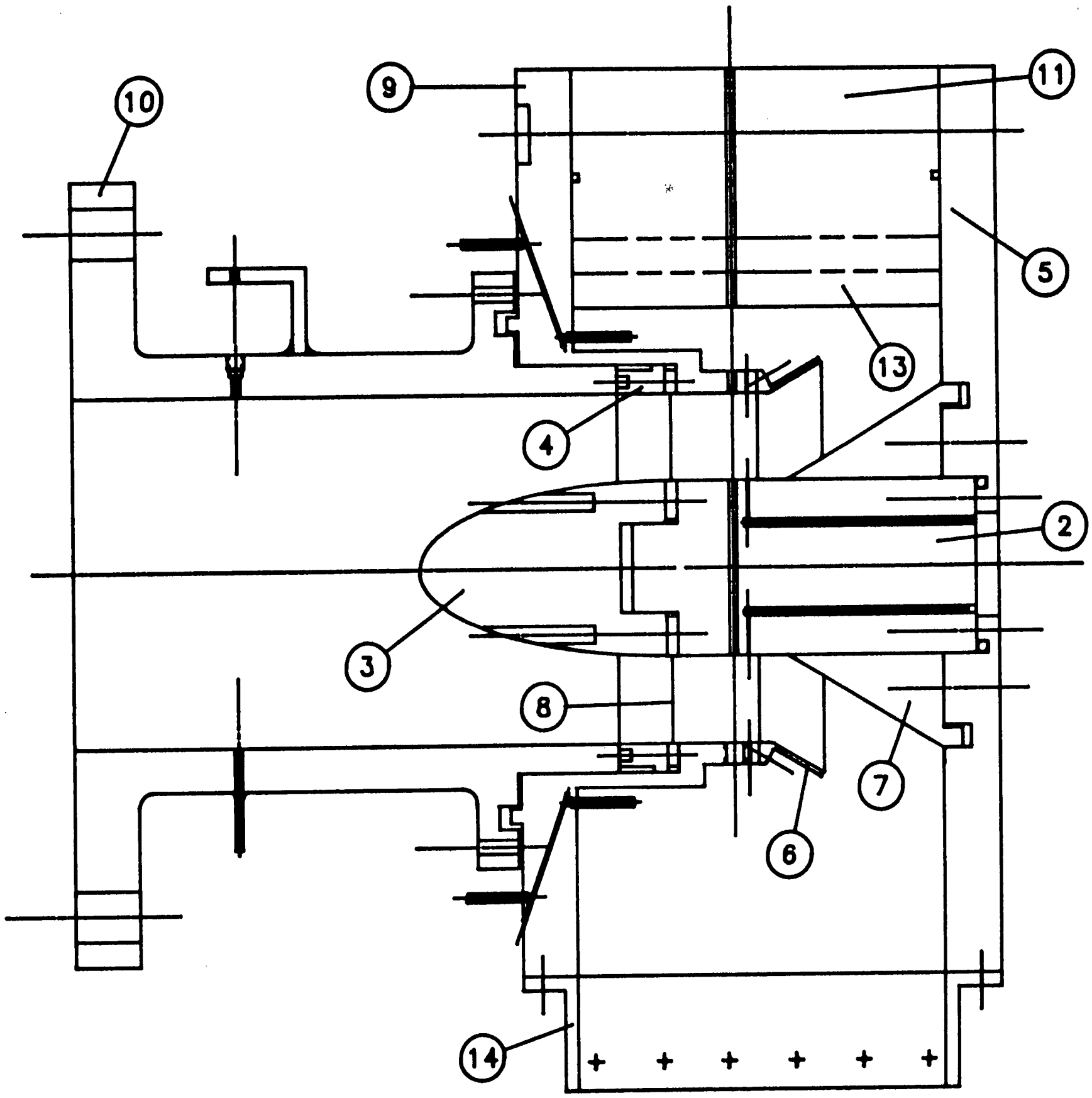

PART NO.	NAME	PART NO.	NAME
2	Hub	5	Back plate
3	Elliptical nose	9	Body
4	Ring piece	10	Upstream pipe
5	Back Plate	11	Shell
6	Guide vane	12	Insert to change width
7	Bearing cone	13	Insert to change height
8	Annulus screen	14	Outlet duct

DRAWING NO. G-1A
ASSEMBLY(ELEVATION VIEW)
SCALE:5/16

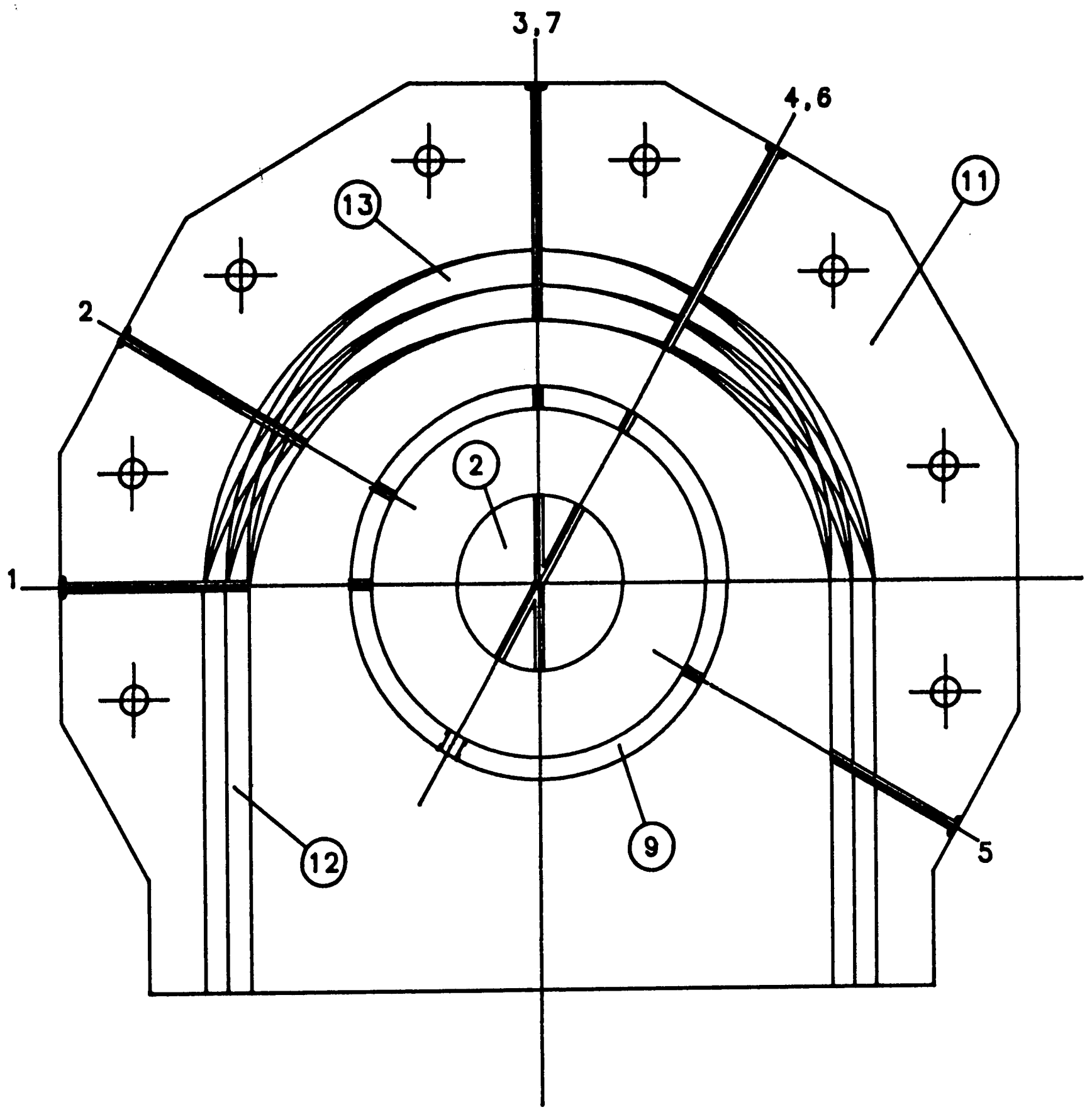

DRAWING NO. G-1B
ASSEMBLY(SIDE VIEW)
SCALE:5/16

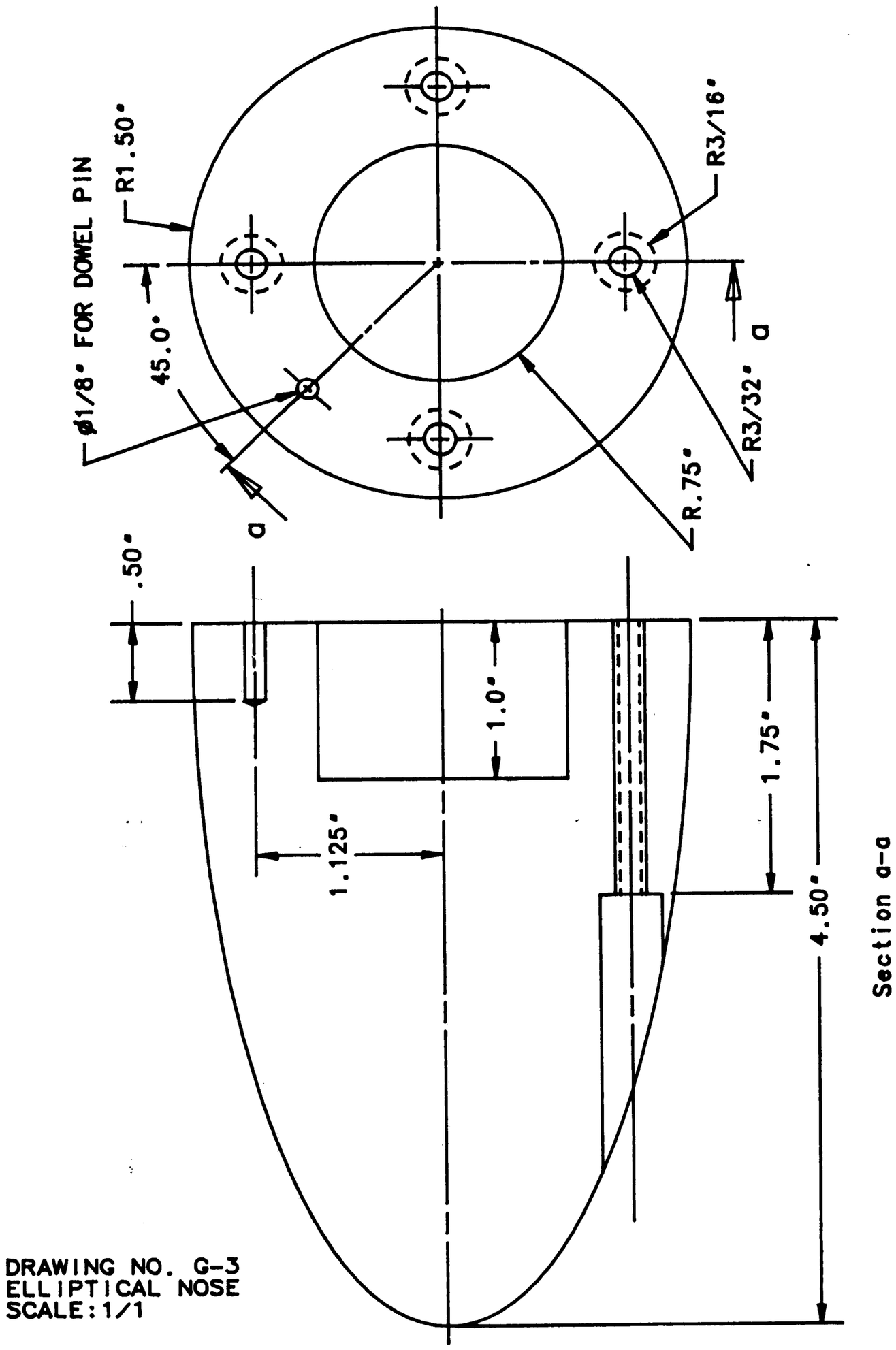

DRAWING NO. G-3
ELLIPTICAL NOSE
SCALE: 1/1

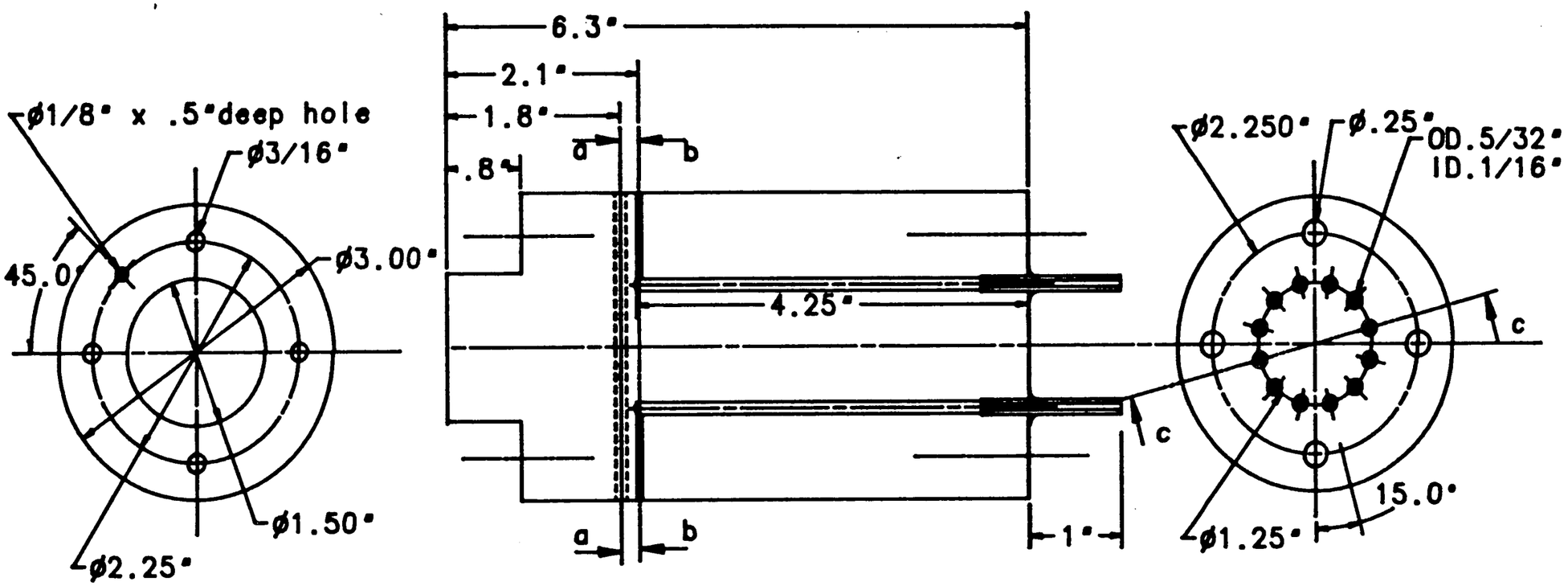

Section c-c

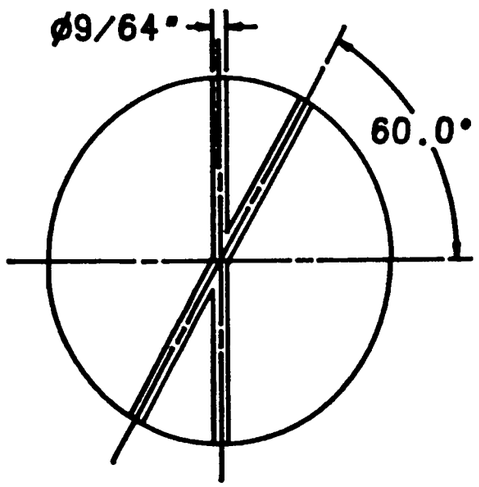

Section a-a

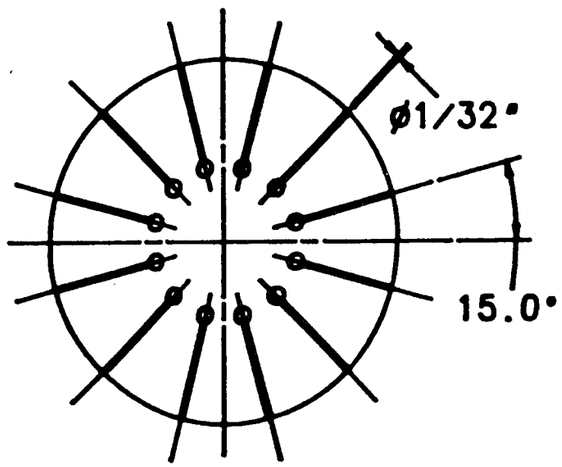

Section b-b

DRAWING NO. G-2
HUB
SCALE: 1/2

76

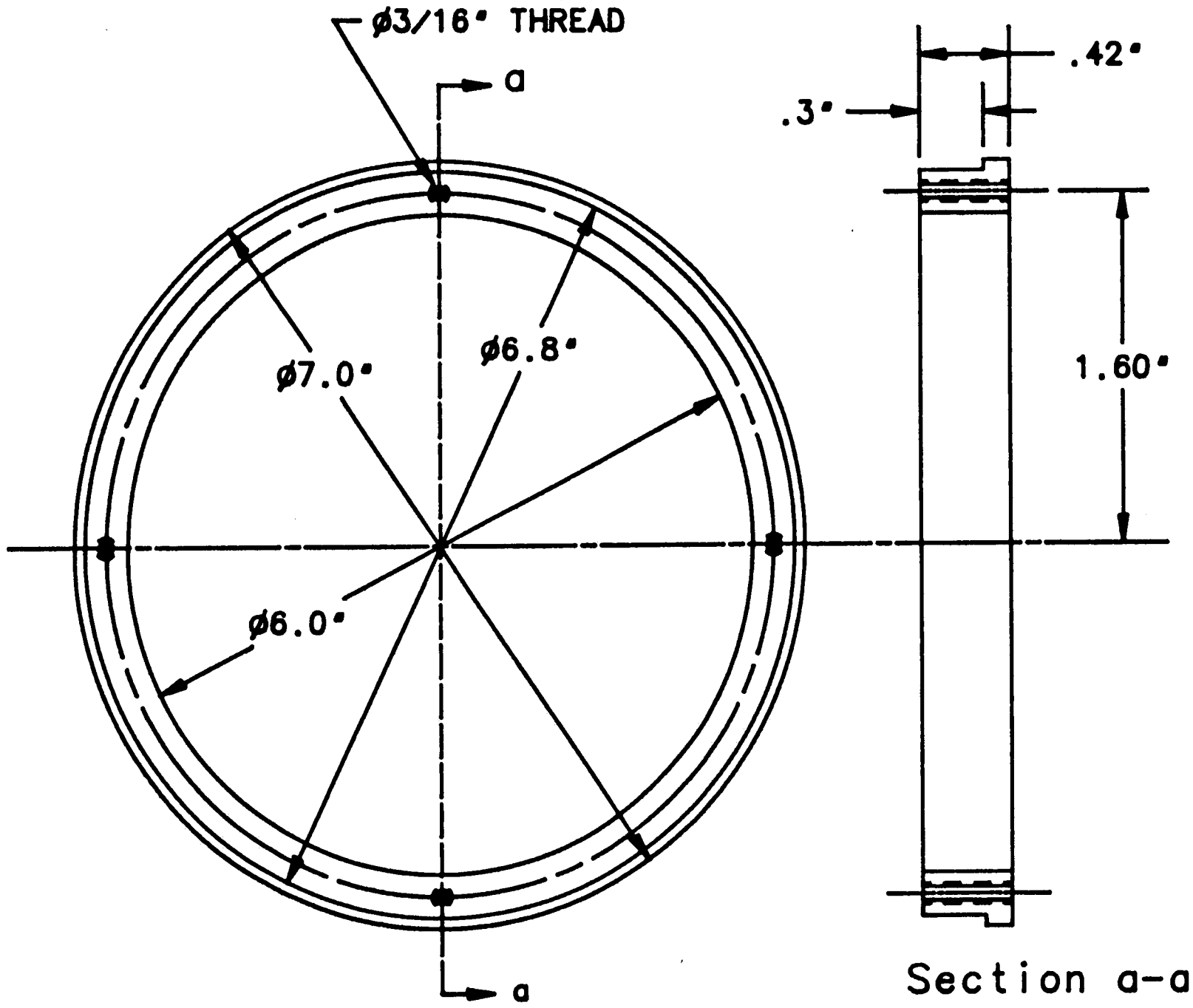

DRAWING NO. G-4
RING PIECE
SCALE: 1/2

DRAWING NO. G-5
BACK PLATE
SCALE: 1/3

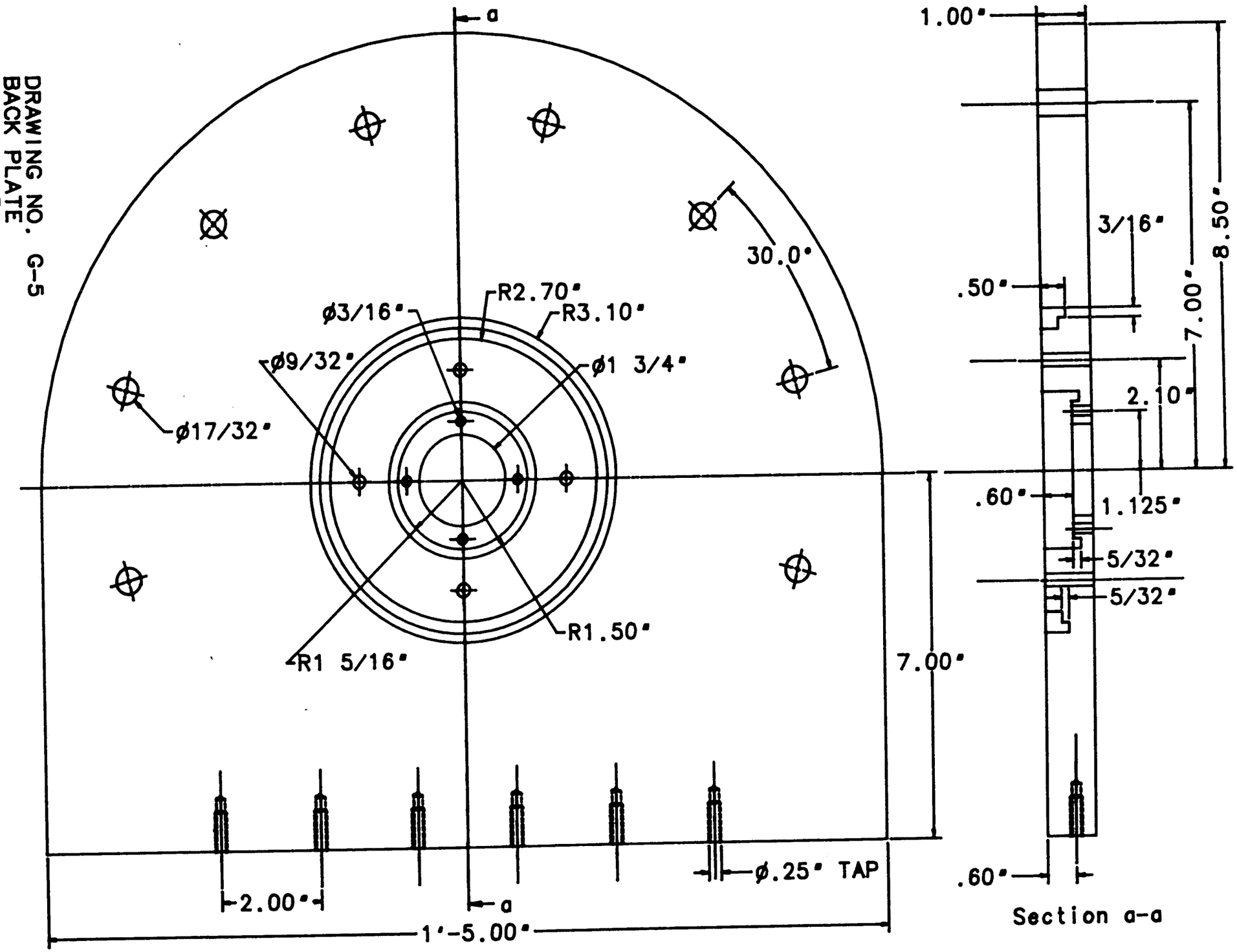

Section a-a

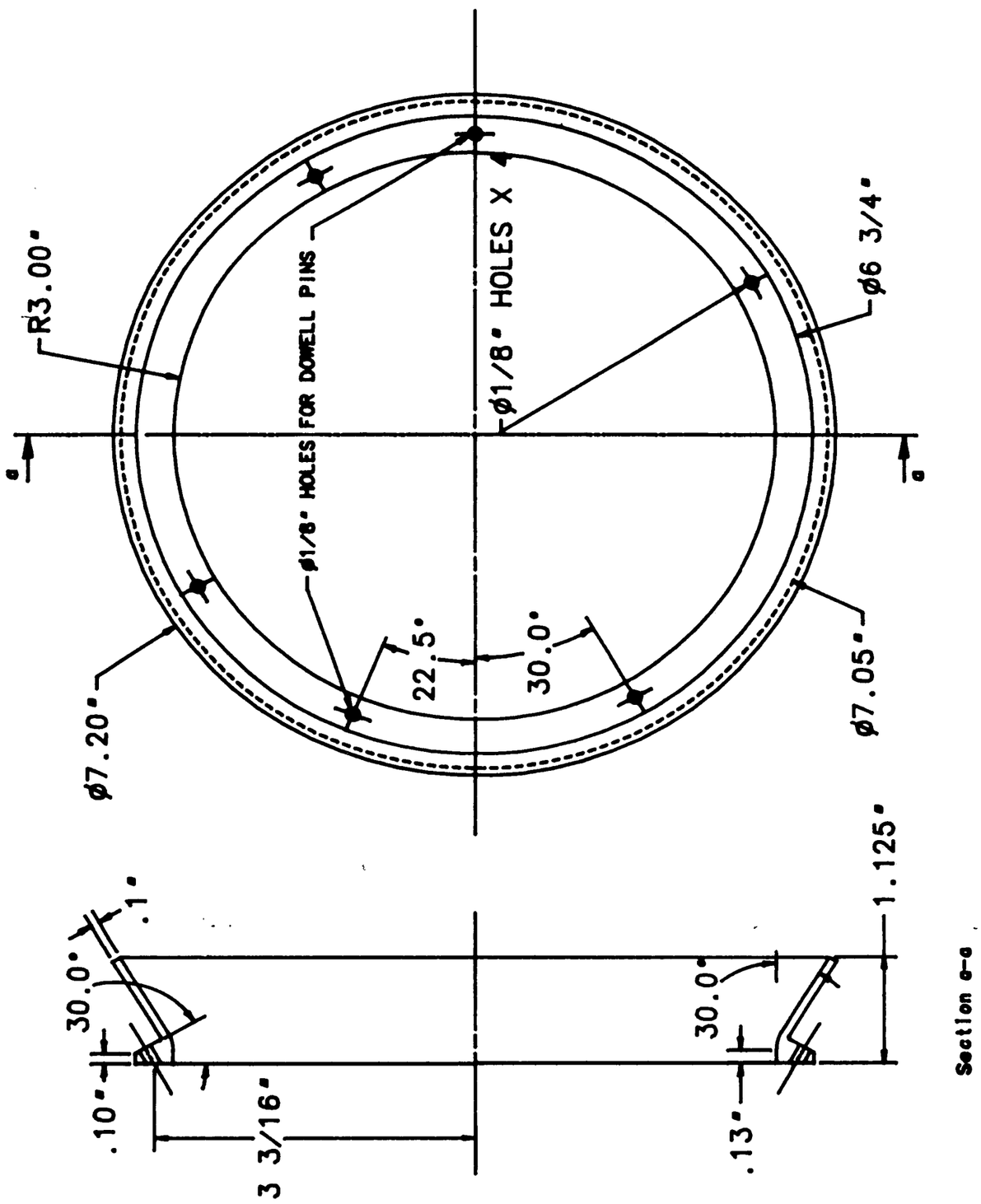

DRAWING NO. G-6
GUIDE VANE
SCALE: 1/2

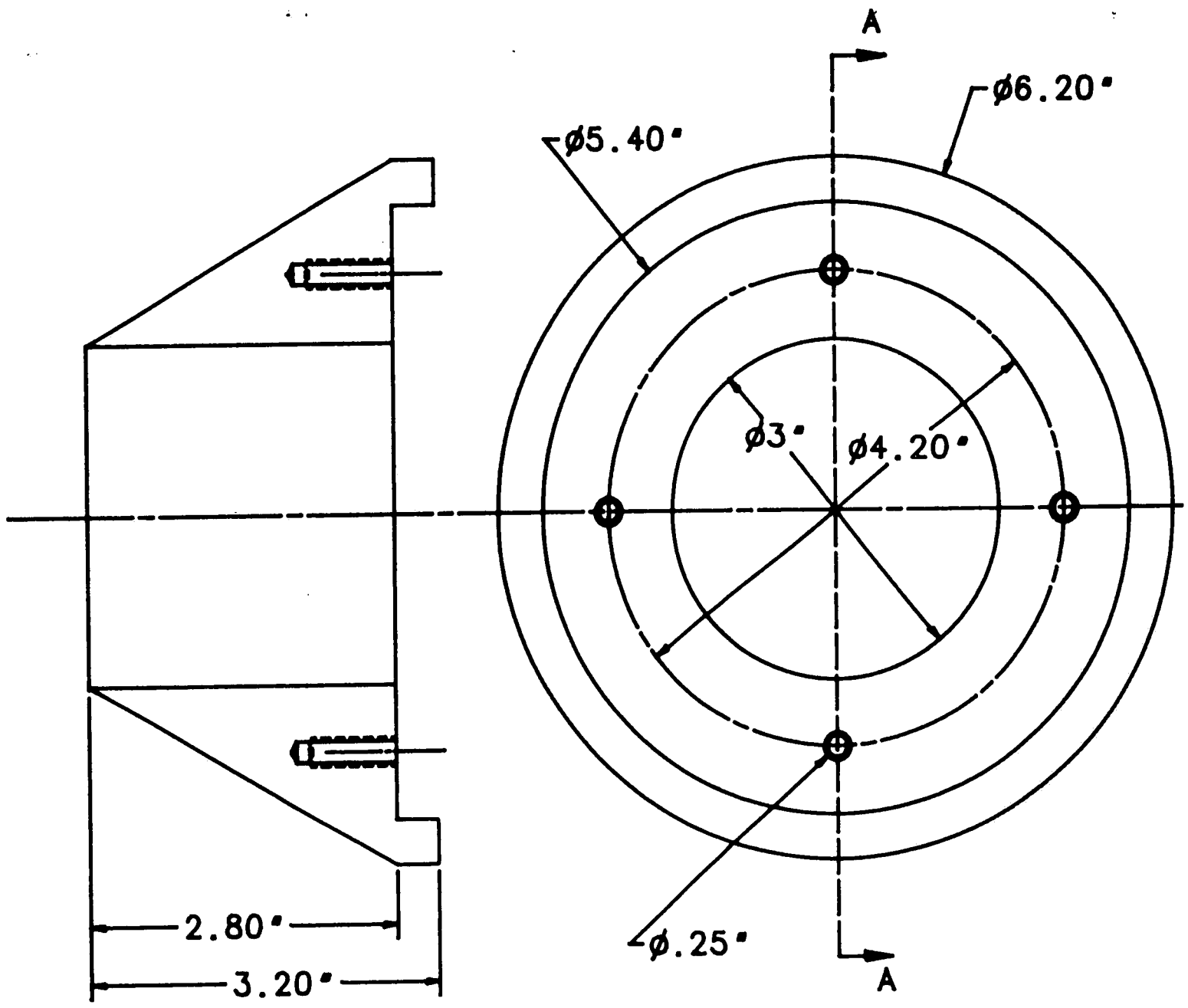

Sention A-A

DRAWING NO. G-7
BEARING CONE
SCALE: 1/2

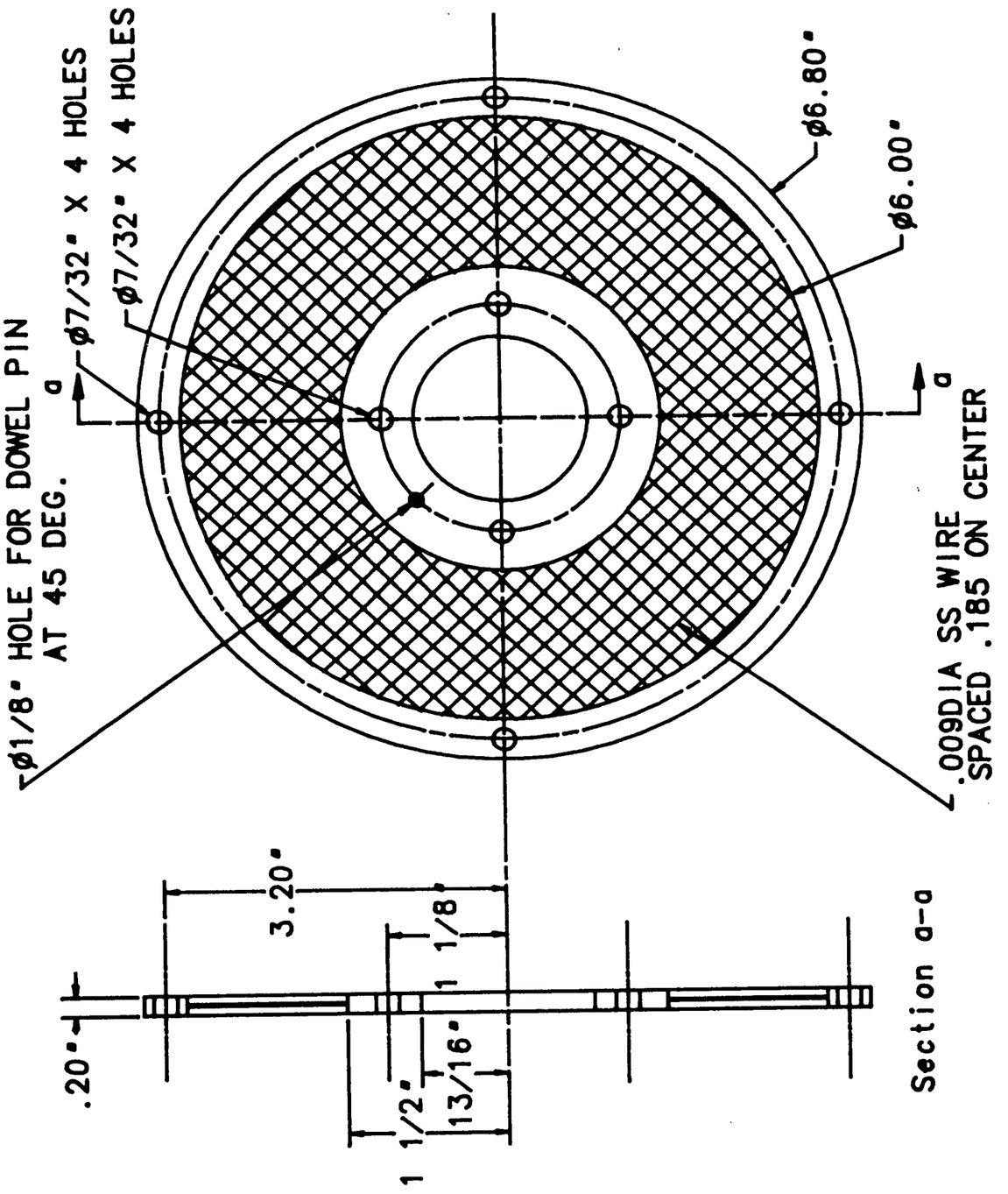

DRAWING NO. G-8
ANNULUS SCREEN
SCALE: 1/2

DRAWING NO. G-9
BODY
SCALE: 1/3

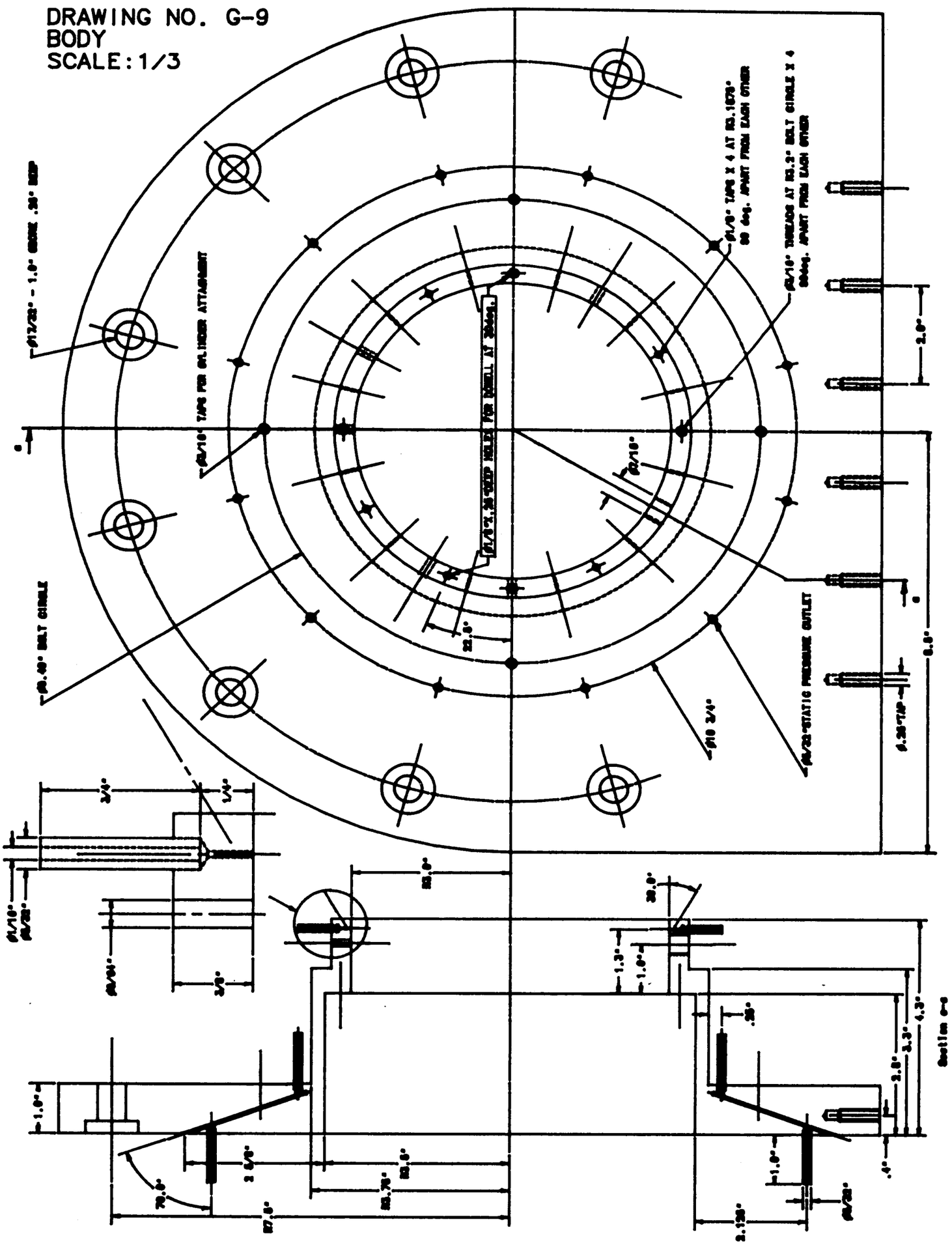

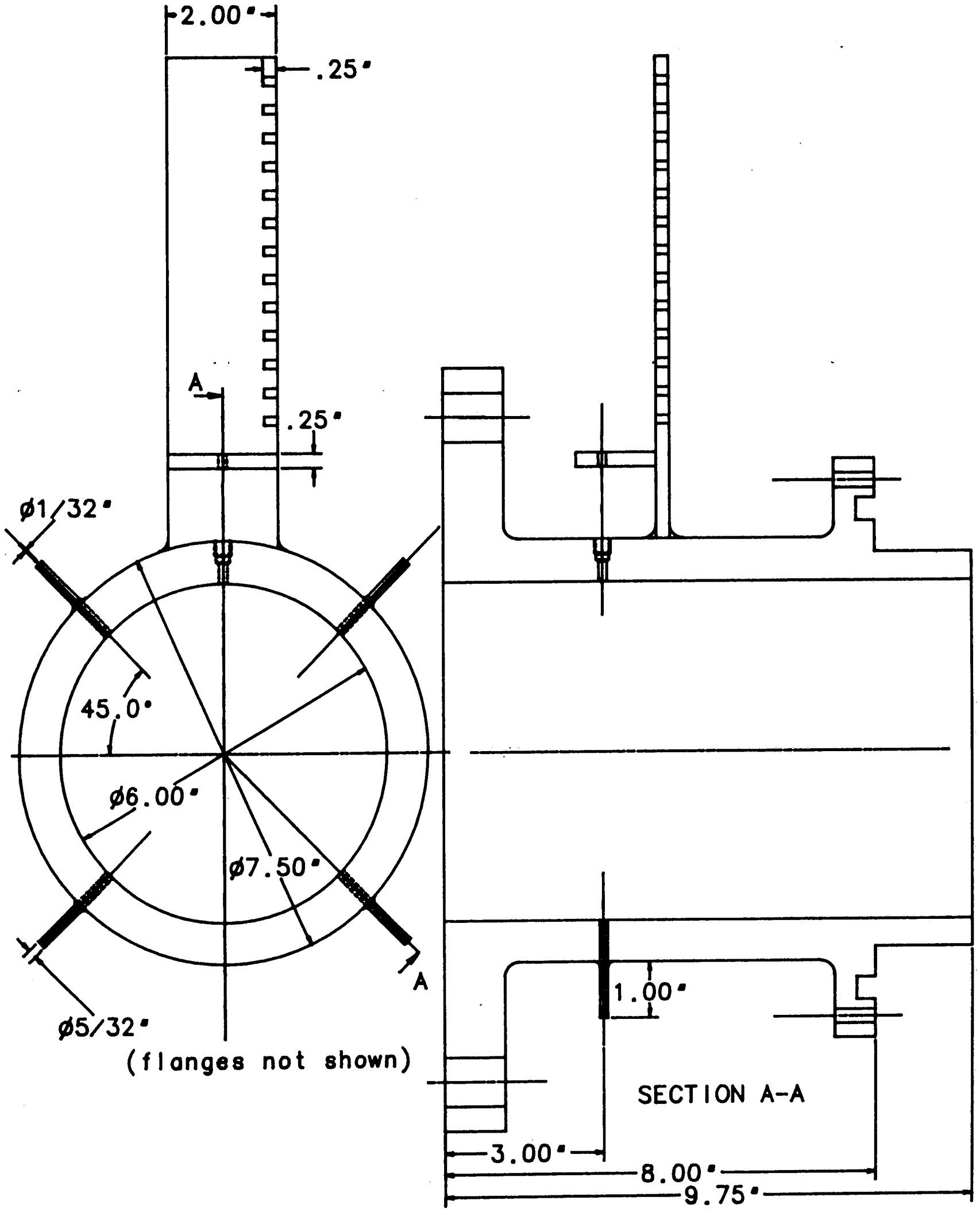

DRAWING NO. G-10A
UPSTREAM PIPE
SCALE:1/3

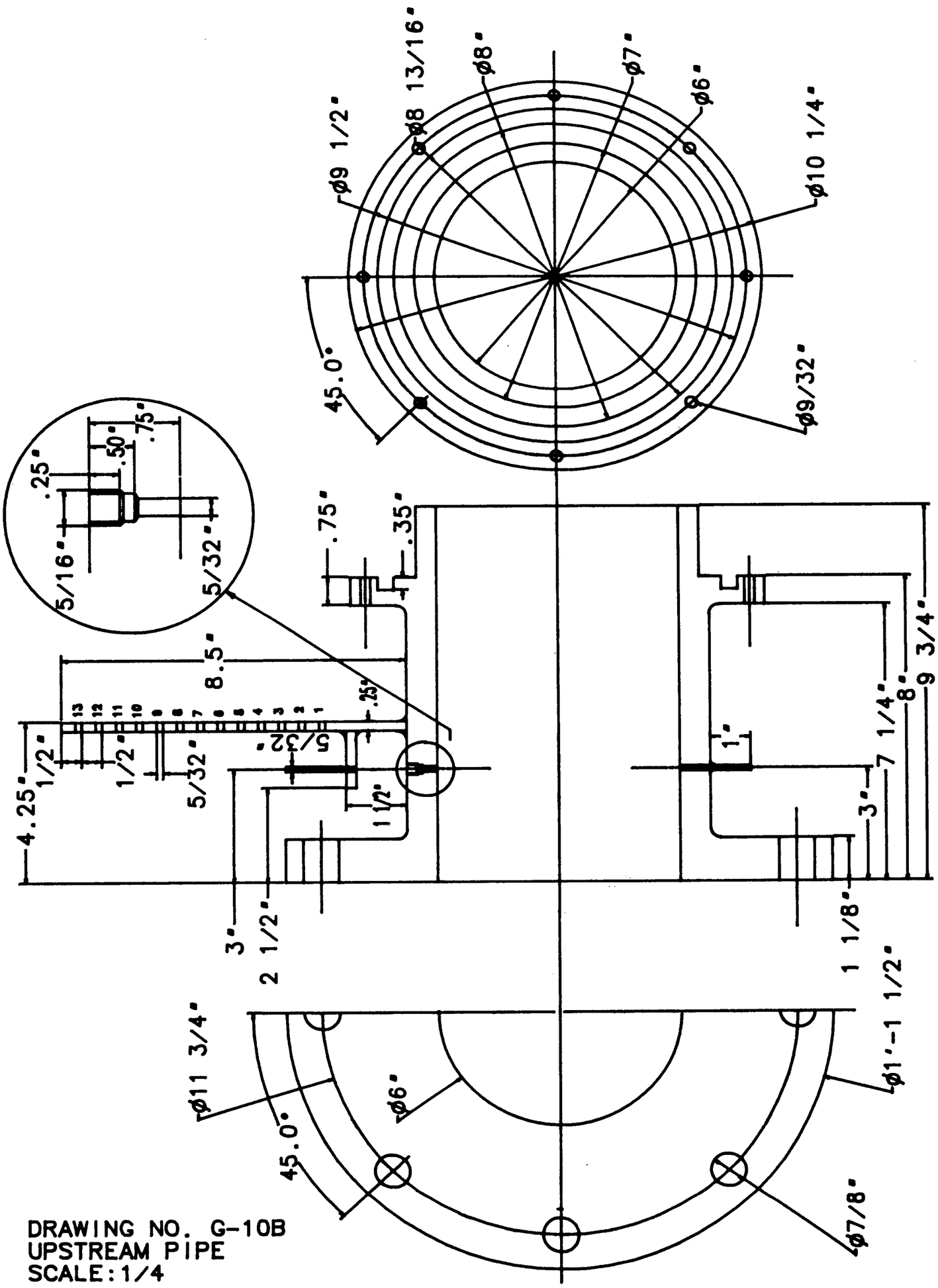

DRAWING NO. G-10B
UPSTREAM PIPE
SCALE: 1/4

DRAWING NO. G-11
SHELL
SCALE: 1/3

TAPS B, SG1, SG3, R1, C1 ALL 10-32 STANDARD

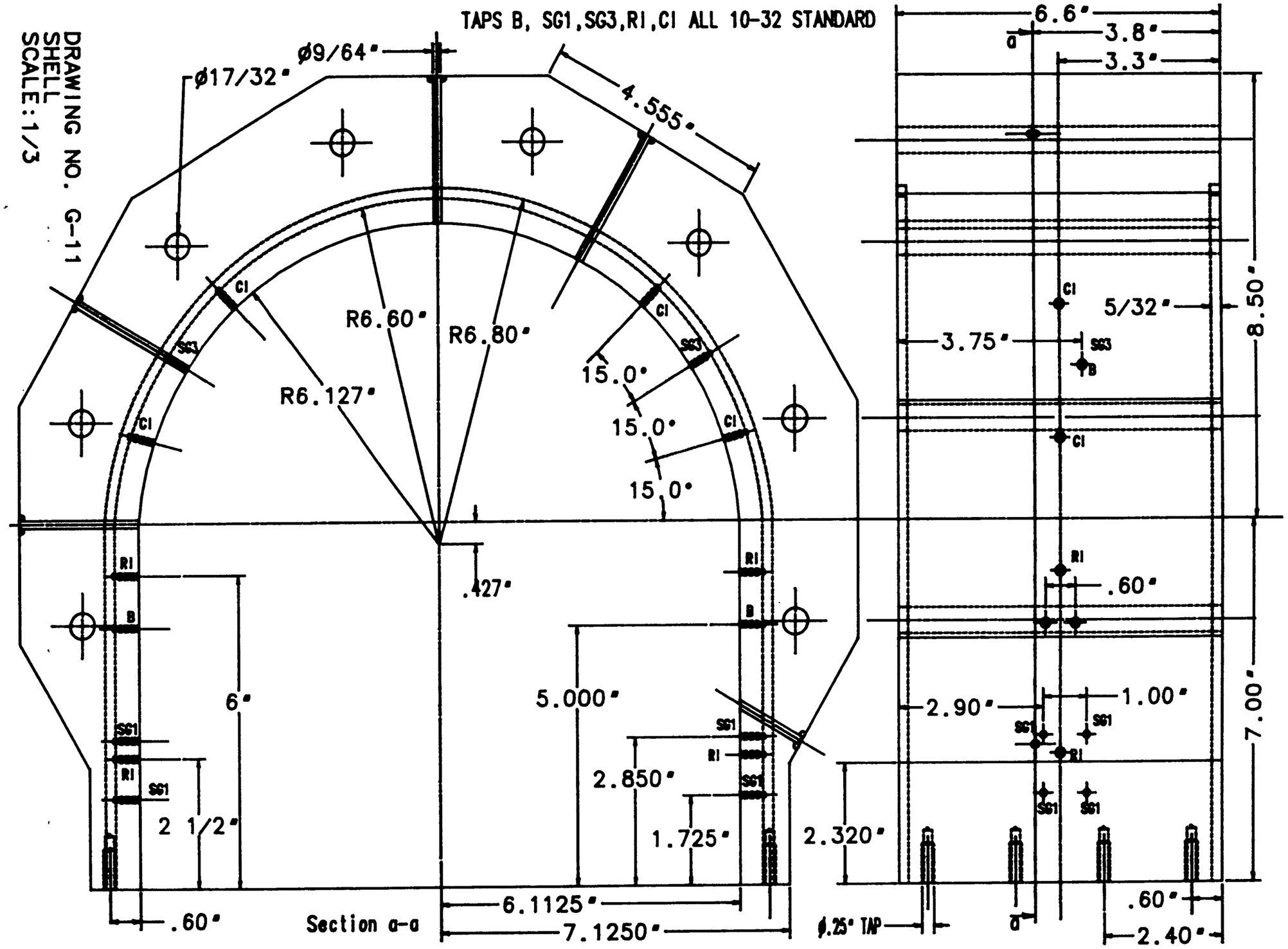

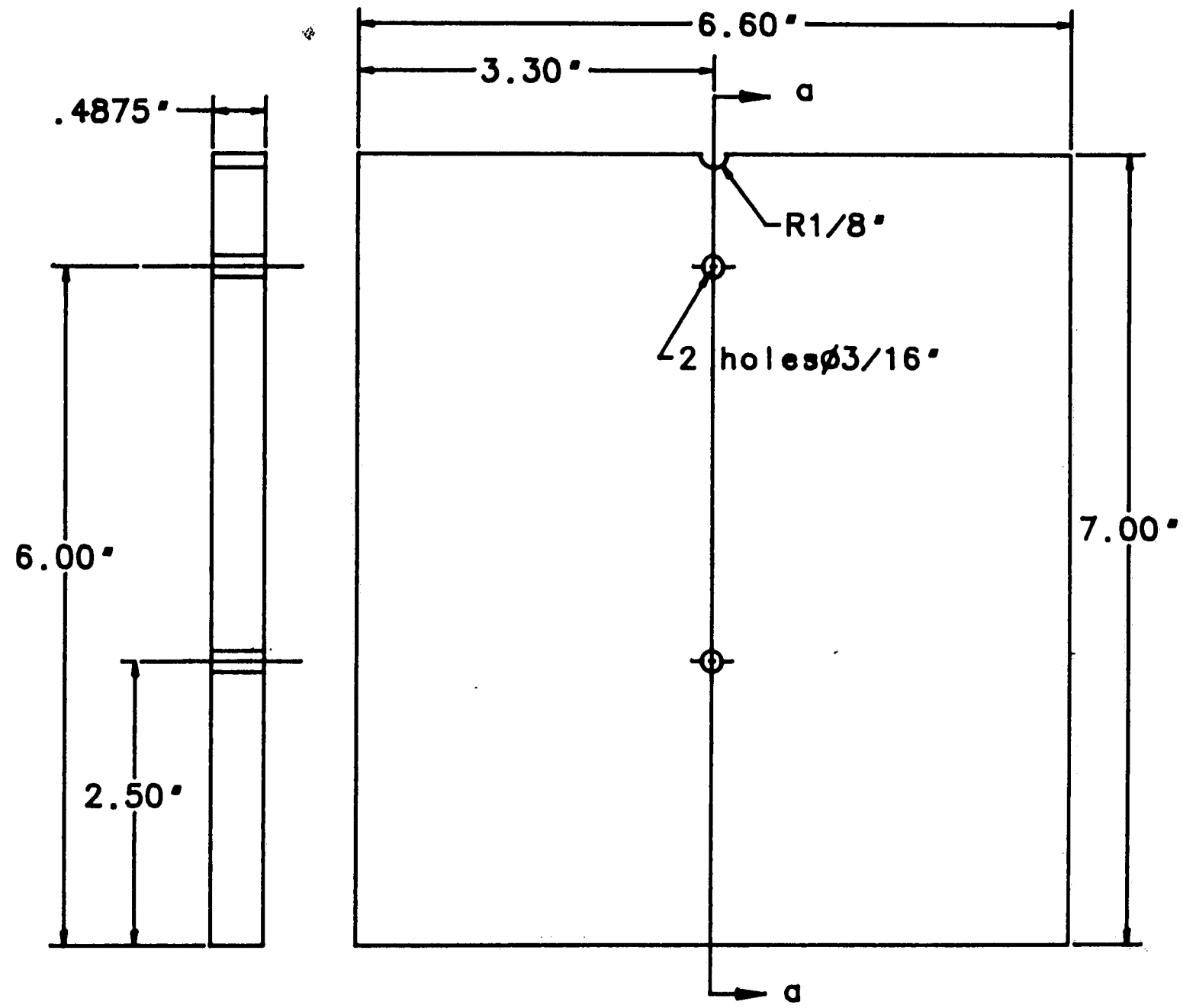

Section a-a

DRAWING NO. G-12A
INSERT TO CHANGE WIDTH
SCALE: 1/2

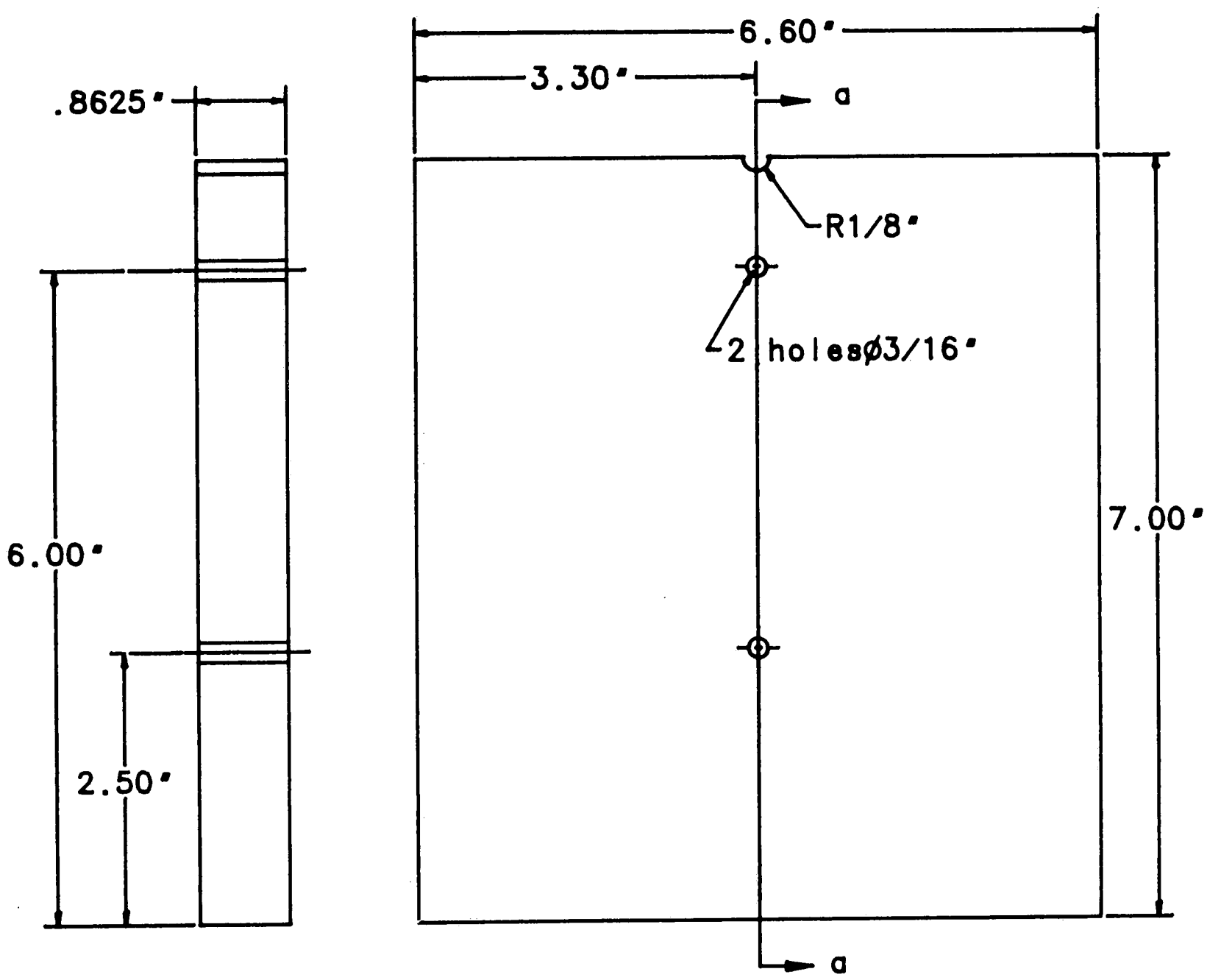

Section a-a

DRAWING NO. G-12B
INSERT TO CHANGE WIDTH
SCALE: 1/2

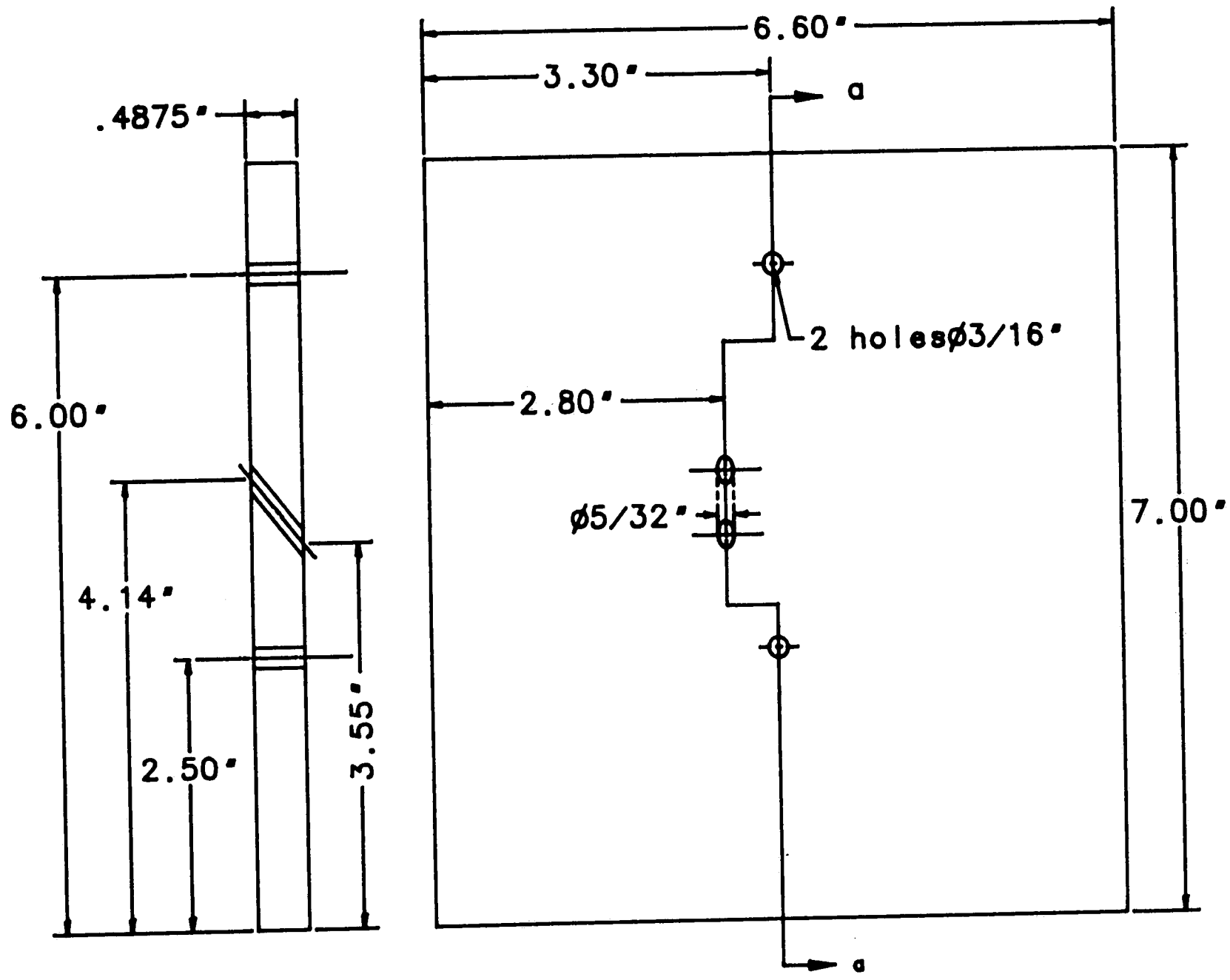

Section a-a

DRAWING NO. G-12C
INSERT TO CHANGE WIDTH
SCALE: 1/2

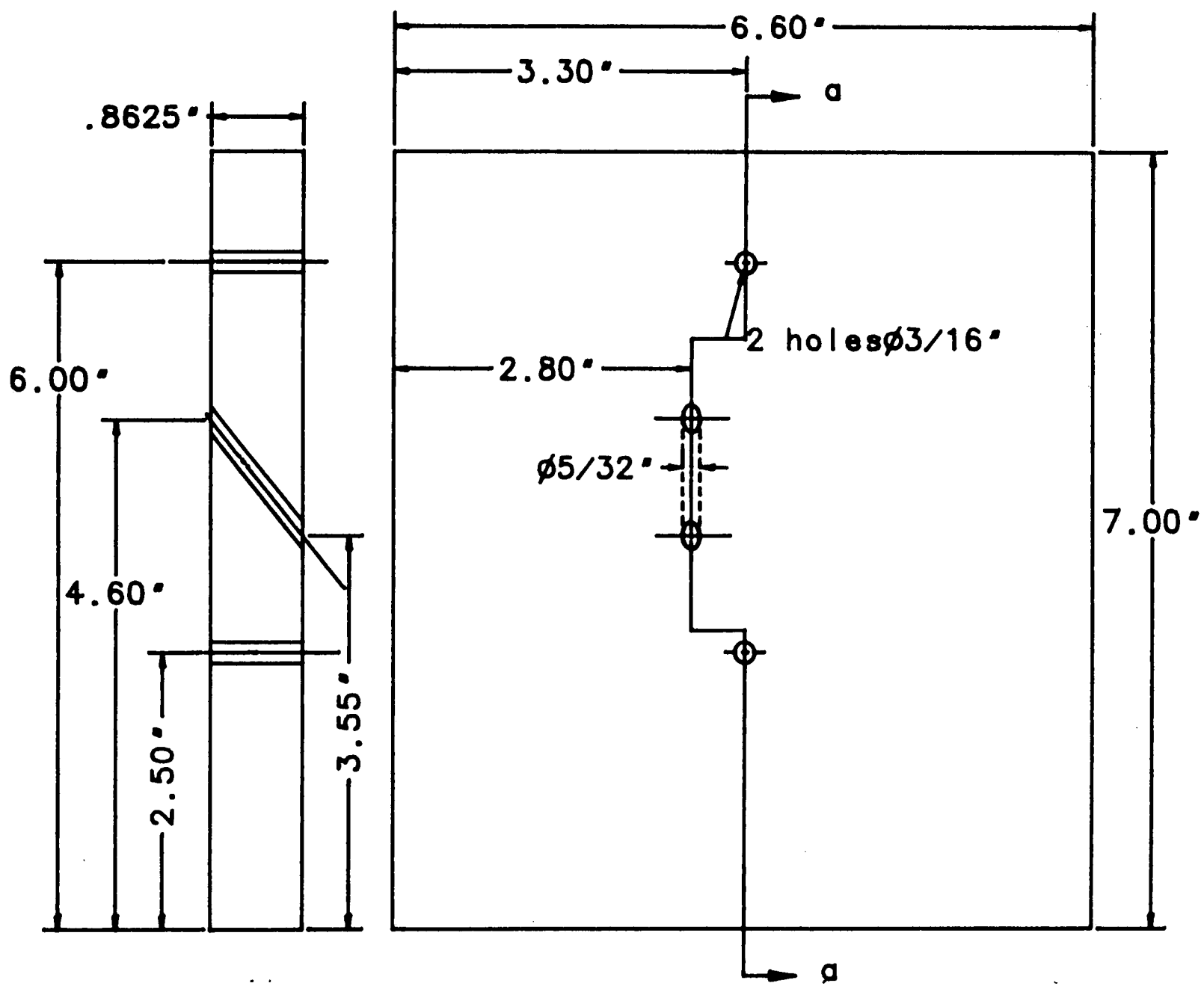

Section a-a

DRAWING NO. G-12D
INSERT TO CHANGE WIDTH
SCALE: 1/2

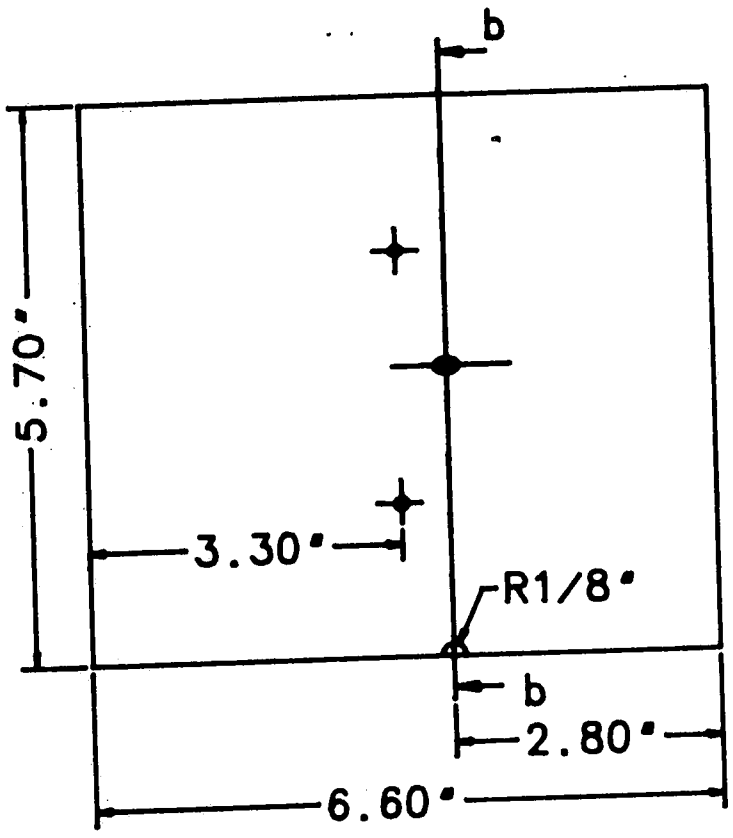

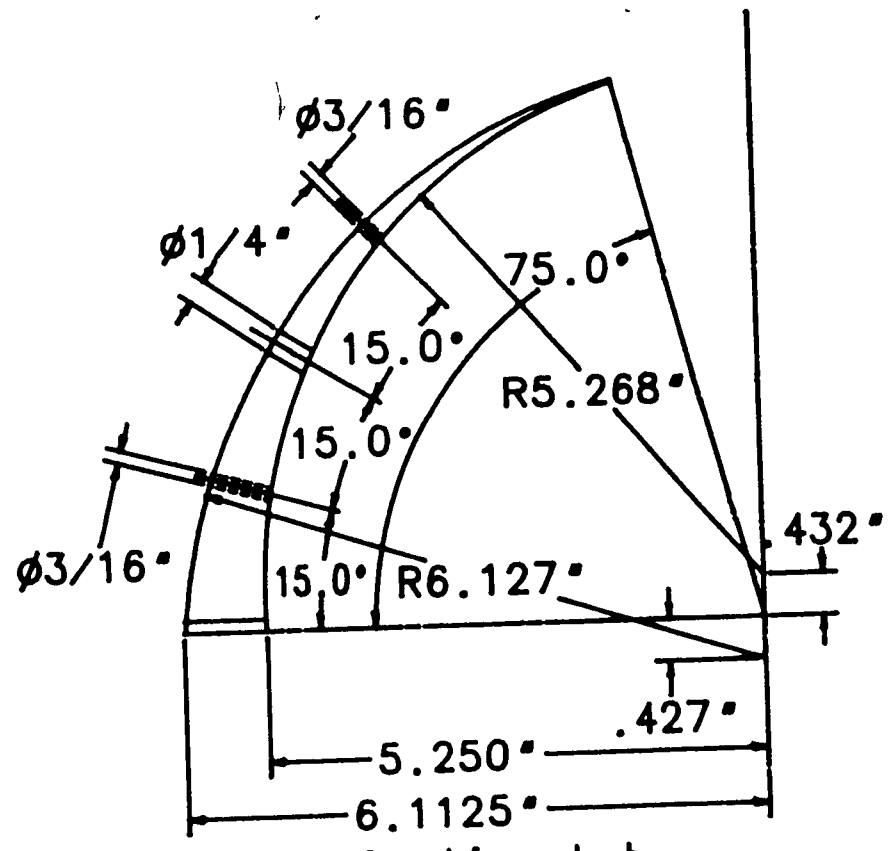

Section b-b

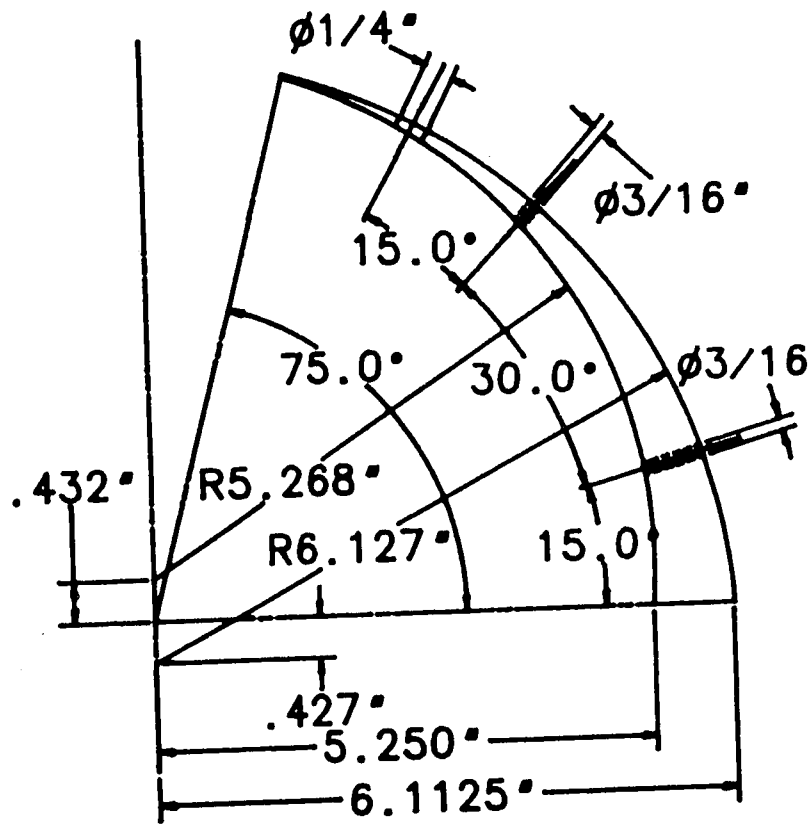

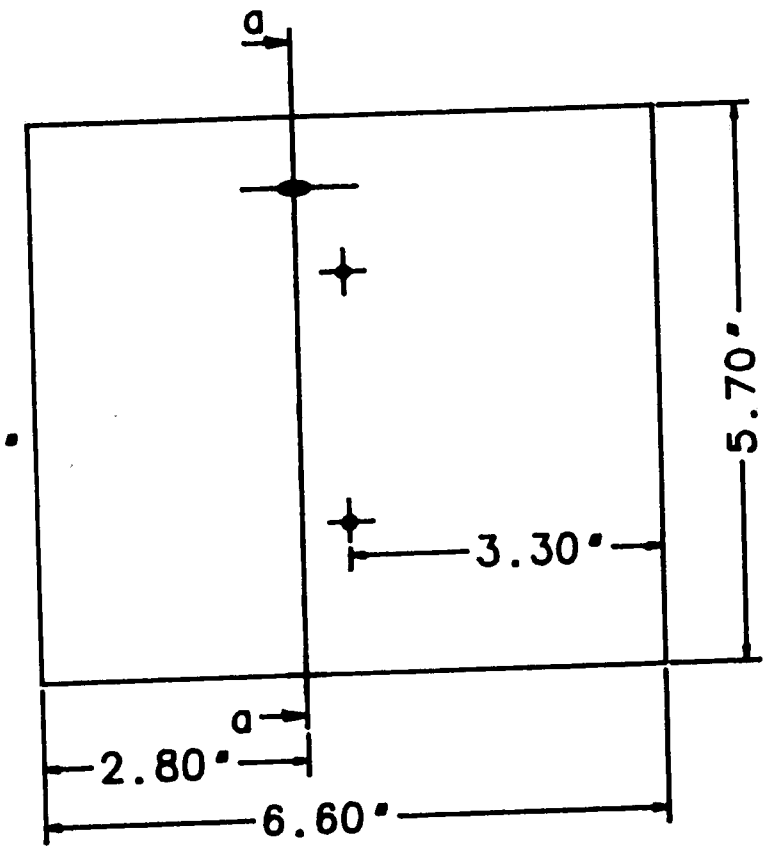

Section a-a

DRAWING NO. G-13A
INSERT TO CHANGE HEIGHT
SCALE:1/3

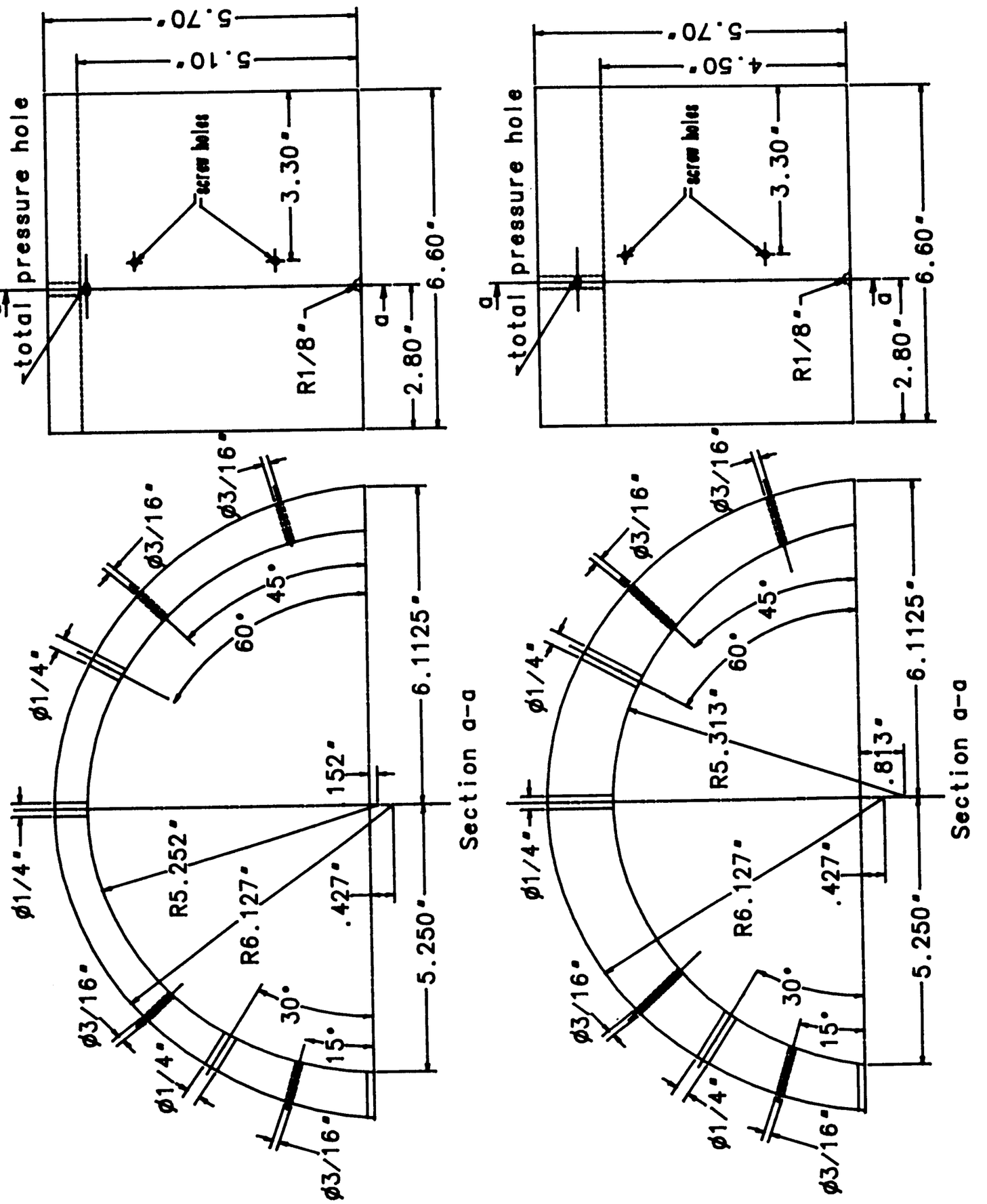

DRAWING NO. G13B
INSERTS TO CHANGE HEIGHT
SCALE: 1/3

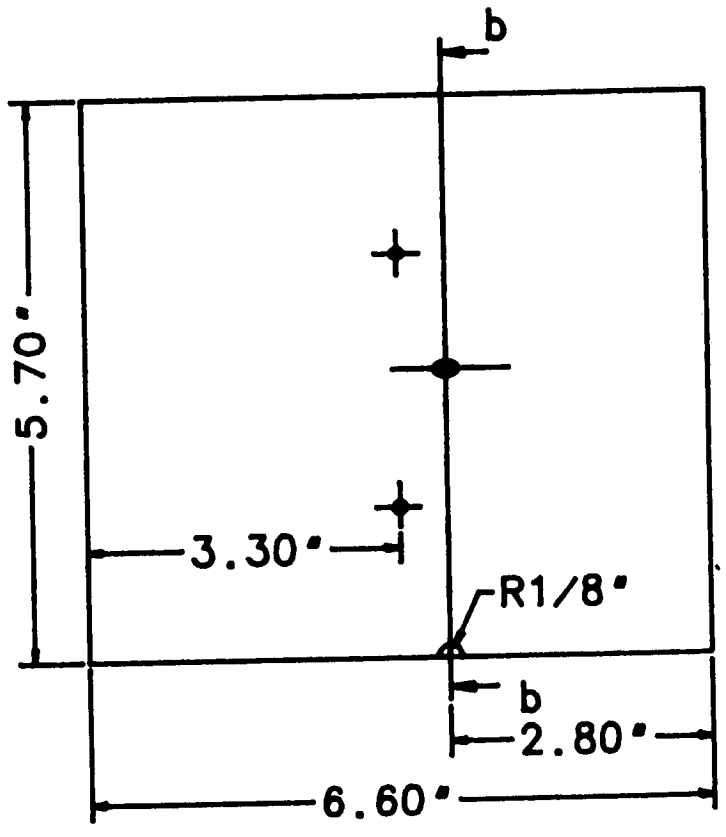

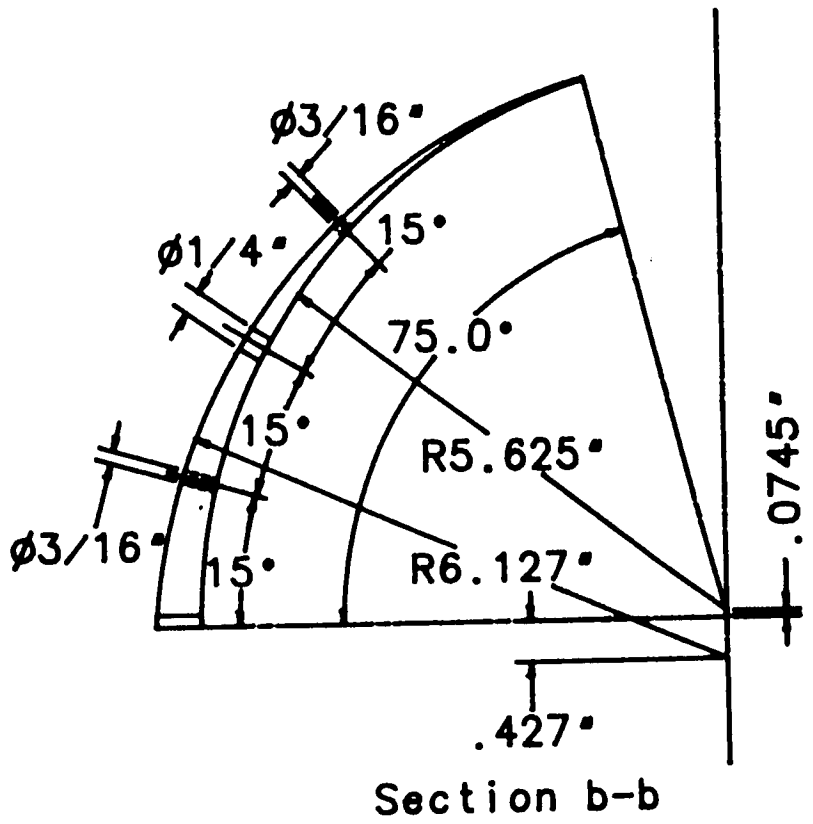

Section b-b

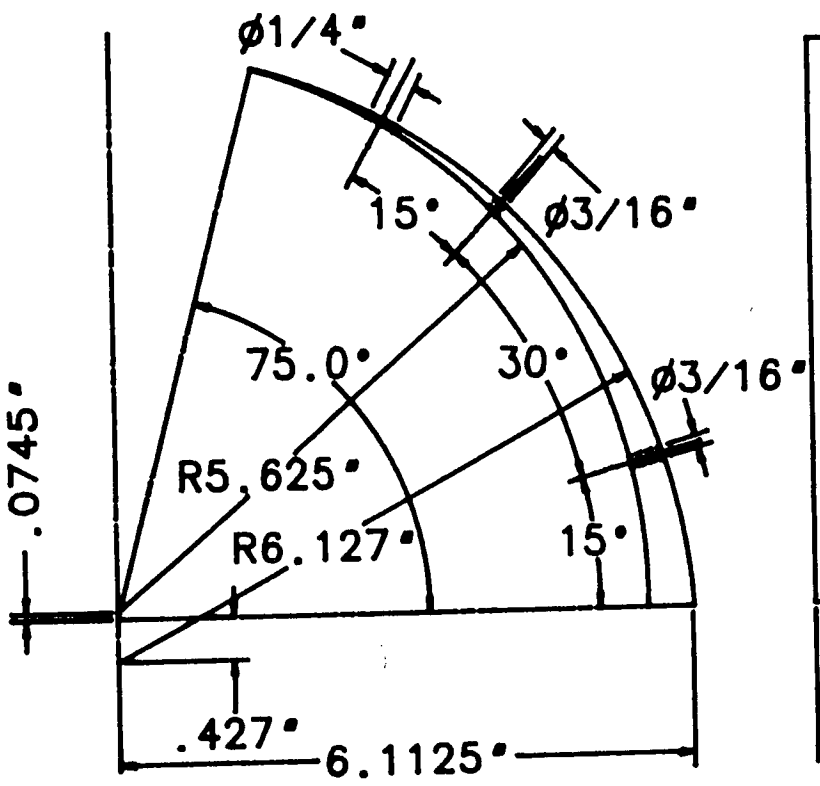

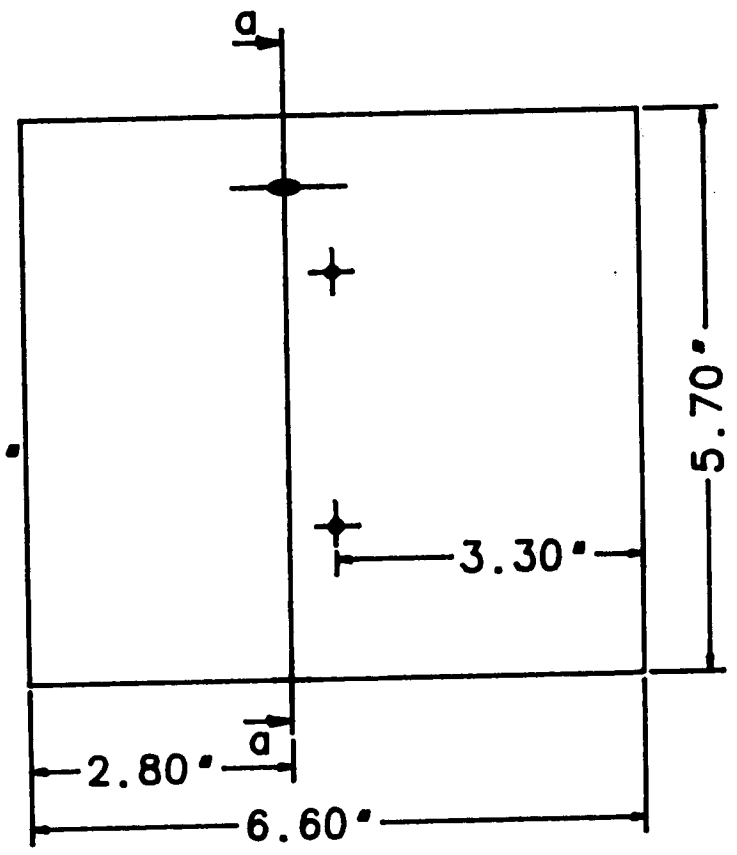

Section a-a

DRAWING NO. G13C
INSERTS TO CHANGE HEIGHT
SCALE: 1/3

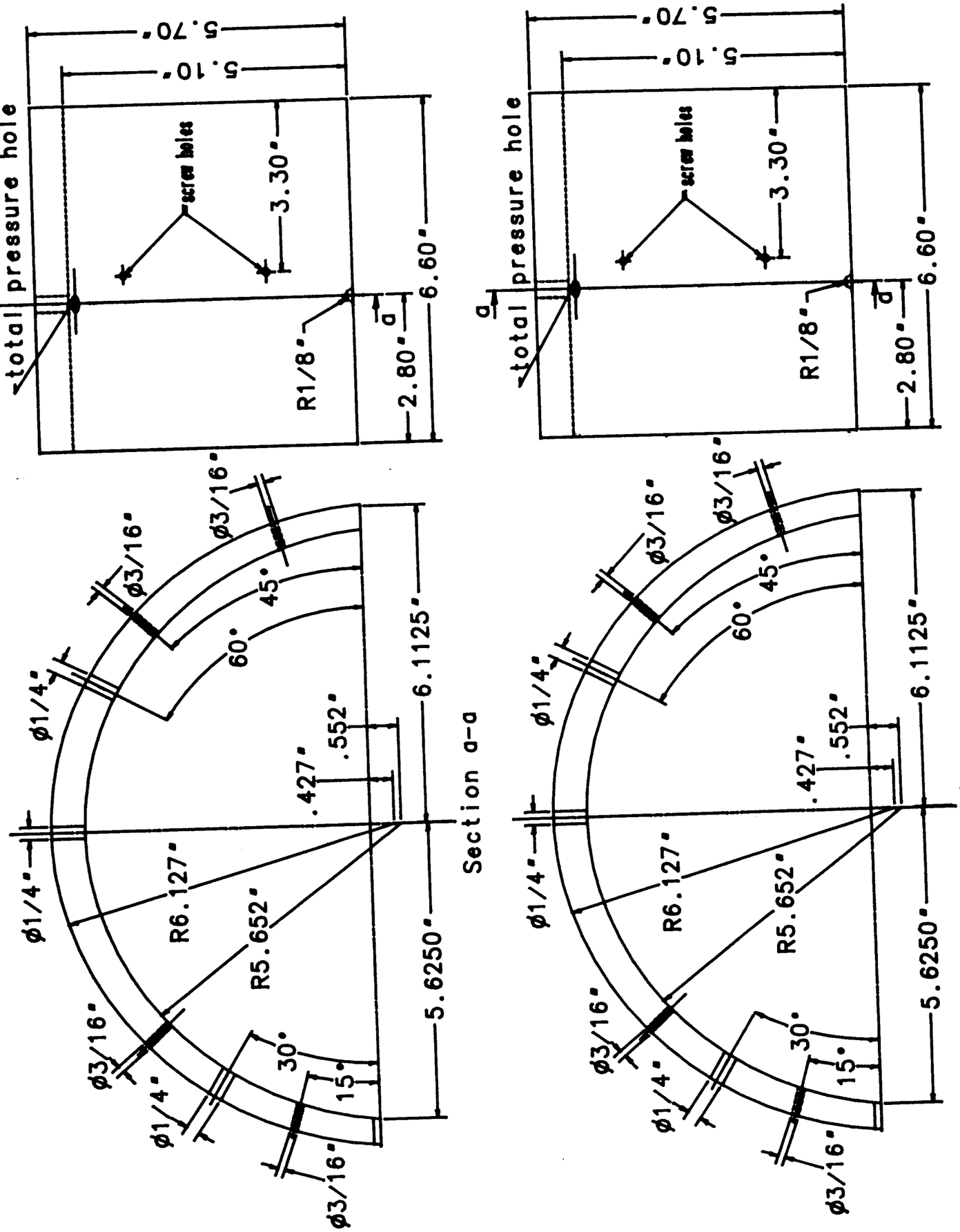

DRAWING NO. G-13D
INSERTS TO CHANGE HEIGHT
SCALE: 1/3

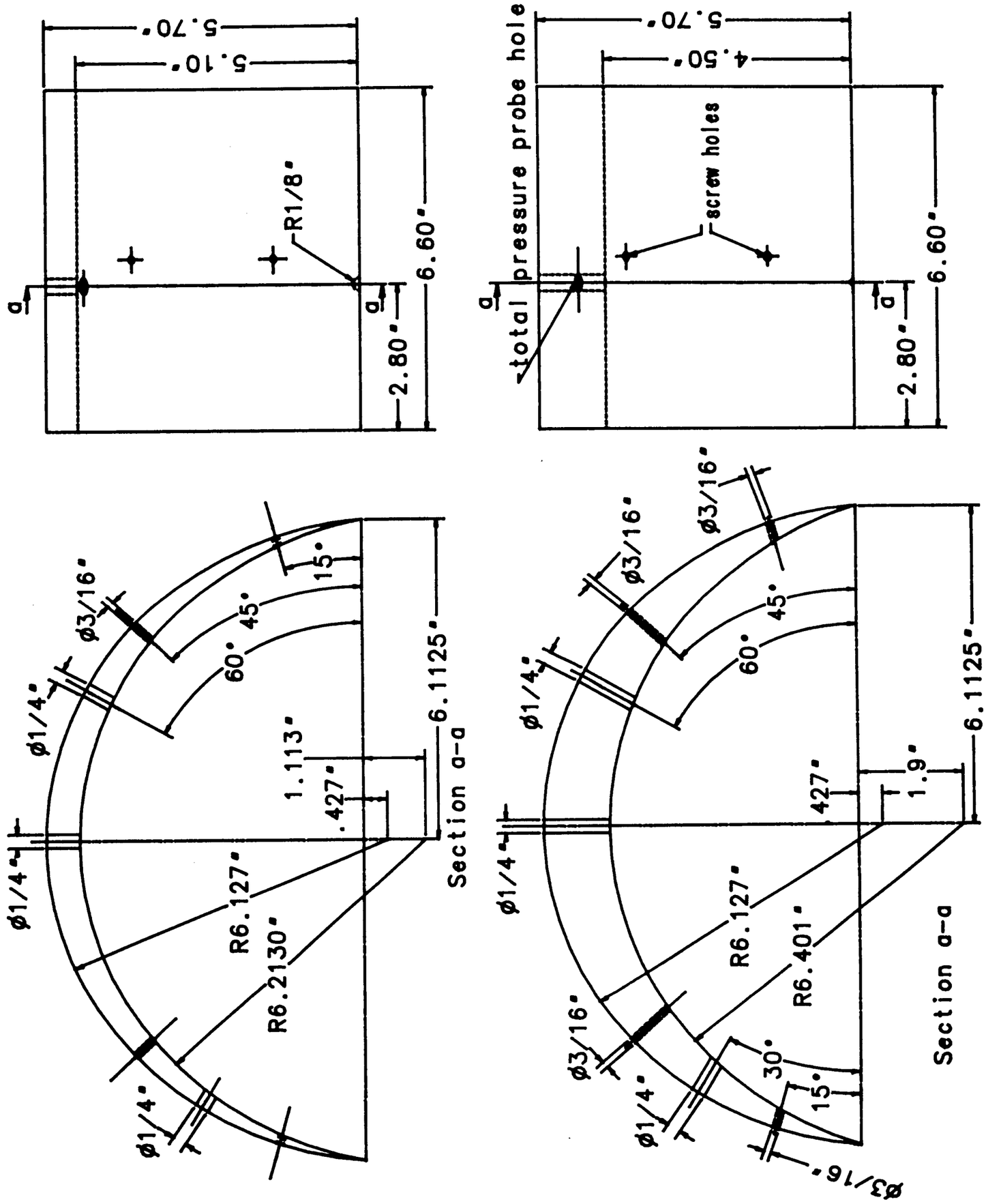

DRAWING NO. G-13E
INSERTS TO CHANGE HEIGHT
SCALE: 1/3

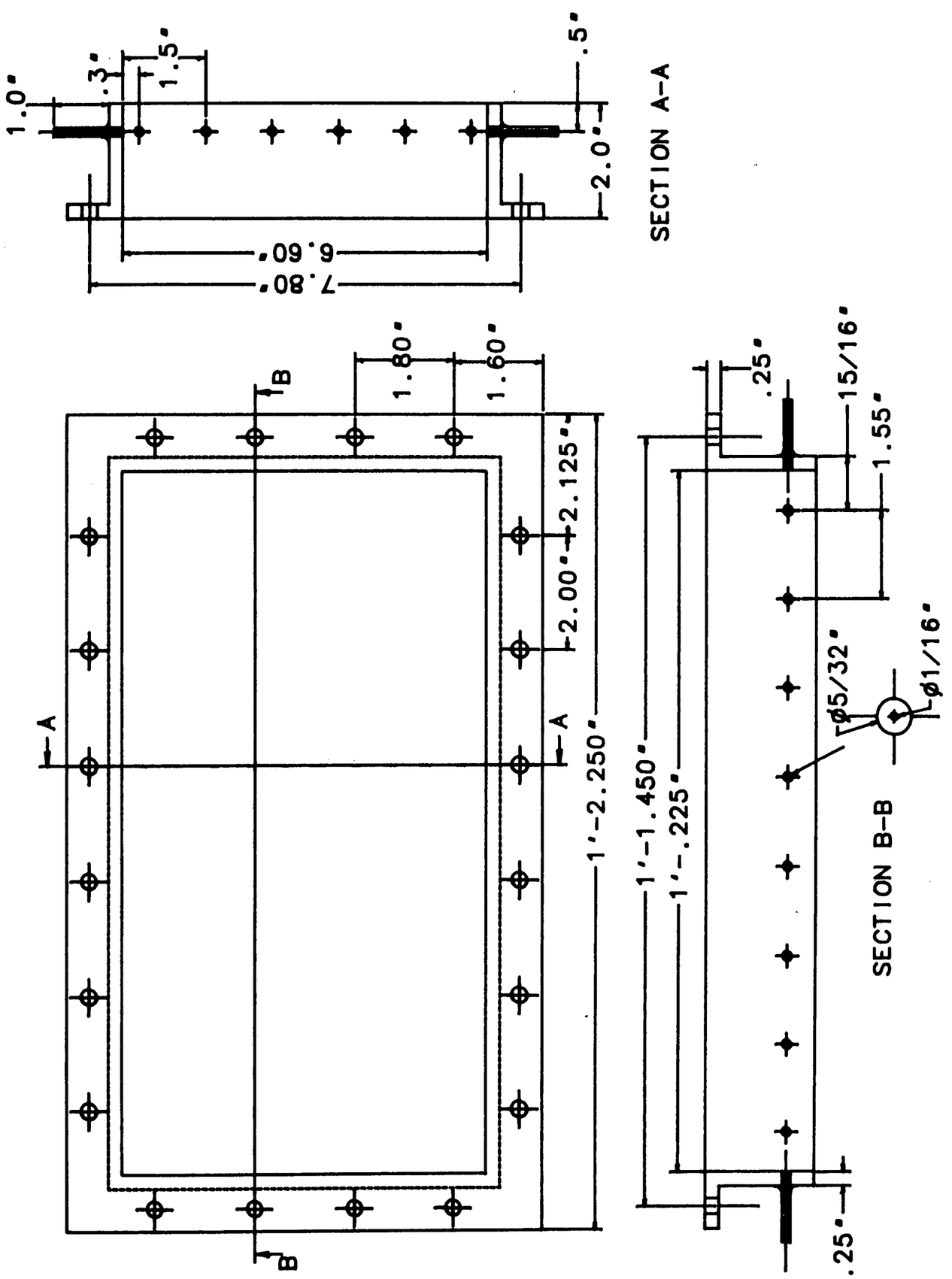

DRAWING NO. G-14A
OUTLET DUCT FOR D/L-8.15
SCALE:1/3

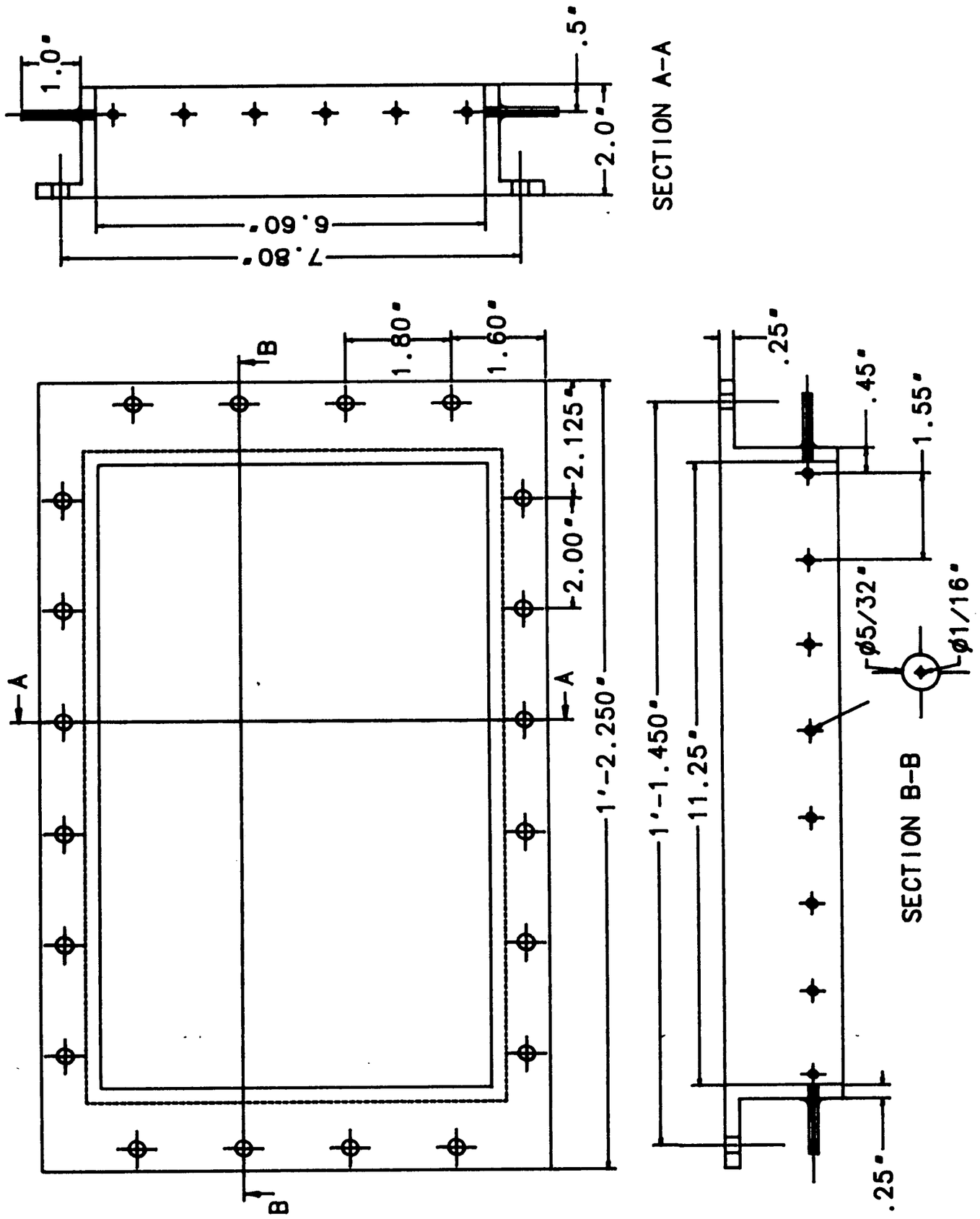

DRAWING NO. G-14B
OUTLET DUCT FOR D/L-7.5
SCALE: 1/3

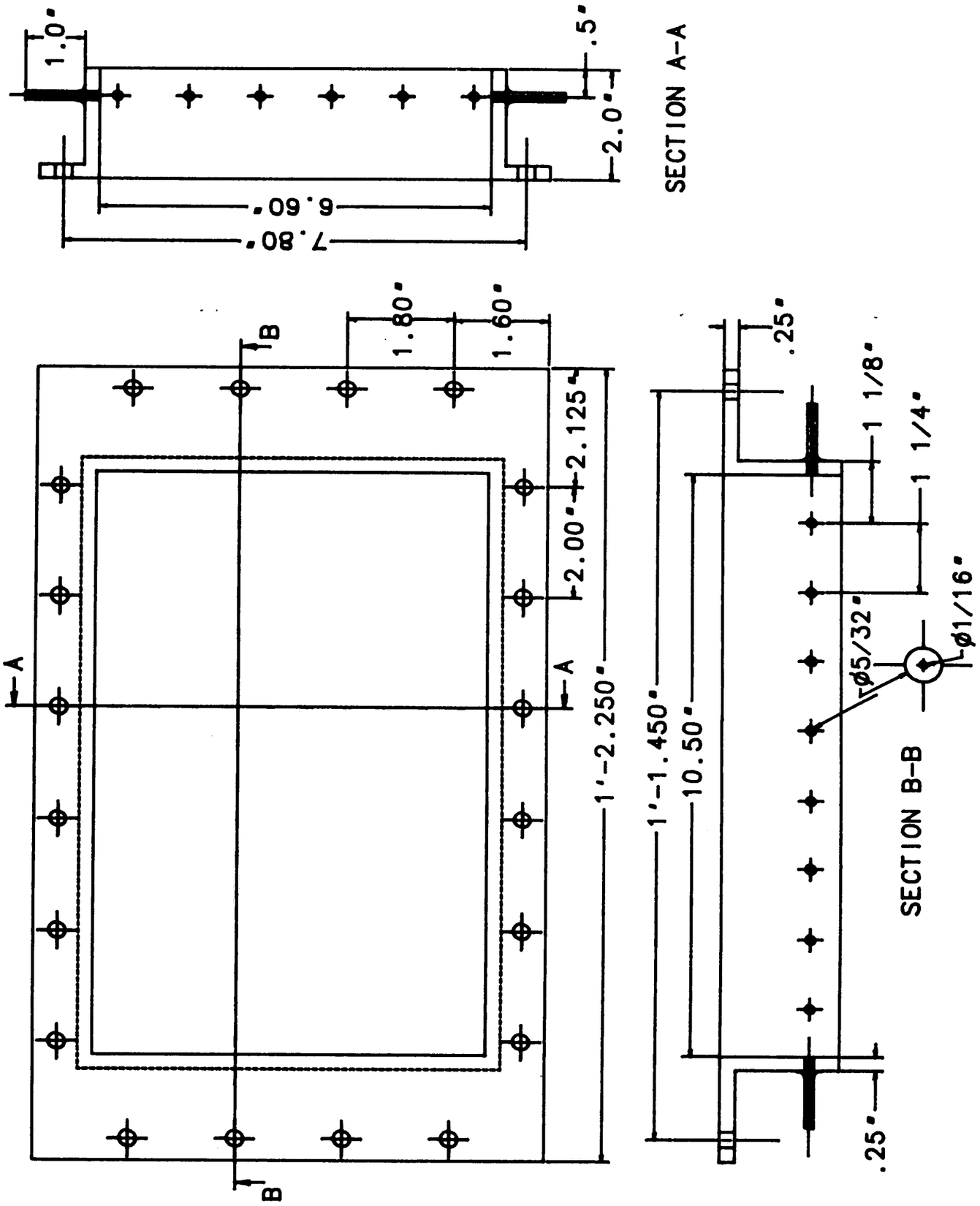

DRAWING NO. G-14C
OUTLET DUCT FOR D/L-7.0
SCALE: 1/3

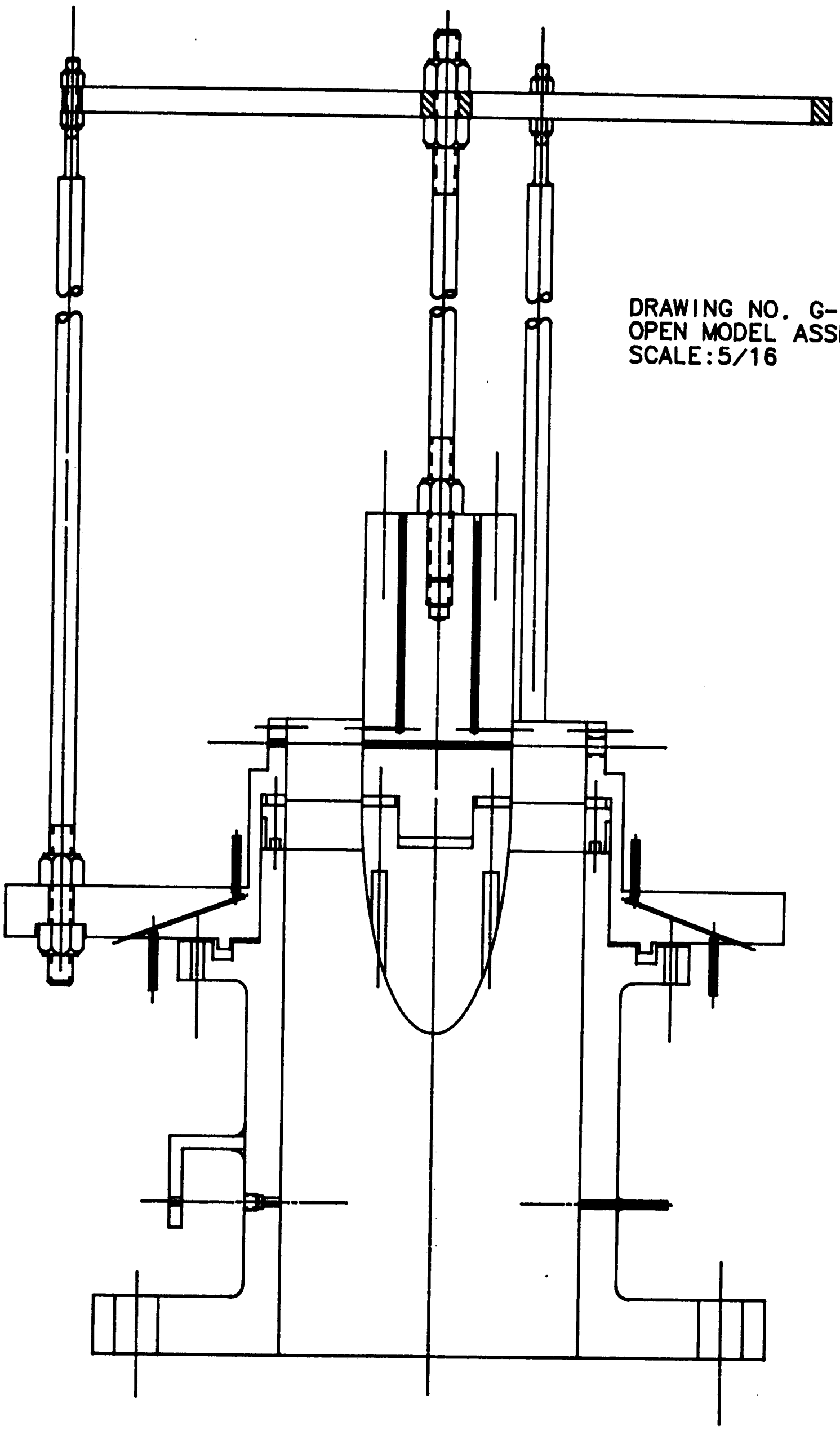

DRAWING NO. G-15
OPEN MODEL ASSEMBLY
SCALE:5/16

APPENDIX H—Hatfield Ferry Unit Drawings

H—1A	Condenser neck plan view
H—1B	Condenser neck (section A—A)
H—1C	Condenser neck (section B—B)

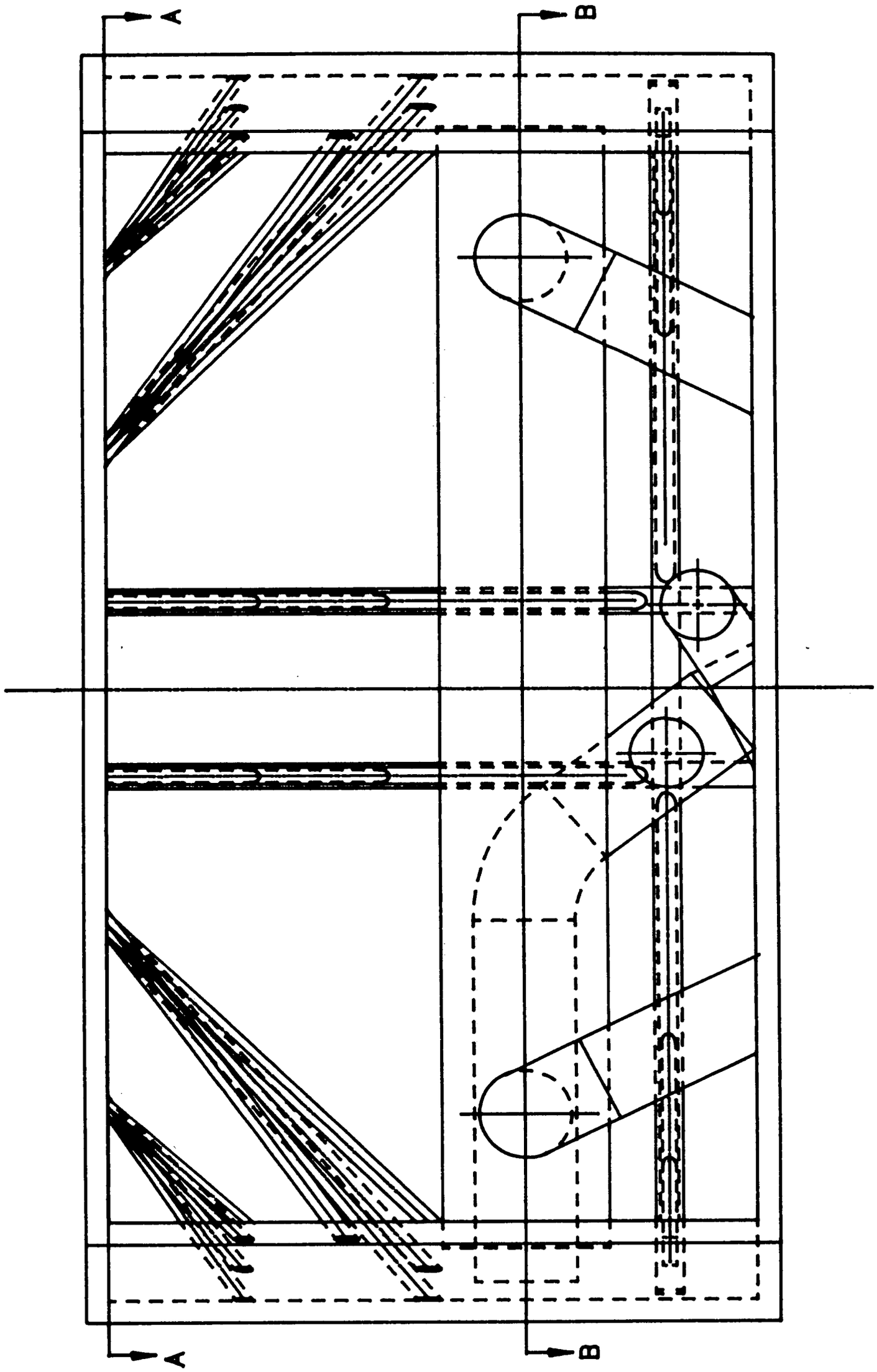

DRAWING NO. H-1A
CONDENSER NECK (PLAN VIEW)
SCALE: 1/2

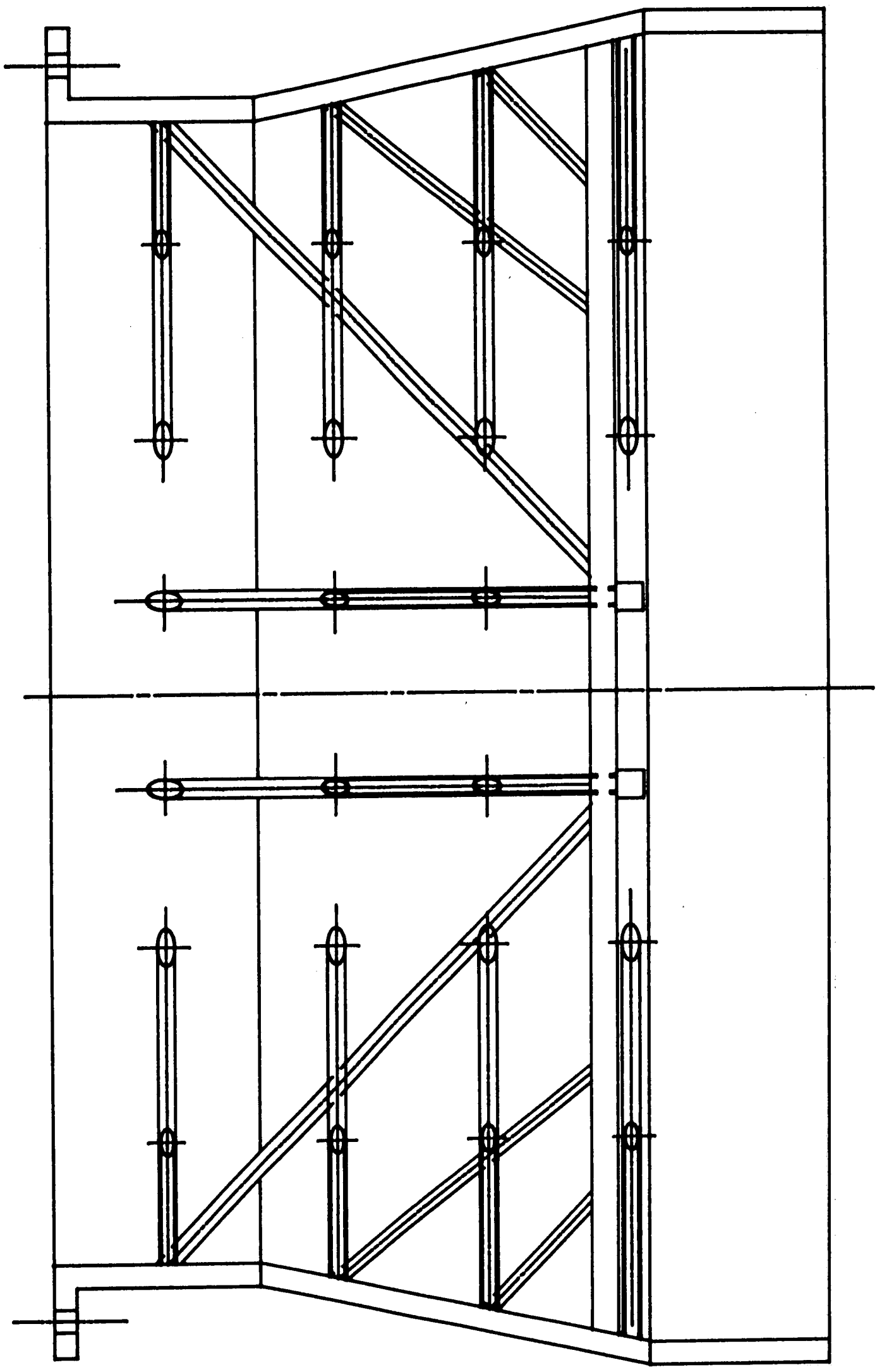

DRAWING NO. H-1B
CONDENSER NECK (SECTION A-A)
SCALE: 1/2

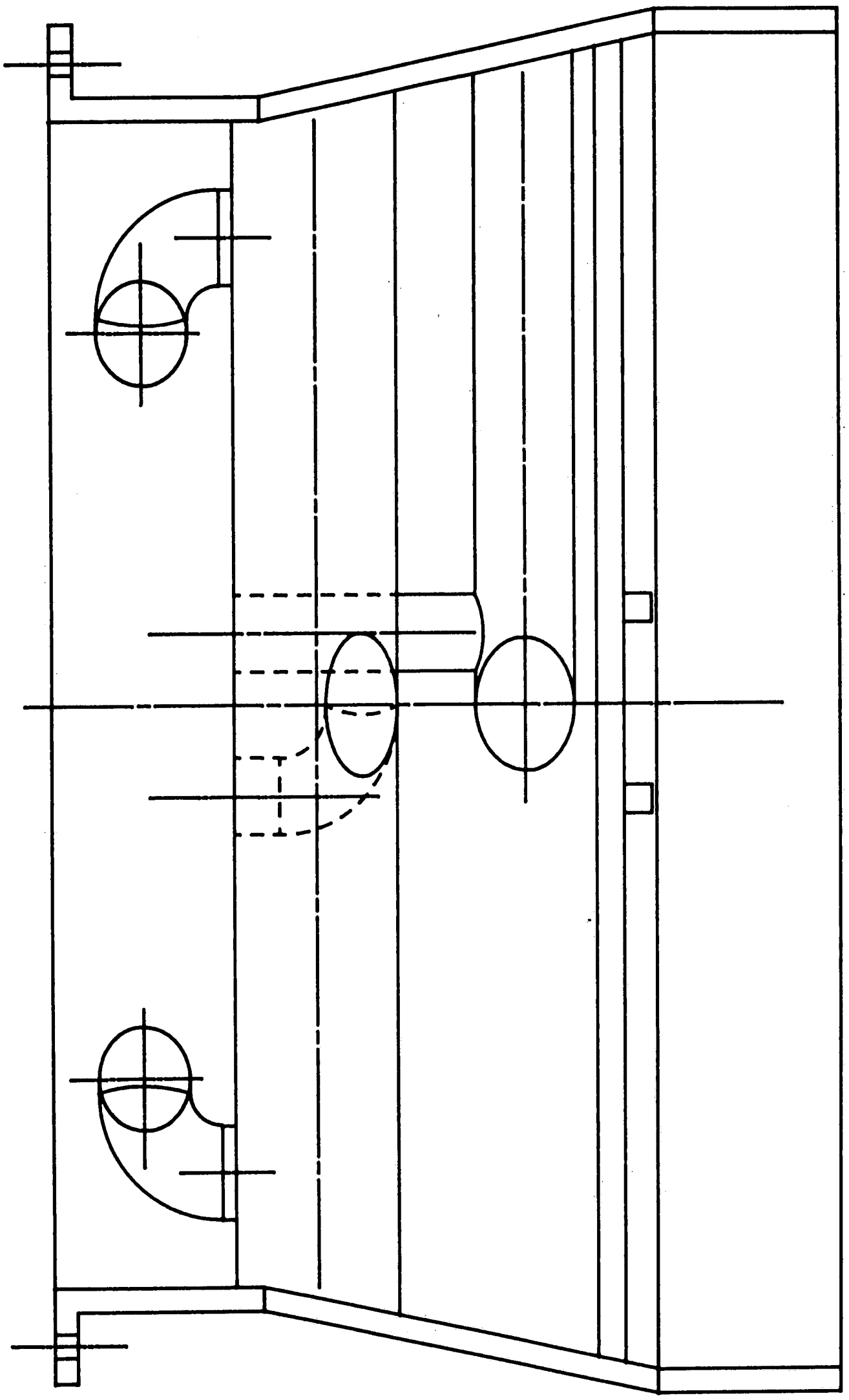

DRAWING NO. H-1C
CONDENSER NECK (SECTION B-B)
SCALE: 1/2

APPENDIX I—Beaver Valley Unit Drawings

BV—1A	Assembly (elevation)
BV—1B	Assembly (plan view)
BV—1C	Side view (section A—A)
BV—1D	Side view (section B—B)
BV—2A	Condenser neck (struts only)
BV—2B	Condenser neck (steam dumps only)
BV—3	Guide vane
BV—4	Bearing cone
BV—5	Insert to change height
BV—6	Insert to change length
BV—7	Outlet duct
BV—8	Extraction piping
BV—9	Strut group 1
BV—10	Strut group 2
BV—11	Strut group 3

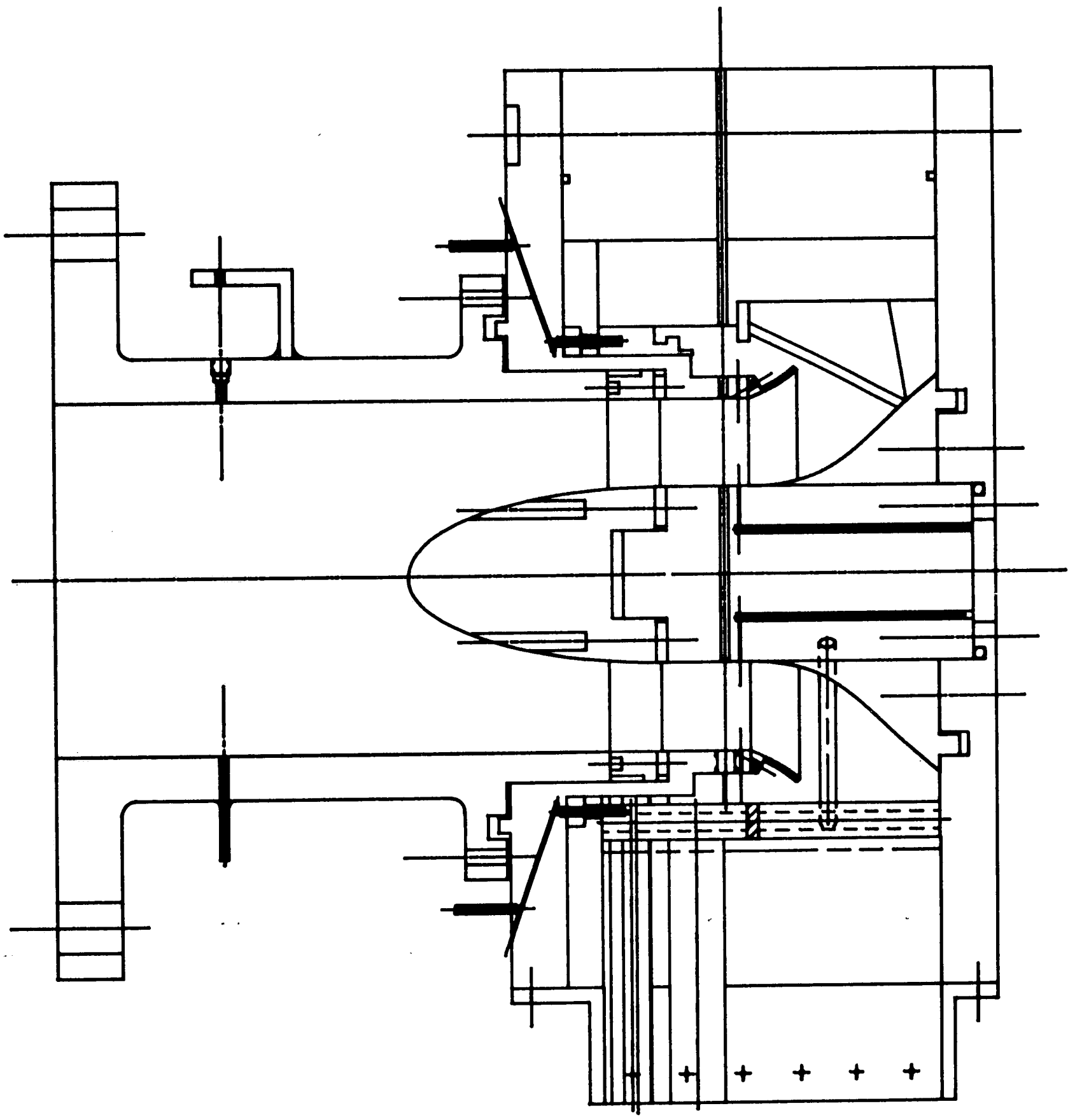

DRAWING NO. BV-1A
ASSEMBLY (ELEVATION VIEW)
SCALE:5/16

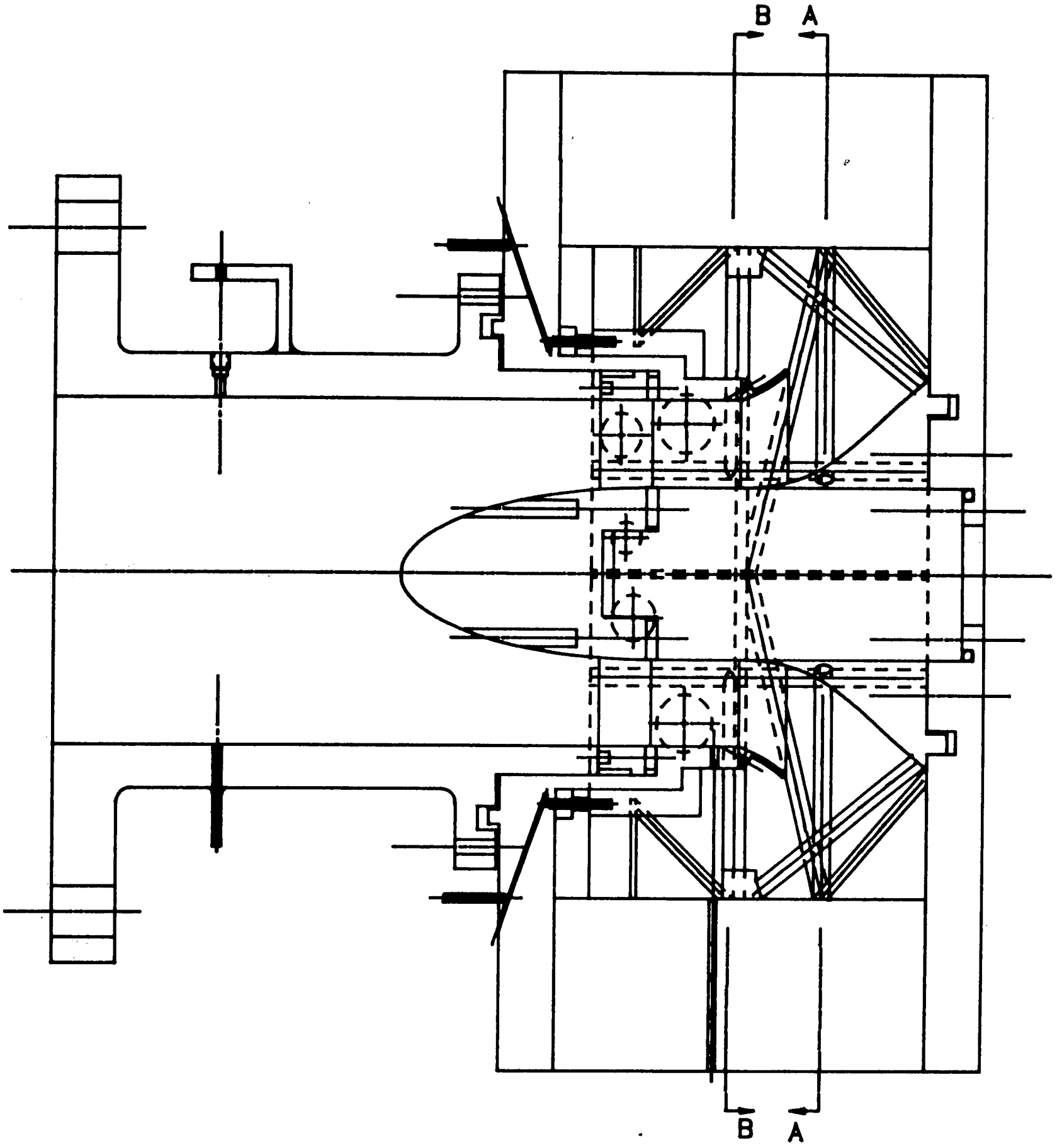

DRAWING NO. BV-1B
ASSEMBLY (PLAN VIEW)
SCALE:5/16

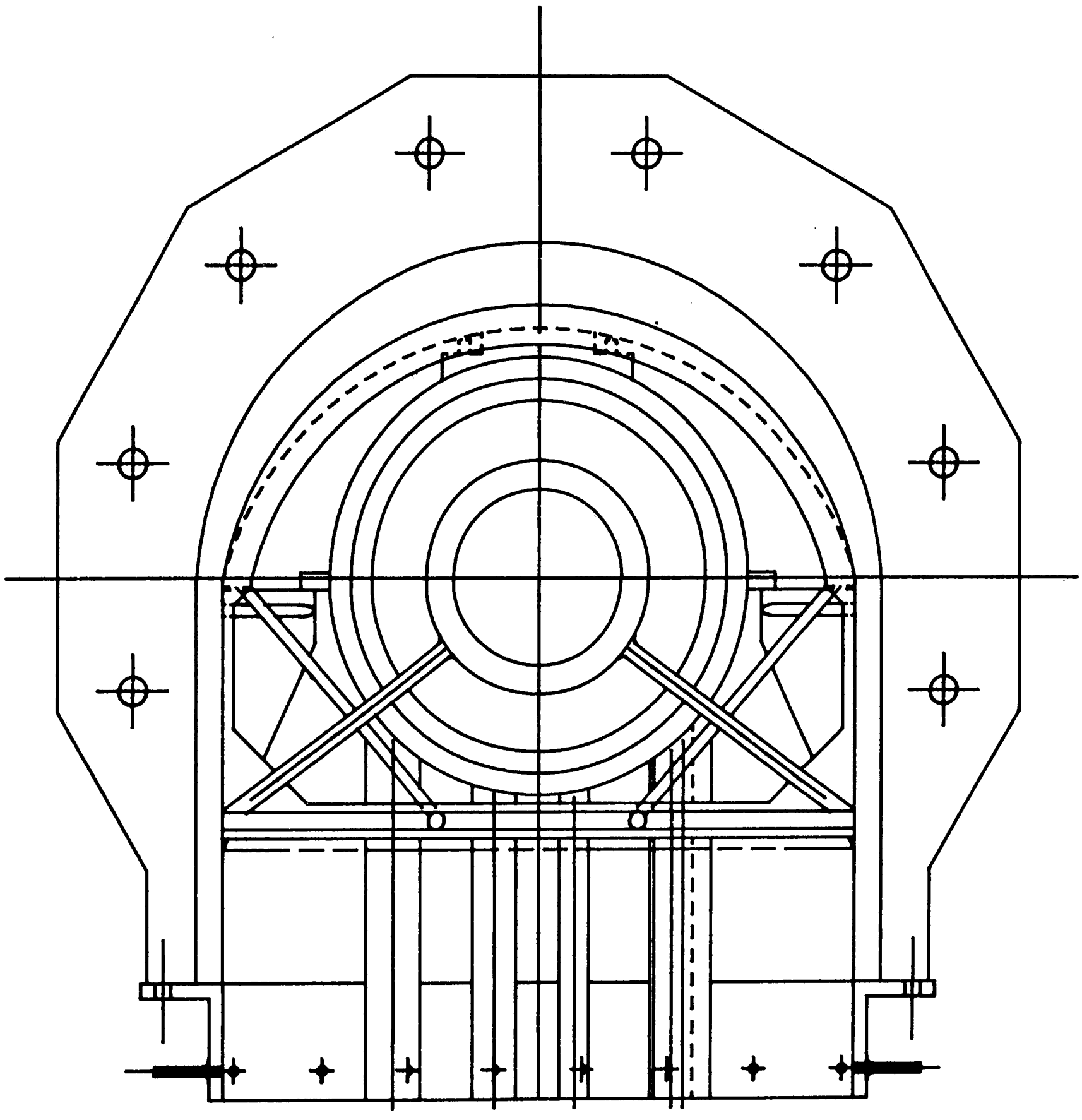

DRAWING NO. BV-1C
SIDE VIEW (SECTION A-A)
SCALE:5/16

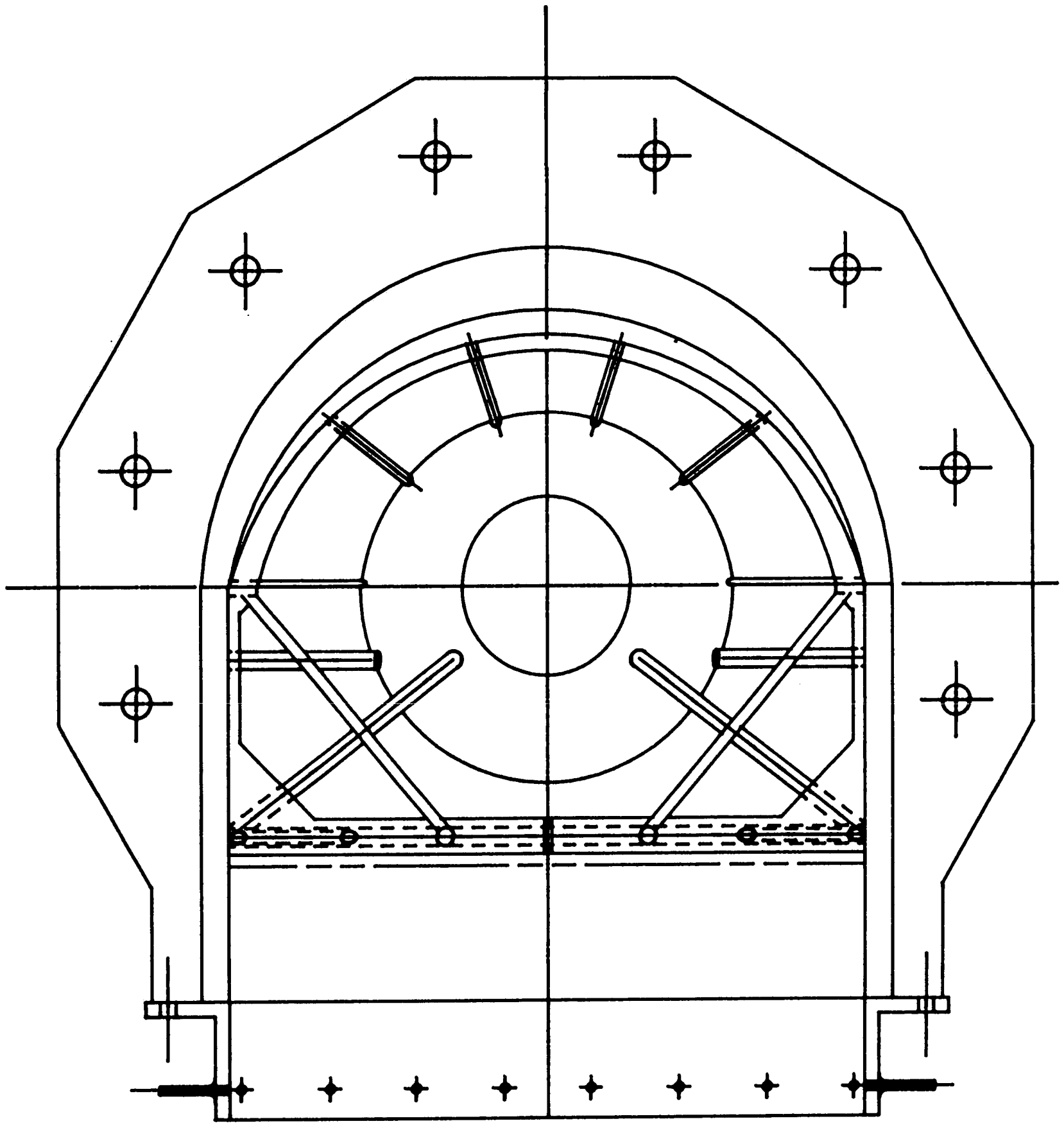

DRAWING NO. BV-1D
SIDE VIEW (SECTION B-B)
SCALE:5/16

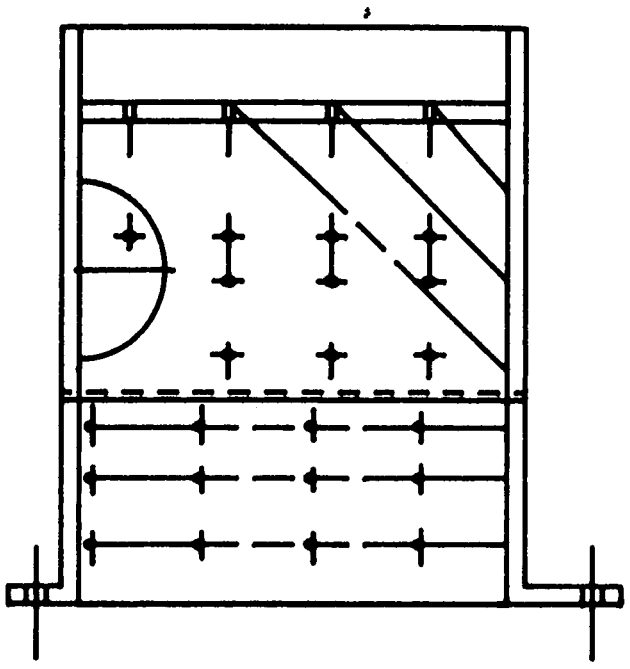

DRAWING NO. BV-2A
CONDENSER NECK (STRUTS ONLY)
SCALE: 1/4

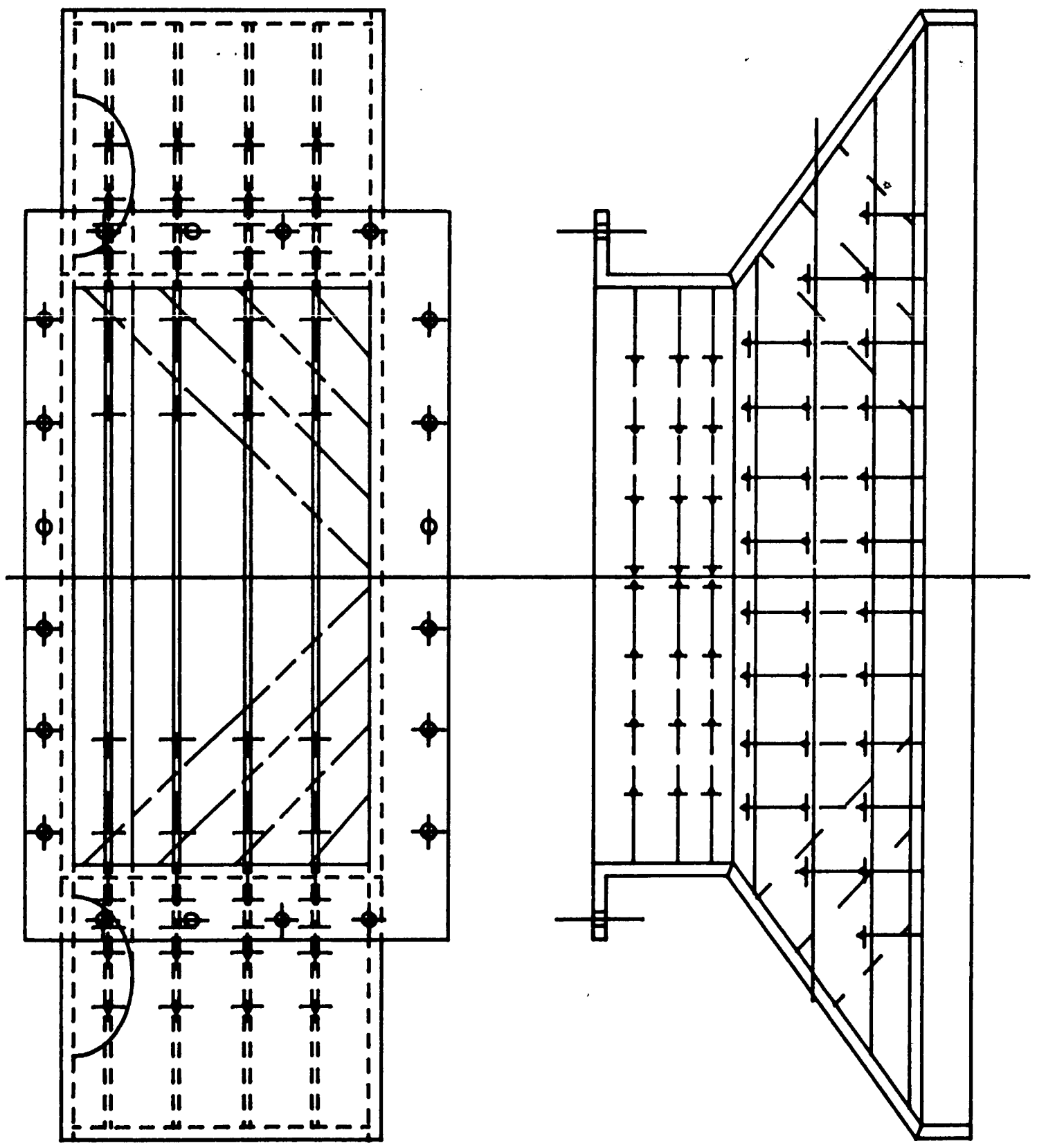

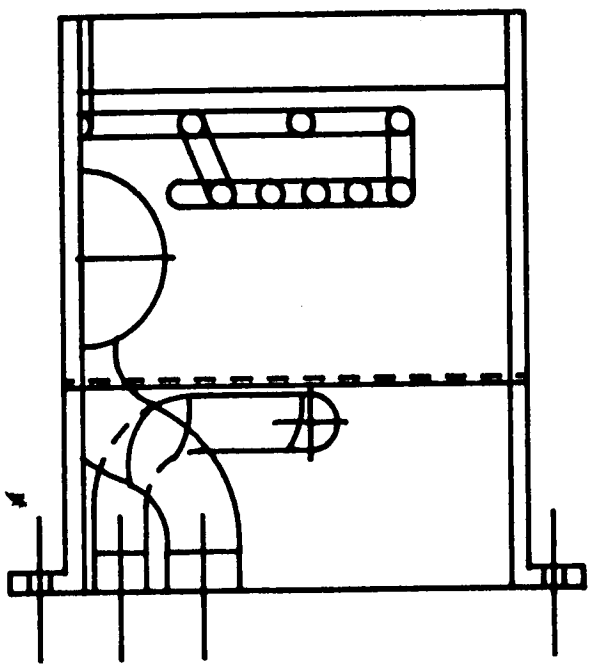

DRAWING NO. BV-2B
CONDENSER NECK(STEAM DUMPS ONLY)
SCALE:1/4

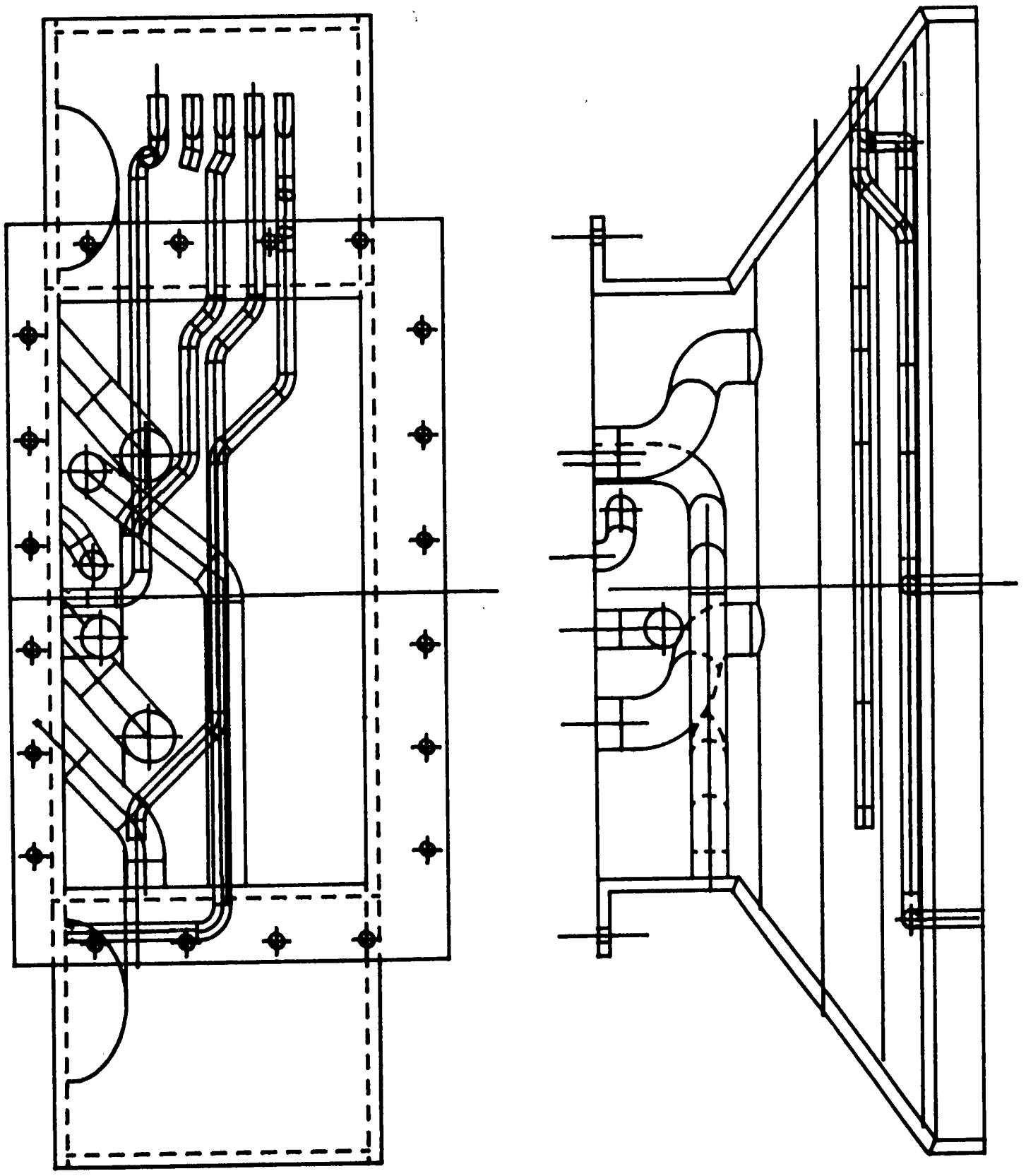

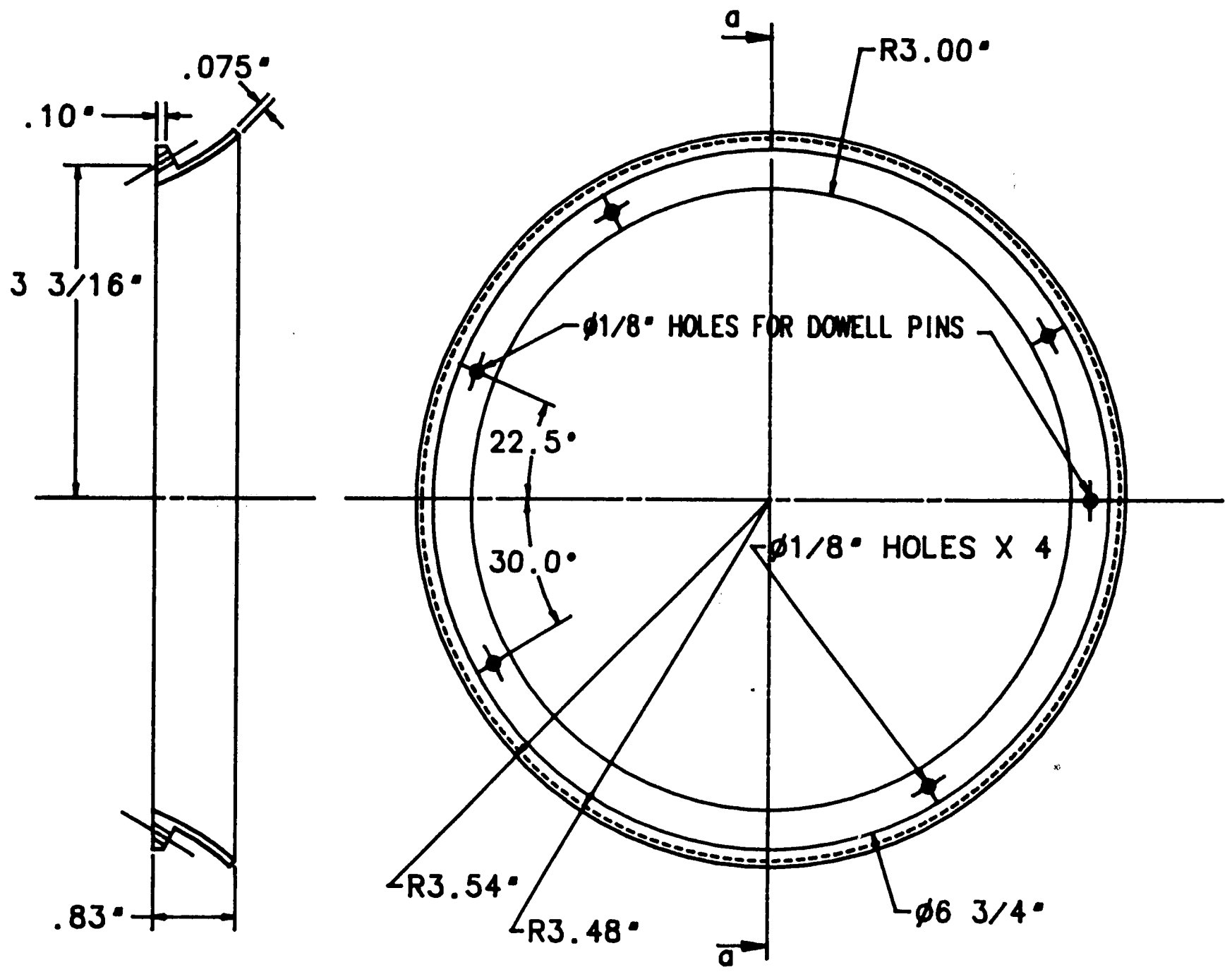

Section a-a

DRAWING NO. BV-3
GUIDE VANE
SCALE: 1/2

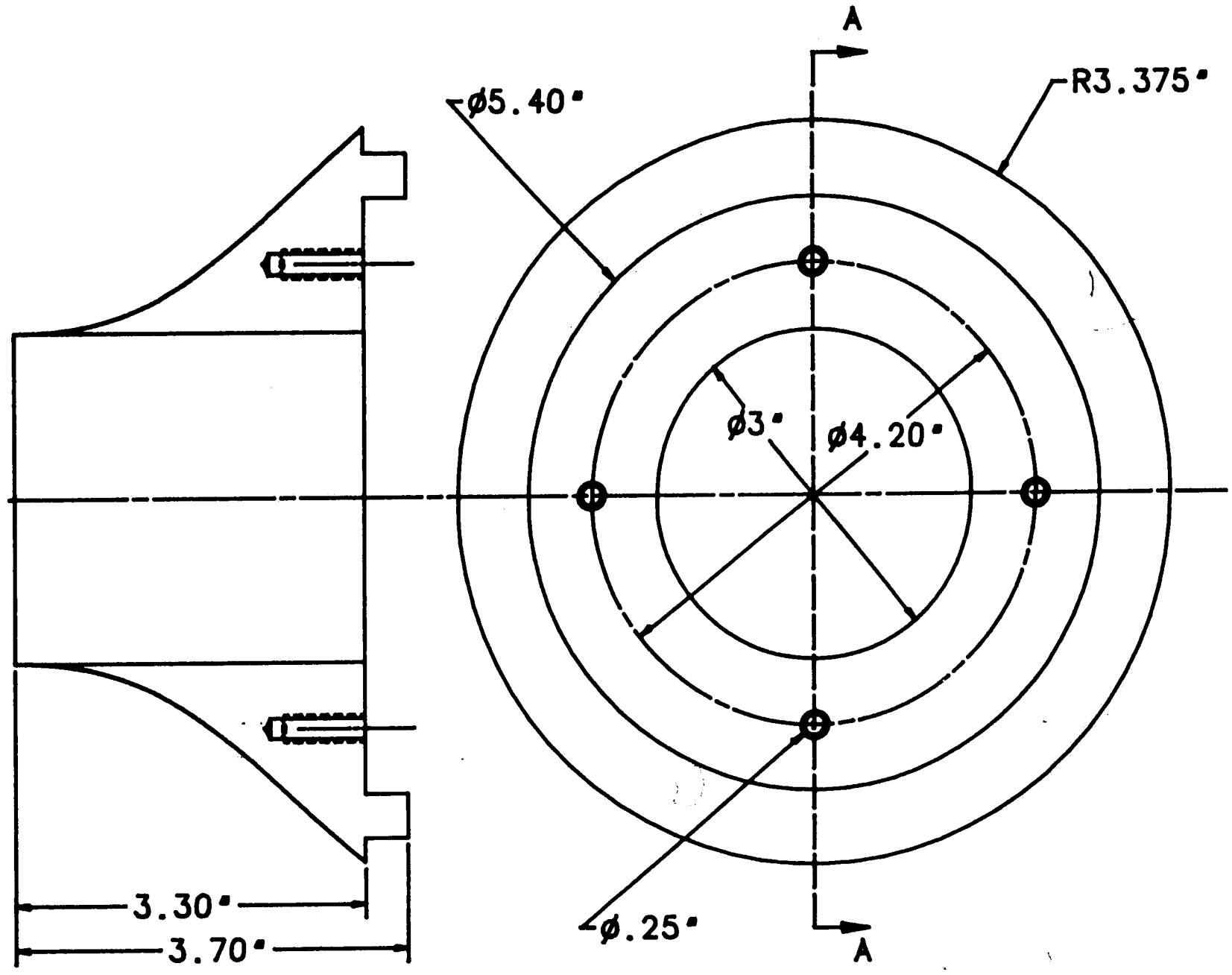

Section A-A

DRAWING NO. BV-4
BEARING CONE
SCALE:1/2

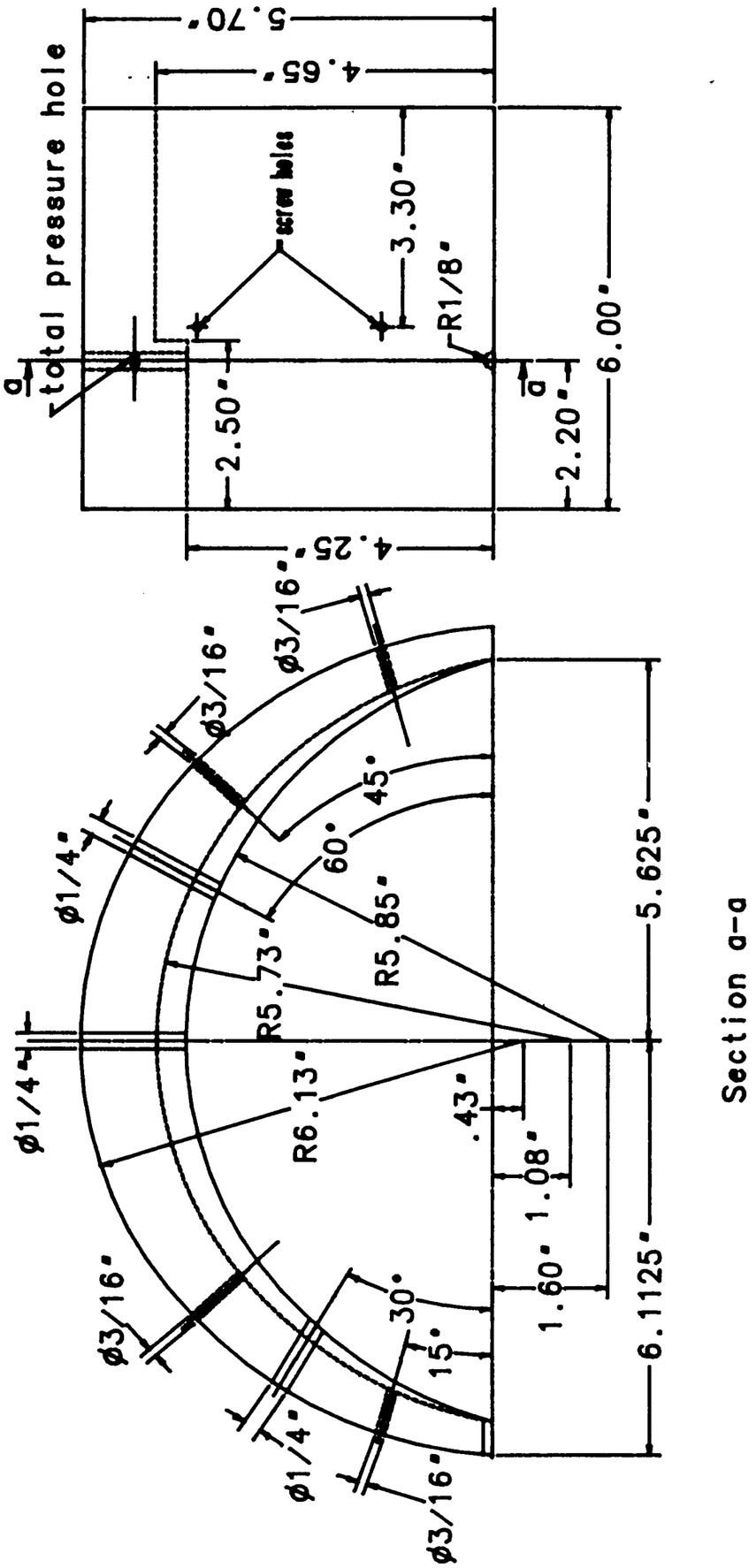

DRAWING NO. BV-5
INSERT TO CHANGE HEIGHT
SCALE: 1/3

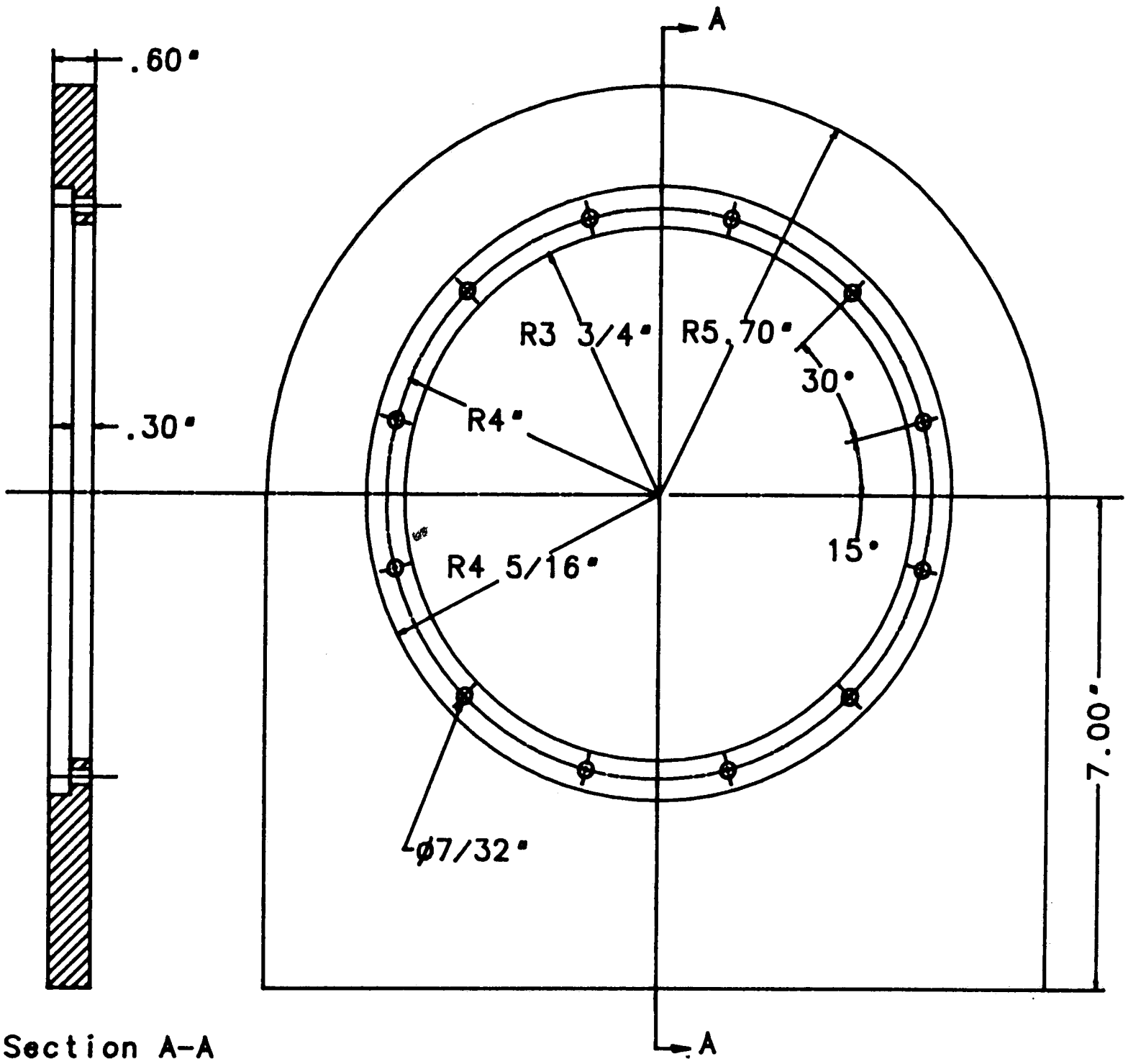

Section A-A

DRAWING NO. BV-6
INSERT TO CHANGE LENGTH
SCALE: 1/3

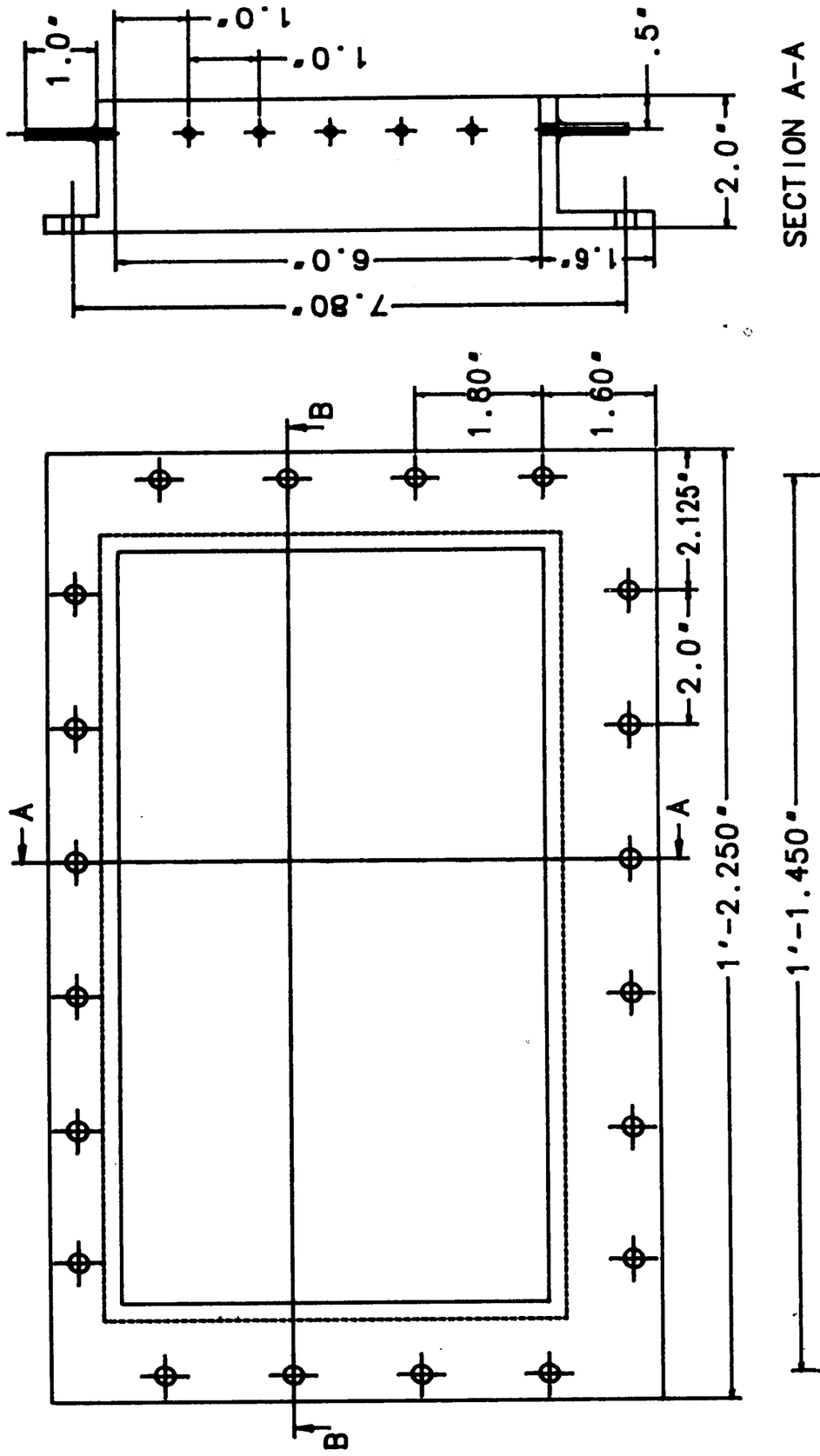

DRAWING NO. BV-7
OUTLET DUCT
SCALE: 1/3

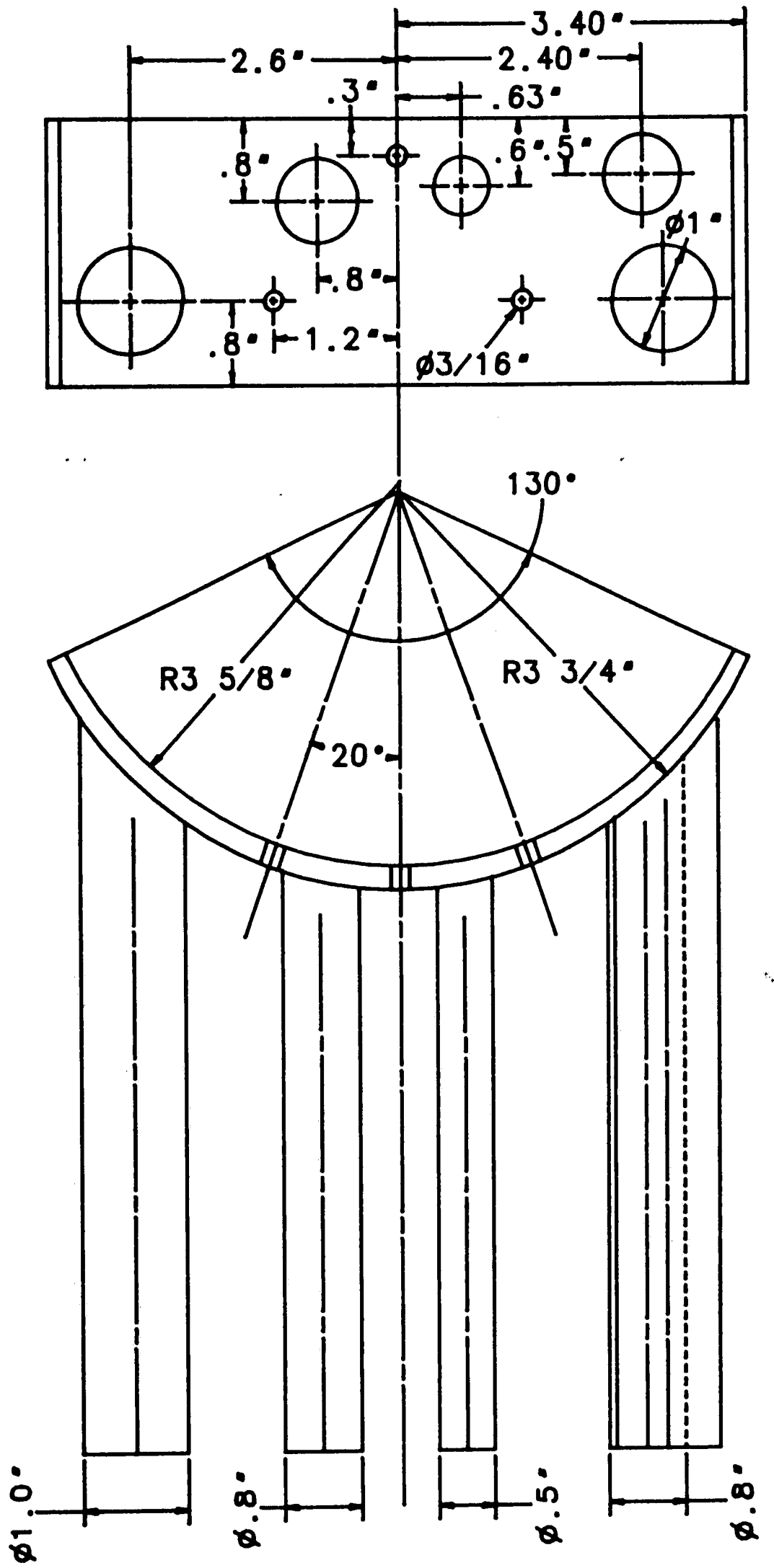

DRAWING NO. BV-8
EXTRACTION PIPING
SCALE: 1/2

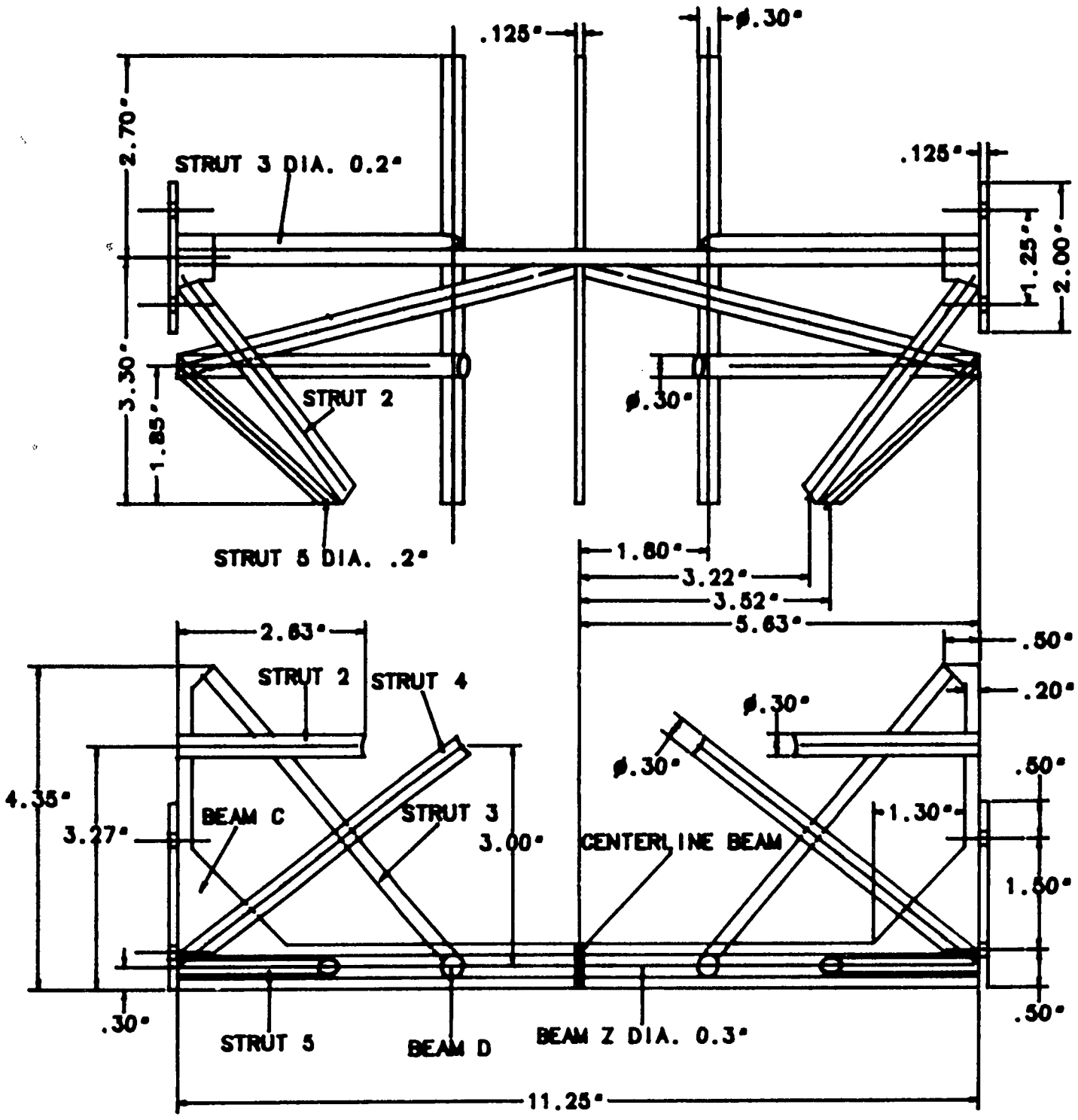

DRAWING NO. BV-9
STRUT GROUP 1
SCALE: 1/3

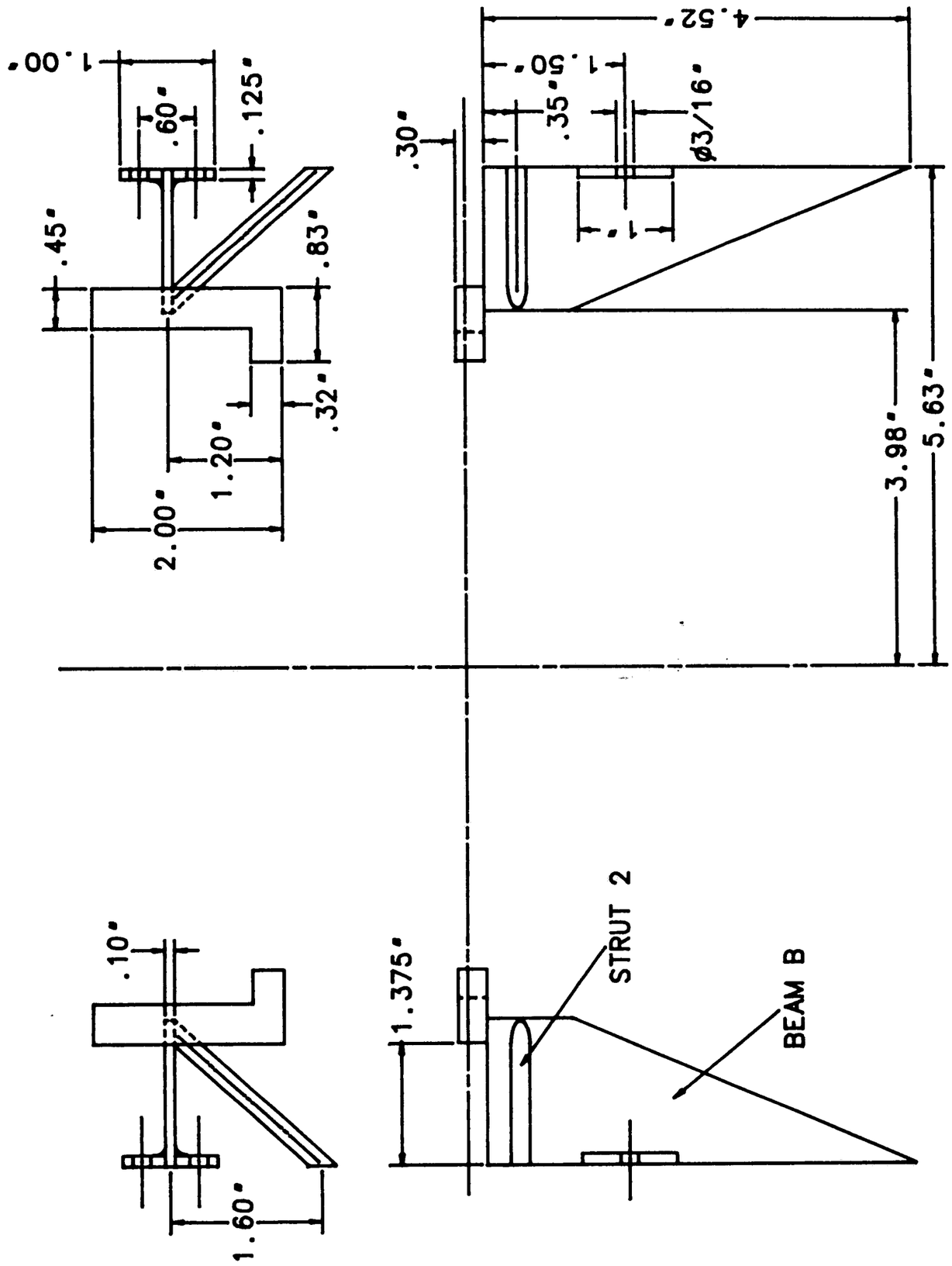

DRAWING NO. BV-10
STRUT GROUP 2
SCALE: 1/2

DRAWING NO. BV-11
STRUT GROUP 3
SCALE: 1/2

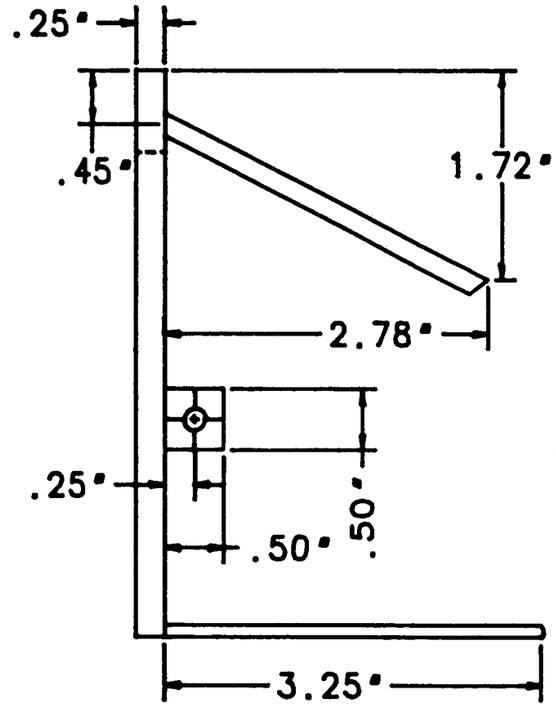

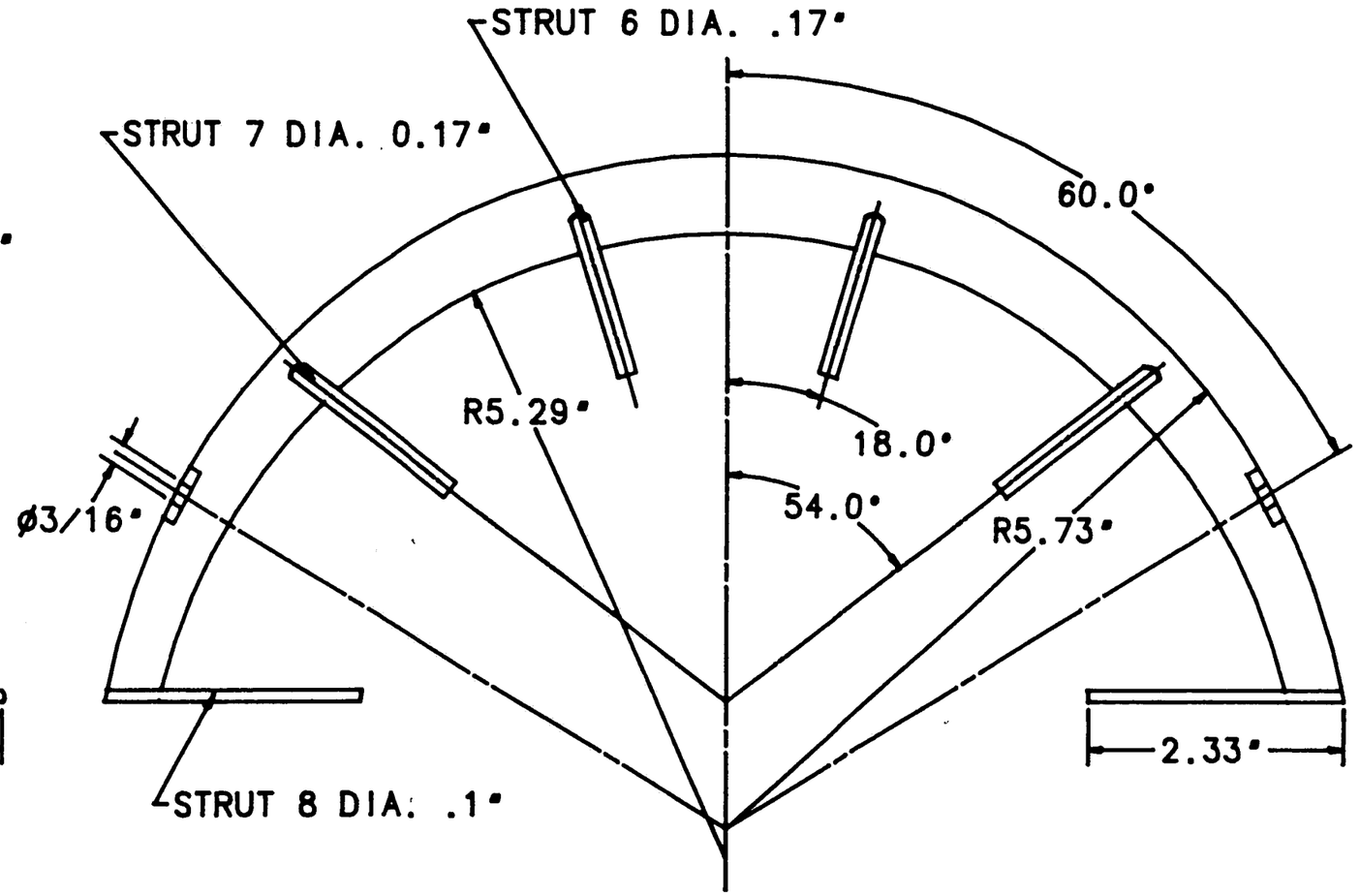

REFERENCES

1. Seglem, C.E., and Brown, R.O., "Turbine Exhaust Losses", ASME Paper No. 60-PWR-7, 1960.
2. Owczarek, J.A., and Warnock, A.S., " Improvement of a Low Pressure Turbine Exhaust End Performance at Indian Point Unit No. 2 Model Experiments ", Energy Research Center Report, Lehigh University, 1989.
3. Rodes, N., " The Prediction of Turbine Exhaust Performance ", ASME Trans., Latest Advances in Steam Turbine Design, Blading, Repairs, Condition Assessment, and Condenser Interaction, PWR-Vol. 7, 1989, pp. 99-105.
4. Gray, L., Sandhu, S.S., Davids, J., and Southall, L.R., " Technical Considerations in Optimizing Blade-Exhaust Hood Performance for LP Steam Turbines ", ASME Trans., Latest Advances in Steam Turbine Design, Blading, Repairs, Condition Assessment, and Condenser Interaction, PWR-Vol. 7, 1989, pp. 89-97.
5. Drakonov, A.M., and Zeryankin, A.E., " Investigating the Joint Operation of a Turbine Stage and a Diffuser Exhaust Hood, Teploenergetika, Vol. 19, No. 2, 1972, pp. 66-69.
6. Von Karman Institute for Fluid Dynamics, " Steam Turbines for Large Power Outputs ", Lecture Series 1980-6, 1980.
7. Japikse, ed., Advanced Topics in Turbomachinery Technology, Principal Lecture Series No. 2. Concept ETI, Inc., 1986.
8. Kline, J.S., "On the Nature of Stall ", ASME Trans., Journal of Basic Engineering, Vol. 81, September 1959, pp. 305-320.
9. Howard, J.H.G., Henseler, H.J., and Thornton-Trump,A.B., " Performance and Flow Regimes for Annular Diffusers ", ASME Paper No. 67-WA/FE-21, 1967.
10. Hoffman, J.A., and Gonzales, G., " Effects of Small Scale, High Intensity

InletTurbulence on Flow in a Two dimensional Diffuser ", ASME Trans., Journal of Fluids Engineering, Vol.106, June 1984, pp. 121-124.

11. Senoo, Y., and Nishi, M., " Improvement of the Performance of Conical Diffusers by Vortex Generators ", ASME Trans., Journal of Fluids Engineering, Vol. 96, 1974, pp. 4-10.

12. Stevens, S.J., and Williams, G.J., " The Influence of Inlet Conditions on the Performance of Annular Diffusers with Conical Walls ", ASME Trans., Journal of Fluids Engineering, Vol. 102, September 1980, pp.357-363.

13. McDonald, A.T., Fox, R.W., and Van Dewoestine, R.V., " Effect of Swirling Flow on Pressure Recovery in Conical Diffusers ", AIAA Paper No. 71-84, 1984.

14. Lohmann, R.P., Markowsky, S.J., and Brookman, E.T., " Swirling Flow Through Annular Diffusers with Conical Walls ", ASME Trans., Journal of Fluids Engineering, Vol. 101, June 1979, pp. 224-229.

15. Sovran, G., and Klomp, E.D. Experimentally Determined Optimum Geometries for Rectilinear Diffusers with Rectengular, Conical or Annular Cross-section. New York: Elsevier Publishing Co., 1967.

16. Takehira, A., Tanaka, M., Kawashima, T., and Hanabusa, H., " An Experimental Study of the Annular Diffusers in Axial-Flow Compressors and Turbines ", Proceedings of the 1977 Tokyo Joint Gas Turbine Congress, 1977, pp. 319-329.

17. Owczarek, J. A., and Warnock A. S., " Preliminary Proposal for Research Project, Part 2 : Improvement of LP Turbine Hood Performance", Energy Research Center, Lehigh University, 1988.

18. Owczarek, J.A., Fundamentals of Gas Dynamics, International Textbook Co., Scranton, PA., 1964.

19. Howard S. Bean, Fluid Meters, Their Theory and Application, 6th ed., New York, ASME, 1971.

20. Idelchik, I.E., Handbook of Hydraulic Resistance, 2nd edition, Hemisphere Publishing Company, 1986.

21. Morel, T., " Comprehensive Design of Axisymmetric Wind Tunnel Contractions", ASME Paper No. 75-FE-17, 1976.

22. Talapurkara, E.G., and Bhalla, V.V.K., "Experimental Investigation of Morel's Method for Wind Tunnel Contractions", ASME Trans., Journal of Fluids Engineering, Vol. 110, March 1988, pp. 45-47.

23. Cornell, W.G., " Losses in Flow Normal to Plane Screens ", ASME Trans., 1958 80, 791.

24. Fowler, J.E., " Factors Affecting the Design of Turbine-Condenser Connections ", ASME Trans., Journal of Engineering Power, July 1977, pp. 429-436.

25. Chesmejef, S., " Aerodynamic Testing of a Low Stimulus, Efficient Exhaust Hood-Industrial Turbines ", ASME Paper No. 77-JPGC-Pwr-2, 1977.

26. Migai, V.K., Gudkov, E.I., and Nosova I.S., " Increasing the Efficiency of Diffusers of Steam Turbine Exhausts ", Teploenergetika, Vol. 21, No. 12, 1974, pp. 46-50.

27. Deich, M.E., Zeryankin, A.E., and Zatsepin, M.F., " Results of Testing Turbomachine Exhaust Ducts with Ring Diffusers ", Teploenergetika, Vol. 12, No. 5, 1965, pp. 46-50.

28. Holden, P.C., and Barsness, E.J., " Condenser-Exhaust Hood Air Model Tests ", ASME Paper No. 63-WA-245, 1963.

VITA

Behzat Turegun was born in Sivas, Turkey, on August 3rd, 1967. After attending Sarkisla High School and Ankara Mimar Kemal High School, he obtained his High School degree from Ankara Etlik High School. He received his B.S. degree in Mechanical Engineering from the Middle East Technical University in June 1989. Upon graduation, he enrolled in the graduate program in Mechanical Engineering Department of Lehigh University. During his graduate study at Lehigh, he worked as a Research Assistant, Teaching Assistant and as a Student Consultant in the Lehigh University Computer Center.